The Role of *Mga* in the Survival of Pluripotent Cells During Peri-implantation Development

Andrew J Washkowitz

Submitted in partial fulfillment of the
Requirements for the degree of
Doctor of Philosophy
In the Graduate School of Arts and Sciences

COLUMBIA UNIVERSITY
2013

ABSTRACT

The Role of *Mga* in the Survival of Pluripotent Cells During Peri-implantation Development

Andrew J Washkowitz

The dual specificity transcription factor *Mga* contains both a T-box binding domain and a basic helix-loop-helix zipper (bHLHZip) domain. Loss of *Mga* leads to embryonic lethality by E5.5. *In vitro* blastocyst culture and embryonic stem (ES) cell culture identify a lack of pluripotent inner cell mass (ICM) derived cells as the cause of embryonic lethality. Loss of *Mga* leads to increased apoptosis in E4.5 embryos, though there is no decrease in the amount of cell proliferation. Embryos with mutant *Mga* have fewer pluripotent ICM cells during delayed implantation, though the number of differentiated primitive endoderm cells remained initially stable. Despite the loss of pluripotent cells, there is no change in the pattern of expression of Nanog or Oct4, pluripotent cell markers, or Gata4, a primitive endoderm marker. Expression of Ornithine Decarboxylase (ODC), the rate-limiting enzyme in the synthesis of cellular polyamines, was identified as a possible cause of embryonic lethality based on a similar mutant phenotype as well as the presence of E-box sequences in genetic regulation loci. ODC is expressed at lower levels in the ICM of *Mga* mutants. Blastocyst and ES cell culture defects were rescued when cultured in the presence of exogenous putrescine, the metabolic product of ODC. These results suggest a mechanism for Mga to influence

pluripotent cell survival through interactions with other bHLHZip domain proteins in the regulation of the polyamine pool in pluripotent cells of the embryo.

Table of Contents

List of tables and figures

Abbreviations

α-difluoromethylornithine (DFMO)

Basic Helix-Loop-Helix Zipper domain (bHLH-Zip)

Definitive Endoderm (DE)

Embryonic Day (E)

Embryonic Stem (ES)

Extraembryonic Endoderm (ExEn)

Inner cell mass (ICM)

Ornithine Decarboxylase (ODC)

Primitive endoderm (PE)

T-Box Binding Element (TBE)

Trophectoderm (TE)

Zygotic Genome Activation (ZGA)

Acknowledgements

First and foremost, I would like to express my unending gratitude to my mentor, Virginia Papaioannou. She supported me through the ups and many downs of my thesis research and perfectly adapted her mentoring style to my work. She gave me space to experiment when I needed it and steered me away from experiments when they were ill advised. Without her help, I would not have been able to accomplish any of my research and I am forever in her debt.

I would also like to thank my colleagues, especially Ripla Arora, Daniel Concepcion, and Nataki Douglas. From scheduled meetings to discussions at the water cooler, their comments were always appreciated and occasionally heeded. Their advice and support was invaluable throughout my research.

Finally, I would like to thank my wife Sarah and my son Henry. Their unconditional emotional support at home was critical to whatever success I found in the lab. I would also like to thank my brother Peter, sister Emily, mother Barbara and father Alan, as well as my brother-in-law David, father-in-law Mort, and mother-in-law Chris. Though few of them understand what I studied to this day, their support was also critical.

Chapter 1
Introduction

Development of the preimplantation embryo

Preimplantation development of the mouse embryo occurs over the first 4.5 days of embryonic life. During this time, the embryo goes through radical changes on both a morphological and gene expression level to establish the three major cell lineages that will contribute to further development after implantation. When the embryo implants between 4.5 and 5.5 days post coitus (defined as E for embryonic day), there are three major cell lineages that will contribute to the embryo: the epiblast (Epi), the trophectoderm (TE), and the primitive endoderm (PE). The Epi gives rise to all of the tissues that make up the body of the embryo. It remains undifferentiated and pluripotent largely through the action of *Pou5f1 (*referred to here by its common name, *Oct4*), *Nanog*, and *Sox2 (*Avilion et al., 2003; Loh et al., 2006; Nichols et al., 1998; Silva et al., 2009). Pluripotency relies both on the repression of differentiation factors as well as the activation of pluripotency factors. In contrast, the PE and the TE have already undergone initial stages of differentiation and will eventually give rise to most of the extraembryonic structures present during gestation. Development and differentiation of embryonic tissues relies on tight transcriptional control of the embryonic genome.

Activation of the zygotic genome

Transcription in the fertilized egg initially relies on maternally-derived mRNA transcripts deposited during oogenesis. It is not until the late one-cell/2-cell stage that an initial wave of zygotic transcription occurs (Hamatani et al., 2004). This wave of transcription, collectively referred to as the zygotic genome activation (ZGA), is both short-lived and is accompanied by rapid downregulation of ZGA-target genes and degradation of target transcripts. The zygotic genes that become active during initial ZGA are characterized as coding for basic cellular machinery including ribosomal proteins, RNA binding, proton transport, among others. Simultaneously, during the time of ZGA, maternal transcripts are degraded rapidly, allowing the zygotic genome to

become the main source of genetic instructions for further development (Paynton et al., 1988).

It is not until a second wave of transcription from the 4-cell stage to the 8-cell stage that genes specific for development of the pre-implantation embryo begin to be transcribed. While transcription of these genes is transient before being immediately decreased, these are the genes that have been shown to be responsible for patterning the pre-implantation embryo. This wave of transcription includes genes such as *Pou5f1* and *Nanog*, pluripotency factors in the ICM, as well as genes such as *Gata3* and *Irx3*, markers of trophoblast (Tanaka et al., 2002).

The presence of maternal transcripts is essential for development, but is often a complicating factor in the analysis of early gene function. Many genes are essential for embryonic development, but are deposited in the egg as either transcript or protein before ZGA. This makes loss-of-function studies difficult as the embryonic genome may contain loss-of-function alleles while the maternally derived transcripts or proteins are functional. This will mask potential embryonic phenotypes while the maternal transcript or protein persists.

Differentiation of the trophectoderm

The earliest zygotic cell divisions and the activation of the zygotic genome leave all daughter cells with the same developmental totipotency. The first cell lineage restriction is the differentiation of the trophoblast, the tissue that will become the placenta. Initiation of differentiation begins when cells of the 8-cell zygote divide asymmetrically to generate "inner" and "outer" populations of cells (Johnson and McConnell, 2004). During this time, "outer" cells that will eventually become TE upregulate the homeobox gene *Cdx2* (Jedrusik et al., 2008). *Cdx2* appears to be the key factor for the differentiation of trophoblast as embryos mutant for *Cdx2* do not downregulate the ICM markers *Oct4* and *Nanog* in the presumptive trophoblast cells resulting in the death of these "outer" cells (Strumpf et al., 2005). *Cdx2* also plays a role in maintaining the structural integrity of the embryo via E-cadherin adherins junctions present in the trophoblast during blastocyst formation (Strumpf et al., 2005). *Eomesodermin (Eomes)* also plays a role in proliferation of the trophoblast, though

mutants lacking *Eomes* are still able to form a TE layer suggesting that it acts downstream of *Cdx2* (Teo et al., 2011).

Conversely, *Oct4* and *Nanog* are initially expressed throughout the embryo, but eventually become restricted to the ICM by the action of trophoblast and TE differentiation genes such as *Cdx2* and *Eomes*. Both *Oct4* and *Nanog* have been shown to be repressors of early differentiation: *Oct4* represses trophoblast differentiation and *Nanog* represses extra-embryonic endoderm and PE (Mitsui et al., 2003; Nichols et al., 1998). In this way, there is a feedback mechanisms where cells of the trophoblast downregulate ICM genes, and cells of the ICM downregulate trophoblast genes.

Differentiation of the primitive endoderm

The second cell lineage restriction in the embryo is the formation of the PE, a monolayer of cells underlying the Epi that will eventually give rise to the yolk sac. The differentiation of the PE begins at E3.5 when cells of the ICM begin to differentially express the pluripotency marker *Nanog* and the PE marker, *Gata6* in a "salt and pepper" pattern (Chazaud et al., 2006). *Gata6* is upregulated by Fgf signaling through the adaptor protein *Grb2*, though the mechanism for targeting only a subset of ICM cells is not understood (Chazaud et al., 2006). Tracking of presumptive PE cells using another marker of PE, *Pdgfrα,* shows that they can either migrate to the PE monolayer or undergo apoptosis, suggesting a role for cell adhesion molecules in the sorting and survival of PE cells (Plusa et al., 2008). Once PE cells are formed, they rely on the Epi to survive as Nanog-deficient embryos are able to initially form a PE, which then degenerates (Silva et al., 2009).

The T-box transcription factors in preimplantation embryonic development and pluripotency

The necessity of transcriptional control of differentiation during preimplantation development suggests that different families of transcription factors can contribute to this process. The T-box transcription factors are an ancient and evolutionarily conserved family of transcription factors necessary for a large number of developmental processes

(Naiche et al., 2005). In mouse, there are 17 T-box factors that can be subdivided into 5 subfamilies based on sequence similarity. All of the T-box factors share a common DNA binding domain, the T-box, which can bind the T-box binding element (TBE), a palindromic sequence with two T-half sites (5'-AGGTGTGAAATT-3') (Kispert and Herrmann, 1993). Dimers of Brachyury are able to bind this sequence, with each monomer binding one T-half site of the TBE (Papapetrou et al., 1997). Different T-box factors bind their respective T-sites in various homo- and heterodimeric combinations, as well in competition with each other or other transcription factors (Habets et al., 2002; Sinha et al., 2000).

Although detected in other organisms as early as the oocyte stage of development, most T-box factors are only functionally necessary during gastrulation and organogenesis (Gibson-Brown et al., 1998; Greulich et al., 2011; Showell et al., 2004). Nonetheless, there is evidence of a role for two T-box genes during blastocyst formation and in the maintenance or acquisition of pluripotency.

Tbx3

Tbx3 transcripts are first detected in the ICM of E3.5 blastocysts (Bollag et al., 1994; Chapman et al., 1996). Despite this expression, the role of *Tbx3* in the ICM is unclear. Homozygous loss-of-function *Tbx3* mutants have no phenotype at E3.5, though there is 50% embryonic lethality by E11.5 with the rest dying by E16.5, most likely due to yolk sac or cardiac deficiency (Davenport et al., 2003; Mesbah et al., 2008).

Nonetheless, *Tbx3* is critical for the function of embryonic stem (ES) cells. Similar to their *in vivo* analog, the ICM, undifferentiated ES cells express *Tbx3*. This expression decreases as the ES cells differentiate implicating *Tbx3* in the maintenance of pluripotency (Lu et al., 2011). This function is supported by the detection of *Tbx3* in a pluripotency transcriptional module involving factors such as Oct4 and Nanog that is able to activate transcription of pluripotent factors and repress differentiation genes (Kim et al., 2008). Moreover, ectopic *Tbx3* expression from a viral plasmid leads to increased efficiency of derivation of induced pluripotent stem cells (iPSC) (Han et al., 2010). Rather than promoting pluripotency, though, *Tbx3* appears to function similarly to *Oct4*

and *Sox2* by repressing differentiation, in this case differentiation into mesoderm, ectoderm, and neural crest cell fates (Ivanova et al., 2006).

In contrast to its role in repression, *Tbx3* is also able to promote differentiation of ES cells into extraembryonic endoderm (ExEn). Overexpression of *Tbx3* in ES cells induces differentiation of ExEn cells as gauged both by morphology and *Gata6* expression (Lu et al., 2011). This duality suggests that, like other factors involved in pluripotency, *Tbx3* renders ES cells poised to differentiate when the proper signals are received. These transcription factors act as repressive factors when ES cells are to remain pluripotent, but can quickly switch to activators when differentiation is induced (Bernstein et al., 2006; Washkowitz et al., 2012).

Eomesodermin

The only other T-box transcription factor that has been shown to play a role in preimplantation development is *Eomes*. *Eomes* is first detected in the trophoblast lineage at E3.5 and continues to be expressed in its derivative, the extraembryonic ectoderm of postimplantation embryos (Hancock et al., 1999; Russ et al., 2000). *Eomes* homozygous mutations are embryonic lethal soon after implantation due to a defect in trophoblast development and failure of formation of trophoblast stem cells. *Eomes* likely acts downstream of the homeobox factor *Cdx2* in the proliferation and development of the trophoblast (Strumpf et al., 2005).

In the pluripotent ICM and Epi, *Eomes* is repressed by *Nanog, Sox2*, and *Oct4*. Later, during gastrulation, *Eomes* promotes the differentiation of the embryonic germ layers by repressing mesoderm and pluripotency genes and activating definitive endoderm (DE) genes (Teo et al., 2011). *Eomes* also regulates the E-cadherin-mediated epithelial-to-mesenchymal transition critical for cell movement and mesoderm specification, thus providing cues for cell specification along the anterioposterior axis (Arnold et al., 2008).

The Max network of basic-helix-loop-helix-leucine zipper transcription factors in early embryonic development and pluripotency

Another group of transcription factors known to play a role in preimplantation development is the basic-helix-loop-helix-leucine zipper (bHLHZip) domain genes of the Max network. The Max network proteins are transcription factors that bind the canonical DNA sequence, the E-box (5'-CACGTG-3') (Grandori et al., 2000; Hurlin and Huang, 2006). This network is composed of the bHLHZip genes *Max* and *Mga*, as well as members of the *Myc*, *Mad*, and *Mnt* families of genes. Most of these genes were identified by the binding of their gene products to Max, highlighting the centrality of Max in the function of this network (Ayer et al., 1993; Hurlin et al., 1999; Hurlin et al., 1995; Meroni et al., 1997; Zervos et al., 1993).

Max lies at the center of this transcriptional network and is required for all proteins of the network to function. Though Max alone is able to homodimerize and bind the canonical E-box, it is transcriptionally inert. Similarly, the other members of this family are unable to bind DNA alone leaving them also transcriptionally inert as monomers. It is only through heterodimerization with Max that the other proteins in the network are able to activate or repress transcription of their E-box-containing target genes. In this way, each protein's activity is modulated by the presence or absence of the other proteins in the network (Baudino and Cleveland, 2001; Meroni et al., 2000; Walker et al., 2005). *Mga* is unique among the members of the bHLHZip domain family members because of the presence not just of the bHLHZip DNA binding domain, but a T-box binding domain as well (Hurlin et al., 1999).

The importance of this network was first noted in 1981 when the amplification and overexpression of the proto-oncogene *c-Myc* was found in Avian Leukosis Virus (ALV)-induced lymphoid leucosis (Hayward et al., 1981). *Myc* has since been linked to more than 40% of human cancers (Zeller et al., 2003). Despite their importance in a variety of cellular contexts, only a subset of the Max-interacting transcriptional network appears to play a role in early embryonic development.

Max

In both mouse and zebrafish, *Max* transcripts are found ubiquitously throughout development (Domashenko et al., 1997; Schreiber-Agus et al., 1993). In mouse, there are maternal stores of Max in unfertilized eggs, as well as zygotic Max produced in all cells of the embryo throughout development (Shen-Li et al., 2000).

Despite its near universal expression, zygotic *Max* appears to be dispensable for development through the preimplantation period, though the maternal stores of the protein could abrogate a need for newly produced Max. Homozygous *Max* mutant embryos are recovered at a mendelian frequency at E3.5, but are recovered at a lower rate at E6.5 and are not recovered at all by E8.5. Mutant embryos at E6.5 are 50-70% smaller than controls and have no demarcation between embryonic cell layers and no morphologically distinct embryonic features. Mutant embryos also have lower proliferation rates at E6.5, and though there is no accompanying apoptosis, it is possible that earlier waves of apoptosis were missed during analysis (Shen-Li et al., 2000).

The importance of *Max* during the peri-implantation period suggests a necessity for active Max network transcription factors, though functional redundancy and maternal protein complicate the analysis.

c-Myc

c-Myc is first transcribed at the 4-cell stage and continues to be expressed until the formation of the blastocyst (Domashenko et al., 1997). The importance of this early expression is unclear as *c-Myc* homozygous mutant mice survive until E10.5 when they die with abnormalities in the heart, pericardium, neural tube, and other structures (Davis et al., 1993). When *c-Myc* deletion is confined to the Epi, embryos die before E12 of severe anemia and functionally defective hematopoietic stem/progenitor cells, but have none of the structural deficiencies in the formation of the heart or neural tube (Dubois et al., 2008). The difference in embryonic lethality when *c-Myc* is deleted in the Epi-derived tissues alone compared to the Epi- and TE-derived tissues suggests separate developmental roles for *c-Myc*: The lack of *c-Myc* in the TE-derived placenta could lead to placental insuffiency and contribute to the E10.5 lethality of mutant *c-Myc* embryos,

while the lack of a hematopoeitc stem-cell population in the embryo could account for the later lethality of the Epi-restricted mutant *c-Myc* embryos.

Complementary to *c-Myc*'s role in the development of a multipotent hematopoietic stem-cell population, *c-Myc* has also been found to expressed in pluripotent ES cells (Murphy et al., 2005), though its role there is unclear. *c-Myc* mutant ES cells are grossly normal and *c-Myc* is not part of the core pluripotency network of *Oct4*, *Sox2*, and *Nanog* (Davis et al., 1993; Kim et al., 2008). Nonetheless, *c-Myc*'s importance in pluripotency is evident as efficient derivation of iPS cells with *c-Myc* is not possible (Takahashi and Yamanaka, 2006). This discrepancy may be explained by the presence of the closely related protein N-myc in ES cells. Indeed, ES cells that have both mutant *c-Myc* and mutant *N-myc* do not maintain pluripotency or self-renewal, highlighting a necessary role for these genes in ES cells (Varlakhanova et al., 2010).

c-Myc has also been proposed to form the core of a transcriptional module that serves to amplify global transcription in ES cells (Nie et al., 2012). In activated lymphocytes, *c-Myc* was shown to bind to the promoters of virtually all genes that were upregulated compared to non-activated lymphocytes, regardless of whether they contained E-boxes in them. The binding of *c-Myc* to promoters of expressed genes with or without E-boxes correlated with an increase in their expression levels in ES cells. This binding was also associated with an increase in RNA polymerase II. Because *c-Myc*-mediated amplification of transcription was not limited to genes with E-boxes in their promoters, *c-Myc* may function as a global transcriptional modulator for the entire genome (Nie et al., 2012). This functionality is also present in T-lymphocytes and Burkitt's lymphoma cells suggesting a universal mechanism for *c-Myc*–mediated gene regulation (Lin et al., 2012).

N-myc

As with *c-Myc*, the closely related transcription factor *N-myc* is also thought to play a role in preimplantation development. N-*myc* transcripts were observed at low levels throughout the E6.5 embryo to the exclusion of the TE (Downs et al., 1989). Later, *N-myc* transcripts were detected during gastrulation and embryonic time points thereafter, notably in the developing nervous system. (Stanton et al., 1992). Though not

examined earlier in the embryo, *N-myc* is also expressed in ES cells, suggesting that expression may be found in the ICM (Sawai et al., 1991).

The role of *N-myc* in pluripotency and the development of the early embryo is unclear. Multiple studies using different mutant alleles have found that embryos with homozygous *N-myc* mutations are embryonic lethal during organogenesis (Sawai et al., 1993; Stanton et al., 1992), suggesting that *N-Myc* is dispensable during earlier stages. However, as with *c-Myc*, ES cells that carry disrupted versions of both *c-Myc* and *N-myc* do not maintain pluripotency or self-renewal (Varlakhanova et al., 2010). Derivation of iPS cells is also normal when *N-myc* is substituted for *c-Myc* (Blelloch et al., 2007). Moreover, the transgenic replacement of the coding sequence of *c-Myc* with that of *N-myc* results in viable and fertile mice with no apparent defects, highlighting a redundant role for these two genes (Malynn et al., 2000).

Mga

Mga (MGI: 1352483, synonyms C130042M01Rik, D030062C11Rik, Mad5), the least studied of the Max-network of transcription factors, is also thought to play a role in the development of the embryo. *Mga* was first identified in a yeast two-hybrid screen for interacting partners of Max. *Mga* was identified using E9.5 and E10.5 cDNA libraries and the full length sequence was constructed using an E14.5 kidney cDNA library (Hurlin et al., 1999). *Mga* has since been found to span 73kb of genomic DNA on chromosome 2 and contain 24 exons. The mature RNA is ~9kb and codes for a protein of 3006 amino acid residues. There are two splice forms that differ by the inclusion/exclusion of the 14th exon.

Domain analysis reveals the presence not just of a bHLHZip DNA binding domain, but also a T-box DNA binding domain, making *Mga* a dual-specificity transcription factor. Unlike other T-box transcription factors, the T-box in *Mga* is fully encoded within a single exon leading to the hypothesis that it is the product of the retrotransposition of the T-box of a *Tbx6*-related cDNA, the most closely related T-box transcription factor (Lardelli, 2003)(Fig 1).

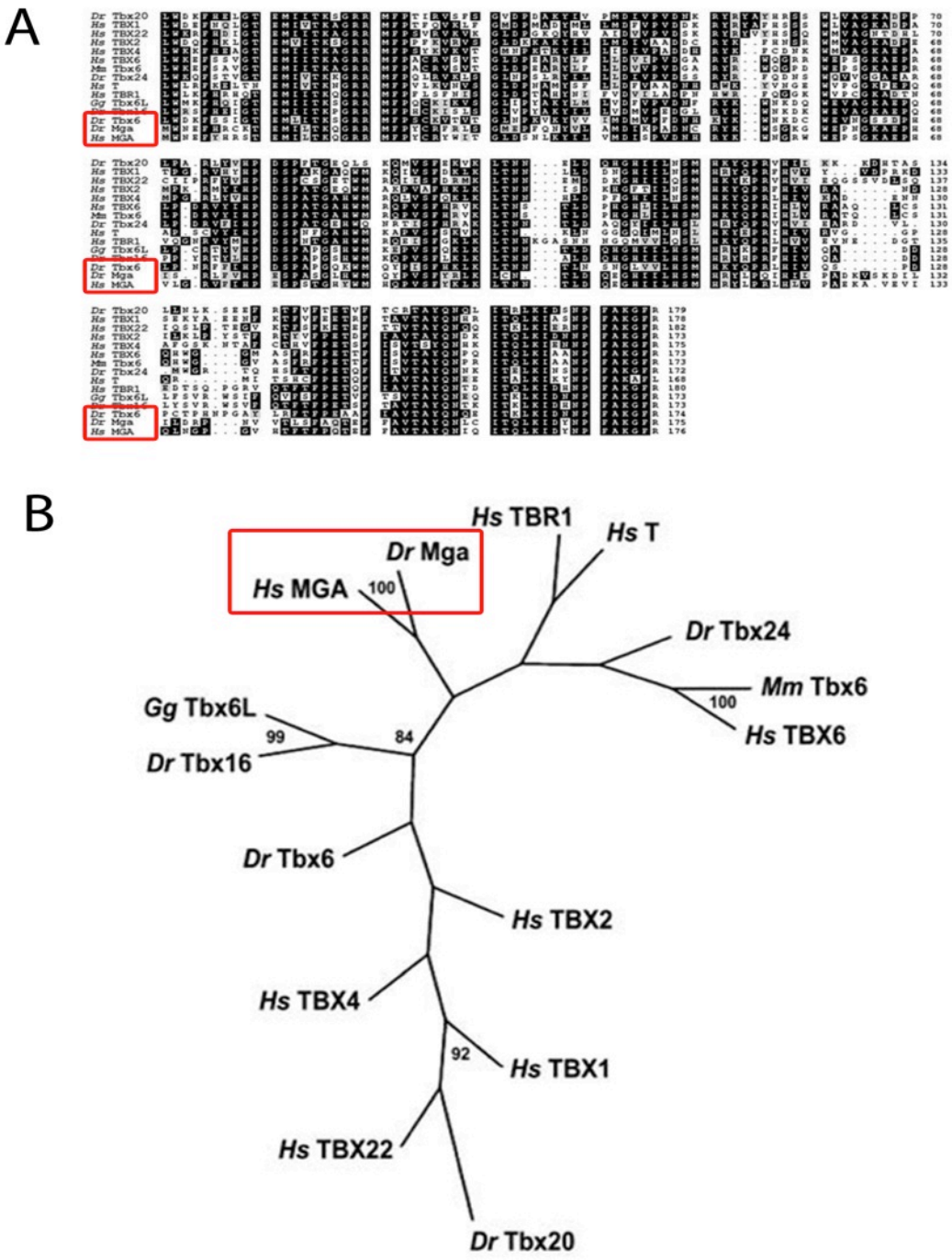

Figure 1. Phylogenetic analysis of vertebrate T-box sequences. A. ClustalW alignment of translated T-box sequences. Mga and Tbx6 are highlighted in red. B. Phylogenetic tree derived by parsimony analysis of alignment of (A). Mga is highlighted in red. Adapted from (Lardelli, 2003). Hs, Homo sapiens; Mm, Mus musculus; Dr, Danio rerio; Gg, Gallus gallus.

In vitro, Mga has been shown to bind the TBE as well as the E-box. Binding of *Mga* to the E-box is dependent on Max dimerization, while binding to the TBE can occur either independently of Max or as a dimer with Max. When bound to E-box sites as a heterodimer, Mga is able to act as a transcriptional activator. However, when bound to a TBE, Mga is able to repress transcription when bound alone, but to activate transcription when bound with Max (Hurlin et al., 1999). This duality suggests that Max can regulate the activity of Mga not only by regulating its binding to the E-box, but also by acting as a switch of transcriptional activity on T-box targets.

Mga appears to be widely expressed during development. In zebrafish, *Mga* mRNA was detected as a maternal transcript in the fertilized egg at the 1-cell stage and is expressed widely throughout later development (Rikin and Evans, 2010). In mouse, the expression is more restricted with mRNA first detected at E3.5 and later at E6.5 through E10.5 (Hu et al., 2009). *In situ* hybridization localized E3.5 expression to the pluripotent ICM (Yoshikawa et al., 2006), and expression of both RNA and protein has been detected in ES cells, the *in vitro* analog of the ICM (Hu et al., 2009; van den Berg et al., 2010). *Mga* RNA was also detected during organogenesis in a variety of organs including the limb buds, branchial arches, and tail region, though control assays were not shown (Hurlin et al., 1999) and independent verification has not been possible (our unpublished results).

Very few studies have addressed the role of *Mga* during embryonic development. In zebrafish, morpholino depletion of *Mga* in fertilized eggs results in defects in the brain, heart, and gut derivatives, though no common mechanism was found. In the heart, there was an absence of looping that was partially a result of overexpression of *Gata4* transcripts, indicating a transcriptional repression role of *Mga*. The brain, however, was shown to have an increase of apoptosis that was p53 dependent, indicating a cell survival role for *Mga* (Rikin & Evans, 2010).

In mouse, *Mga* appears to have a role in the pluripotency program. In ES cells, Mga has been shown to be in a complex with the pluripotency factor Oct4, a necessary transcriptional activator for pluripotency (Hammachi et al., 2012). When *Mga* is depleted with siRNA, ES colonies showed a decrease in the transcription of *Oct4*, *Sox2*,

and *Nanog* suggesting a transcriptional activation role for Mga in ES cells (Hu et al., 2009; van den Berg et al., 2010).

In addition to its role as a transcription factor, Mga may also modulate transcription by recruiting other complexes to target genes. Mga has been found in polycomb repression complexes with PRC1B and E2F-6 in both ES cells and HeLa cells (Illingworth et al., 2012; Ogawa et al., 2002). In HeLa cells, the presence of Mga in this complex allows chromatin modification and silencing of T-box and E-box targets, suggesting that Mga is able to regulate transcription both on a direct transcriptional level as well as an epigenetic level.

Aims of this research

Our initial experiments indicated that *Mga* was critical for peri-implantation development. It is possible that *Mga* is necessary for peri-implantation development because it regulates key transcriptional targets through its interaction with Max network proteins. We studies how *Mga* affects preimplantation development using 4 primary systems. First, we used blastocyst culture of embryos lacking *Mga* to directly observe the growth and development of the peri-implantation embryo in the absence of *Mga*. Second, we derived ES cells with a conditional *Mga* allele to observe any effects that mutation of *Mga* has on the growth and differentiation of ICM analogues. Third, we used immunofluorescence of E4.5 day embryos to assess the expression of cell layer differentiation and characterize the growth and apoptosis of embryos lacking *Mga*. Finally, we used hormonally induced diapause to assay maintenance of pluripotency in embryos lacking *Mga* in the absence of the rapid cell division characteristic of peri-implantation development.

Chapter 2
Results

The role of *Mga* in preimplantation development

Function of the Mga mutant allele

A conditional *Mga* mutation was generated by the German Gene Trap Consortium (GGTC), Mouse Genome Informatics (MGI) allele $Mga^{Gt(E153E01)Wrst}$. This is a multipurpose allele from which additional alleles can be derived. In the following, the alleles are referred to as Mga^{GT} (for gene trap), Mga^{Inv} (for FLP-recombinase inverted gene trap) or $Mga^{Re\text{-}inv}$ (for Cre-recombinase re-inverted gene trap).

The *Mga* allele was made with a gene trap construct that contains a splice acceptor and β-galactosidase-neomycin resistance (β-geo) fusion protein cassette that is flanked by 4 sets of heterotypic LoxP and FRT sites (Fig 2). In its original Mga^{GT} orientation, the upstream exon donates a splice site that is accepted by the gene trap cassette rather than the endogenous allele. This creates a truncated fusion protein that carries a β-geo reporter under the control of the *Mga* promoter. When treated with Flp recombinase, the cassette is inverted to the Mga^{Inv} configuration and the splice acceptor is put in the wrong orientation to accept the upstream splice, allowing the wild type transcript to be produced. When treated with Cre recombinase, the cassette is flipped to the $Mga^{Re\text{-}inv}$ configuration, once more producing the β-geo fusion protein. These mechanisms allow the Mga^{GT} and $Mga^{Re\text{-}inv}$ alleles to act as mutant reporters and the Mga^{Inv} allele to act as a conditional-mutation allele (Fig 2)(Schnutgen et al., 2005).

ES cell clones were isolated from E14Tg2a ES cells (Sv129P2) after retroviral infection using rsFlpRosaβgeo (FlpRBG; www.genetrap.de). The insertion of FlpRBG in intron 3 of *Mga* was identified by splinkerette PCR (Horn et al., 2007).

Breeding with Mga *mutants*

All embryos and adults produced during the course of experiments were routinely genotyped by PCR. $Mga^{GT/+}$ mice genotyped at weaning were recovered at the expected Mendelian frequency (46/88 from $Mga^{GT/+}$ x $Mga^{+/+}$ matings; $X^2 = 0.18$, $p=0.67$) and were viable and fertile indicating that the mutant allele did not have a heterozygous or

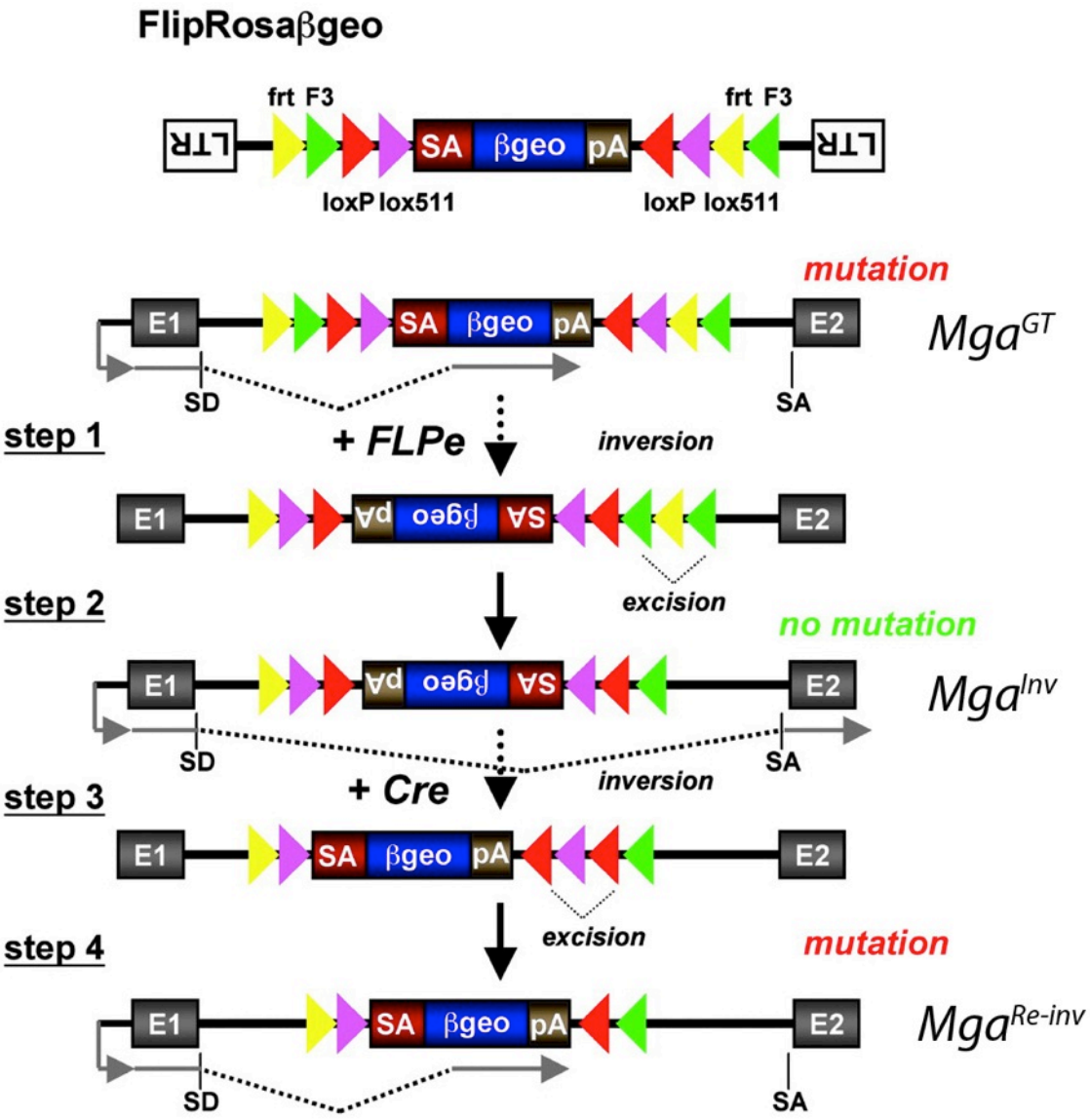

Figure 2. The gene trap cassette and *Mga* mutations produced from the FlpRBG cassette. The FlpRBG targeting vector utilizes a gene trap strategy for the creation of a mutant reporter of *Mga*. The Mga^{GT} allele orients a splice acceptor-β-galactosidase-neomycin resistance cassette (top) to accept the upstream exon's splice site and create a mutant truncated reporter protein. After treatment with Flp recombinase (which results in inversion, step 1 and excision, step 2), the splice acceptor is no longer in the proper orientation to accept the upstream splice and a wild type transcript is produced. After further treatment with Cre recombinase, inversion (step 3) and excision (step 4) occur to produce the $Mga^{Re\text{-}inv}$ allele, which functions like the Mga^{GT} allele: a truncated reporter protein is produced. Adapted from (Schnutgen et al., 2005).

dominant negative effect (Table 1). No $Mga^{GT/GT}$ mice were recovered at weaning in 19 litters from inter se matings of $Mga^{GT/+}$ mice (0/84; $X^2 = 28.64$, $p<0.0001$) indicating homozygous lethality before that time (Table 1). $Mga^{GT/+}$ mice were also bred with a constitutively active FlpE recombinase-expressing mouse to generate the inverted conditional allele, Mga^{Inv} (Fig 2). $Mga^{Inv/+}$ mice were born at the expected frequency (7/13 from $Mga^{Inv/+}$ x $Mga^{+/+}$ matings; $X^2 = 0.33$, $p = 0.56$) indicating that the conditional $Mga^{Inv/+}$ allele did not have a heterozygous or a dominant negative effect (Table 1). Homozygous $Mga^{Inv/Inv}$ mice, however, were recovered at only ~50% of the expected frequency (19/150 from $Mga^{Inv/+}$ x $Mga^{Inv/+}$ matings; $X^2 = 13.45$, $p = 0.001$) indicating that the conditional Mga^{Inv} allele is not fully functional (Table 1). This conditional allele was insufficient to compensate for the Mga^{GT} mutation of a second allele as no $Mga^{GT/Inv}$ mice were recovered (0/22 from $Mga^{Inv/Inv}$ x $Mga^{GT/+}$ matings; $X^2 = 22$, $p<0.0001$) (Table 1).

The role of Mga *during implantation*

Dissection of the uteri of females from inter se $Mga^{GT/+}$ matings at E9.5 – E11.5 revealed empty implantation chambers with cellular debris or a few trophoblast giant cells in approximately ¼ of the deciduae examined (6/25; from the Mendelian ratios, $X^2 = 6.37$, $p=0.04$). Trophoblast giant cells from one of these decidua were recovered and proved to be $Mga^{GT/GT}$ when genotyped by PCR. Implantation sites with evidence of embryonic lethality were present at E5.5 as well, where approximately ¼ of the deciduae dissected were empty (9/44; from the Mendelian ratios, $X^2 = 11.69$, $p=0.003$). Histological examination of whole uteri at E5.5 and E6.5 showed instances of cellular debris with isolated trophoblast giant cells in approximately ¼ of the decidual swellings examined (10/39 at E5.5; from the Mendelian ratios, $X^2 = 0.55$, $p=0.46$; 4/10 at E6.5; from the Mendelian ratios, $X^2 = 1.20$, $p = 0.27$) (Fig 3). At E4.5, $Mga^{GT/GT}$ embryos were recovered from uterine flushes at approximately 80% of the expected Mendelian frequency (49/245; $X^2 = 10.91$, $p = 0.004$) and appeared morphologically normal when compared to their wild type or heterozygous littermates (Fig 4). Similarly, $Mga^{GT/GT}$ embryos were recovered at the expected Medelian frequency at E3.5 (21/89; $X^2 = 1.30$, $p = 0.51$) and appeared morphologically normal (Table 2). Taken together, these results

Table 1. Genotype distribution at weaning of progeny from *Mga* mutant crosses. X^2 and p values were calculated assuming a Mendelian distribution.

Mating	Genotype			X^2, p
	+/+	+/-	-/-	
$Mga^{+/+}$ x $Mga^{GT/+}$	46	42	N/A	$X^2 = 0.18$, p=0.67
$Mga^{GT/+}$ x $Mga^{GT/+}$	31	53	0	$X^2 = 28.64$, p<0.0001
$Mga^{+/+}$ x $Mga^{Inv/+}$	5	7	N/A	$X^2 = 0.33$, p=0.56
$Mga^{Inv/+}$ x $Mga^{Inv/+}$	38	93	19	$X^2 = 13.45$, p=0.001
$Mga^{GT/+}$ x $Mga^{Inv/Inv}$	N/A	22 *Inv/+*	0 *GT/Inv*	$X^2 = 22$, p<0.0001

Table 2. Genotype distribution of embryos from $Mga^{GT/+}$ x $Mga^{GT/+}$ crosses. ND indicates that no genotype was obtained though an implantation site (E5.5) or an empty decidua (E9.5-E11.5) was observed. X^2 and p values were calculated assuming a Mendelian distribution of recovered embryos.

Stage	Genotype				X^2, p
	+/+	*+/GT*	*GT/GT*	ND	
E3.5	27	41	21	0	X^2=1.36, p=0.51
E4.5	83	113	49	0	X^2=10.91, p=0.004
E5.5	12	23	0	9	X^2=11.69, p=0.003
E9.5-E11.5	6	13	0	6	X^2=6.37, p=0.04

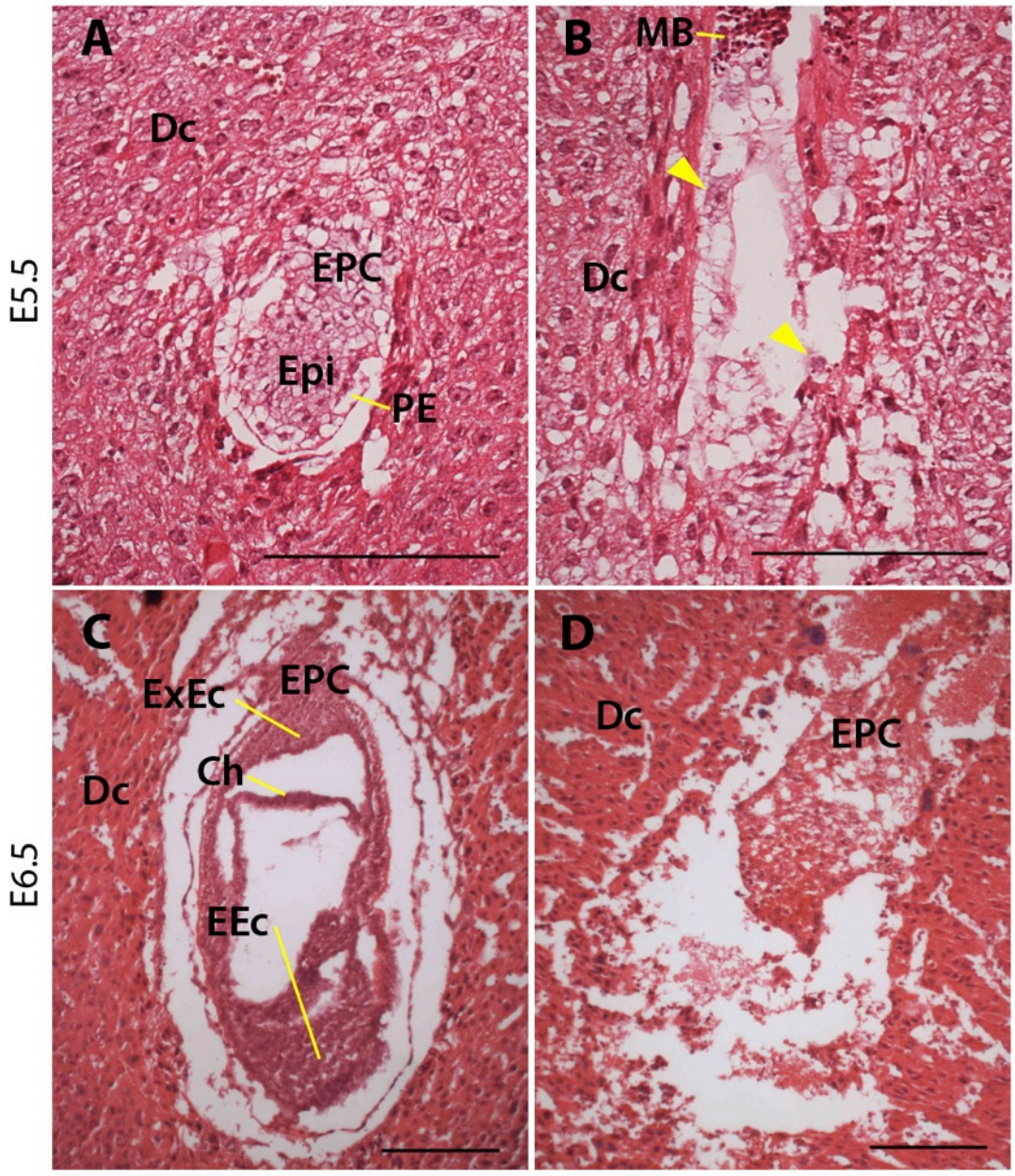

Figure 3. Histological sections of implantation sites at E5.5 and E6.5. Embryo degeneration (B, D) was detected in 10/39 decidual swellings at E5.5 and 4/10 swellings at E6.5 with trophoblast giant cells seen at E5.5 (yellow arrows). Other implantation sites contained morphologically normal embryos (A, C). MB. Maternal blood; Dc. Decidua; Epi. Epiblast; EPC, Ectoplacental cone; PE, Primitive endoderm; ExEc, Extraembryoic ectoderm; EEc, Embryonic ectoderm; Ch. Chorion. Scale bars: 100μm.

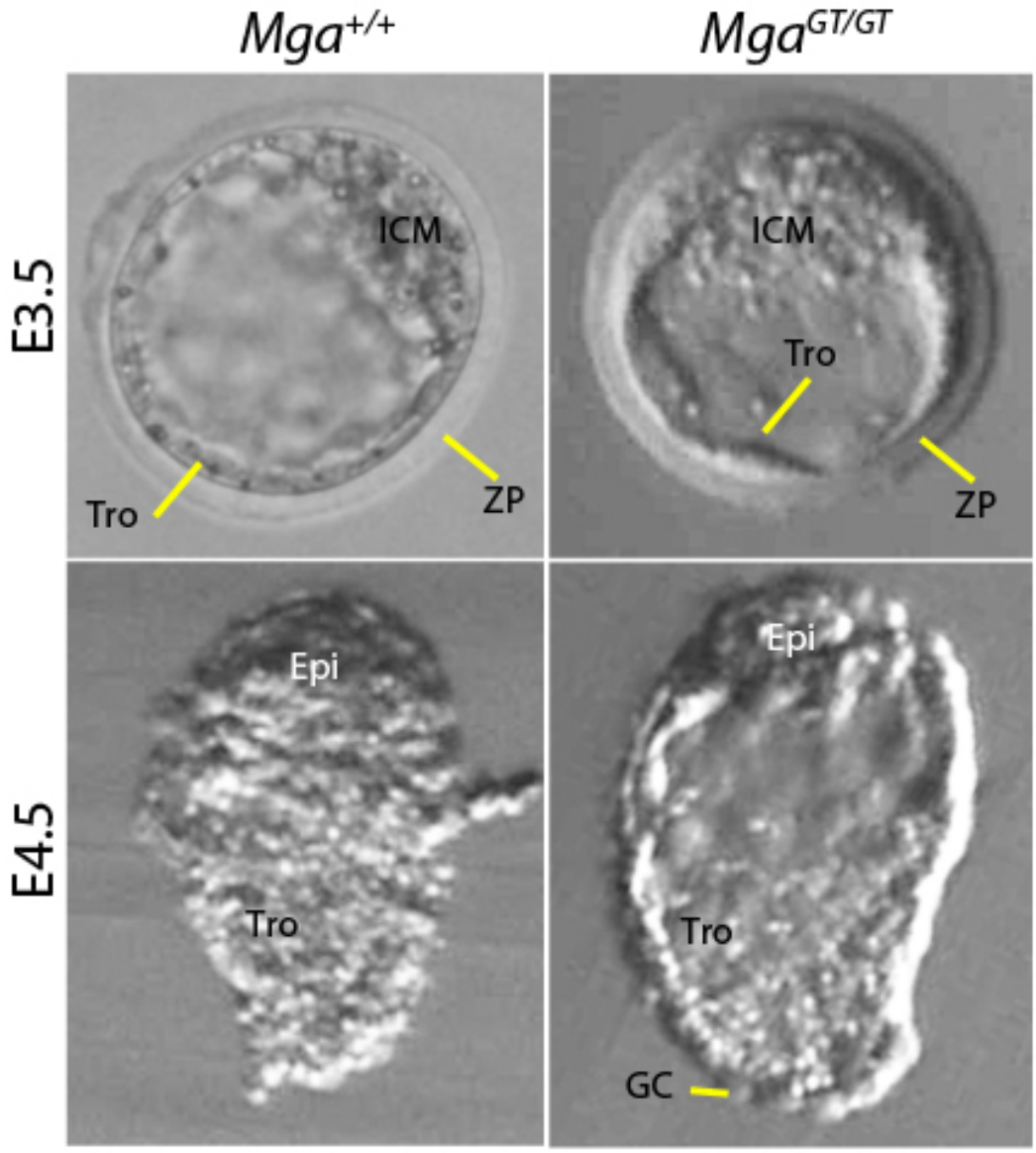

Figure 4. Preimplantation embryos at E3.5 and E4.5. ICM, Inner Cell Mass; Epi, Epiblast; Tro, Trophectoderm; ZP, Zona Pellucida; GC, Giant cells.

indicate that *Mga*$^{GT/GT}$ embryos implant in the uterus but die shortly thereafter; thus it is likely that *Mga* plays an essential role in the peri-implantation development of the embryo.

The function of *Mga* in the development of the ICM

Mga expression in the pluripotent tissues of the embryo

To assess the contribution of *Mga* to peri-implantation development, embryonic expression of *Mga* was assessed using the β-galactosidase reporter functionality of the *Mga*^{GT} allele. There was robust β-galactosidase activity in the Epi of *Mga*$^{GT/+}$ embryos at E5.5, 6.5, and 7.5 to the exclusion of the PE or extraembryonic tissues (Fig 5E-J). Standard X-gal staining was not sufficient for detection in preimplantation stages, but the more sensitive S-gal method for β-galactosidase detection showed staining in the Epi at E4.5 in *Mga*$^{GT/+}$ embryos, but not in *Mga*$^{+/+}$ embryos (Fig 5B, C). While neither X-gal nor S-gal showed staining at E3.5, RT-PCR for *Mga* in wild type embryos demonstrated expression at E3.5 (Fig 5A, D). This was the earliest time point that *Mga* was expressed, as RT-PCR detected no *Mga* expression in embryos at the 1-cell stage (E0.5) or at E2.5 (Fig 5D).

The role of Mga in ICM development

To test the capacity of *Mga*$^{GT/GT}$ for survival and differentiation outside the uterine environment, embryos were isolated at E3.5 from *Mga*$^{GT/+}$ x *Mga*$^{GT/+}$ matings prior to time of death and cultured *in vitro* before genotyping retrospectively by PCR. *Mga*$^{GT/+}$ cultures were stained with X-gal to assess β-galactosidase reporter activity. The ICM of the blastocyst cultures showed strong X-gal staining to the exclusion of the trophoblast 48 hours after starting culture, indicating that the *in vitro* culture system initially recapitulated the embryonic expression of *Mga* in the Epi before vanishing (Fig 6).

While *Mga*$^{GT/GT}$ embryos (n=11) were able to attach to the tissue culture substrate and form an outgrowth consisting of trophoblast giant cells, the ICM derivatives failed to

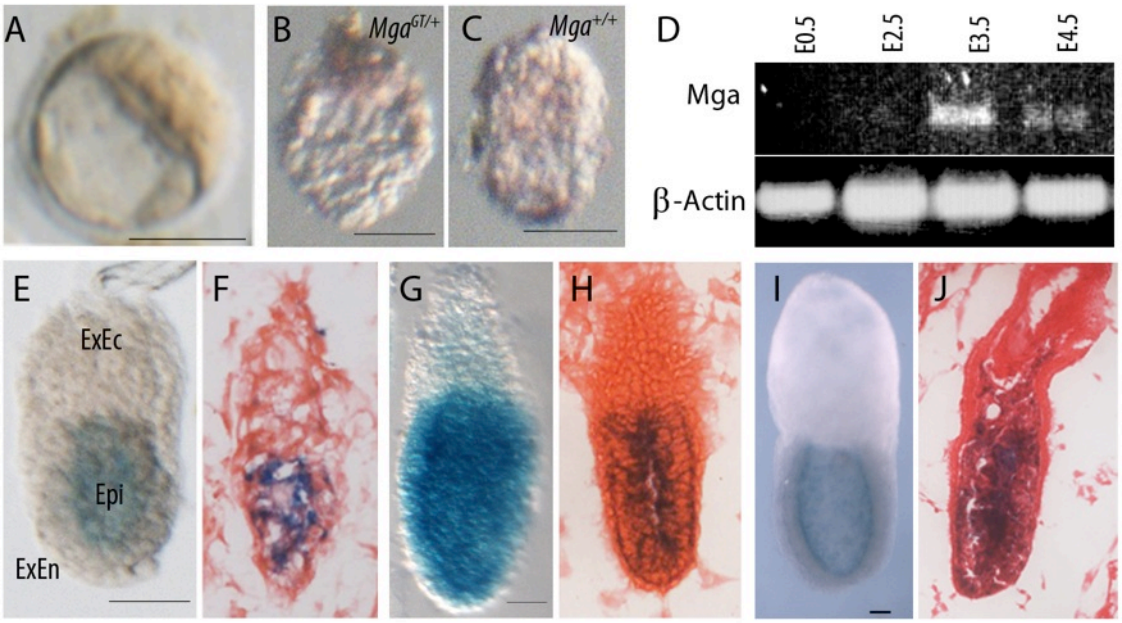

Figure 5. *Mga* expression in embryos using the β-galactosidase reporter and RT-PCR. **A-C**. No β-galactosidase activity was observed in blastocysts at E3.5 using X-gal stain (A). S-gal staining was present in the Epi of E4.5 $Mga^{GT/+}$ embryos (B), but not in $Mga^{+/+}$ embryos (C). **D.** RT-PCR on pooled embryos did not detect any *Mga* transcripts at E0.5 or E2.5, but expression was present at E3.5 and at E4.5. **E-J.** β-galactosidase staining was observed in the Epi of whole mounts at E5.5 (E), E6.5 (G), and E7.5 (I). Parafin sections (nuclear fast red counterstain) confirm Epi staining of β-galactosidase from E5.5 (F), E6.5 (H), and E7.5 (J) embryos. ExEc, Extraembryonic Ectoderm; Epi, Epiblast; ExEn, Extraembryonic Endoderm. Scale bars: 40μm.

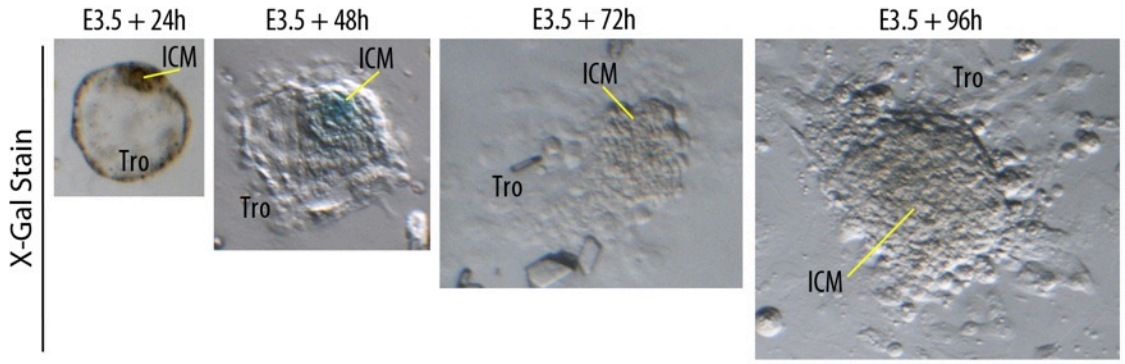

Figure 6. β-galactosidase activity during *in vitro* culture of E3.5 blastocysts. Blastocyst cultures from *Mga*$^{GT/+}$ embryos were stained with X-gal. The ICM of the cultures showed β-galactosidase activity after 48 hours of culture reflecting reporter expression. ICM, Inner cell mass; Tro, Trophoblast.

thrive, resulting in smaller ICM outgrowth surface area by 4 days of culture. In contrast to the normal-appearing trophoblast cells, the ICM cells were sparse and did not form the multicellular or cystic structures of their $Mga^{+/+}$ and $Mga^{GT/+}$ littermates (n=35) when examined 4 days after culture (Fig 7A). Quantification of the surface area of the ICM outgrowth showed similar wild type and mutant ICM outgrowths after 2 days of culture before the mutants either stagnated in their growth or contracted by 4 days of culture (Fig 7B, C). In conjunction with the expression data, this indicates a failure of ICM survival as a contributing factor in the embryonic lethality of $Mga^{GT/GT}$ embryos.

The role of Mga in embryonic stem cell culture

To confirm the importance of *Mga* for the survival of the ICM, we used the *in vitro* analog of the ICM, ES cells. Because $Mga^{GT/GT}$ ICMs did not grow when cultured, we derived ES cells from embryos carrying the conditional allele $Mga^{Inv/Inv}$ that also harbored the inducible Cre recombinase gene *CreERT2* integrated into the *Rosa26a* locus (de Luca et al., 2005). $Mga^{Inv/Inv}$; *CreERT2* ES cells were morphologically indistinguishable from $Mga^{Inv/+}$ ES cells and grew at similar rates when cultured under normal conditions (Fig 8A, B, D). Additionally, $Mga^{Inv/Inv}$*; CreERT2* ES cells expressed pluripotency markers Oct4 and Nanog as expected (Fig 8C).

Upon inversion of the conditional allele by addition of 4-hydroxytamoxifen to the culture, however, $Mga^{Inv/Inv}$*; CreERT2* colonies were sparser and smaller than either $Mga^{Inv/+}$ cells or $Mga^{Inv/Inv}$*; CreERT2* cells treated with ethanol vehicle alone when viewed at low magnification as a population, though the colony morphology was normal in the individual surviving colonies (Fig 9A). Quantification of cell number at 24-hour intervals revealed an approximate 35% decrease in the number of cells in cultures where inversion had been induced when compared to uninduced $Mga^{Inv/Inv}$*; CreERT2* and control cell lines (Fig 9B). Genotyping of the surviving colonies showed that there was incomplete inversion of the Mga^{Inv} allele regardless of the length of tamoxifen treatment (Fig 9C). To ensure that the optimal dose was used to induce inversion, colonies were grown in increasing concentrations of tamoxifen. Both $Mga^{Inv/Inv}$*; CreERT2* and $Mga^{Inv/+}$ cultures had fewer colonies present as tamoxifen dose was increased past previous experimental levels of 0.5μM, but the amount of inversion in $Mga^{Inv/Inv}$*; CreERT2*

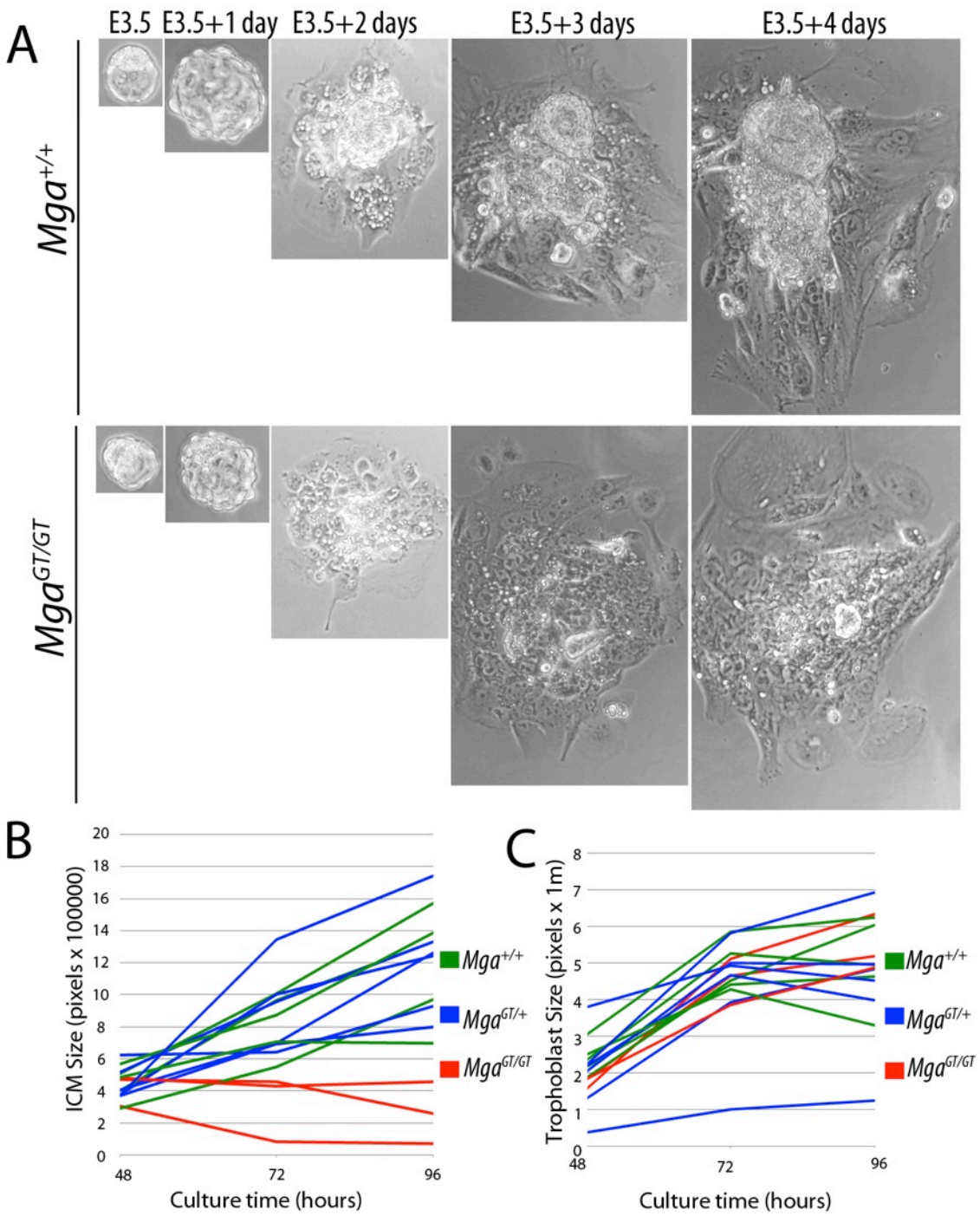

Figure 7. In vitro culture of E3.5 blastocysts. **A.** ICM outgrowth from *Mga*$^{GT/GT}$ embryos appeared smaller than controls at 3 or 4 days of culture by phase contrast microscopy. **B, C**. Measurement of the surface area at 4 days showed that the ICM surface area of *Mga*$^{GT/GT}$ embryos was smaller that controls (B), although the trophoblast outgrowth was similar (C).

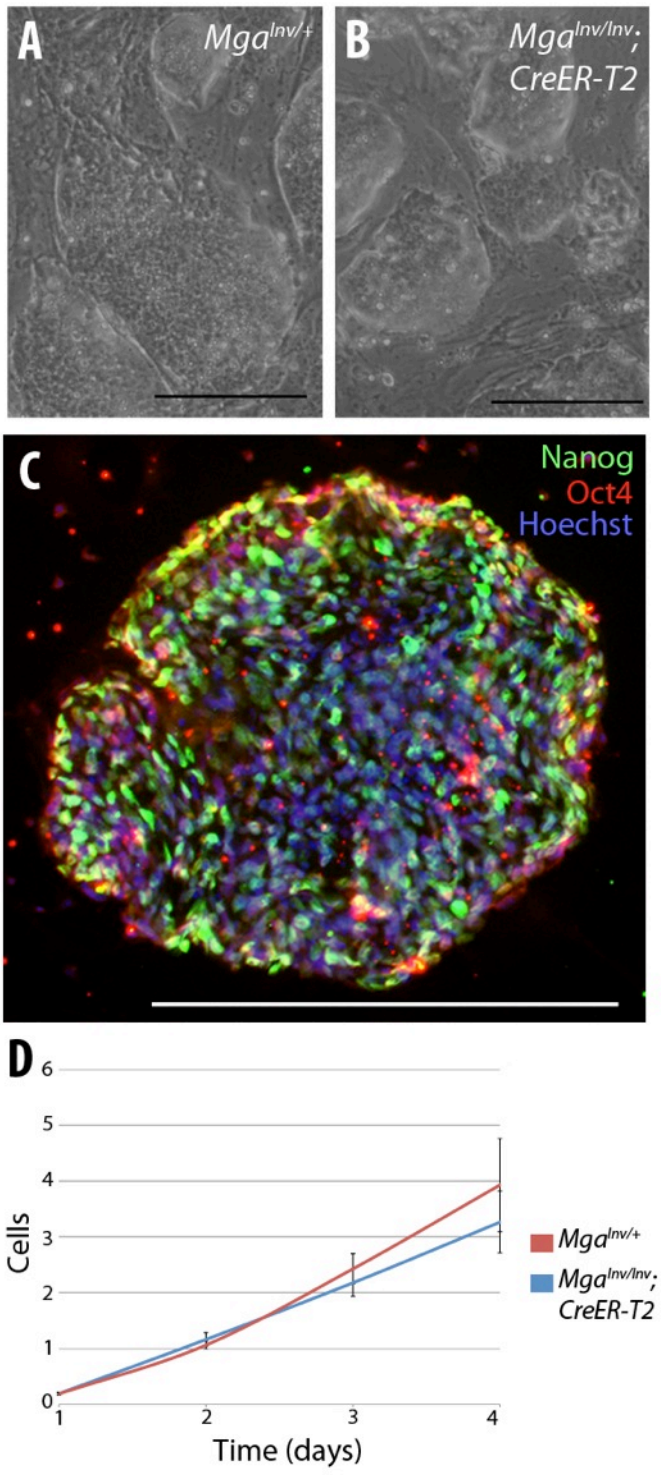

Figure 8. Growth and differentiation of *Mga*$^{Inv/Inv}$*; CreERT2* ES cells. **A-B**. ES cell colonies appeared morphologically similar to *Mga*$^{Inv/+}$ ES cells. **C.** Immunohistochemistry for normally expressed pluripotency markers Nanog (green) and Oct4 (red) in *Mga*$^{Inv/Inv}$*; CreERT2* ES cells. Nucleii are stained with Hoeschst (blue). **D.** *Mga*$^{Inv/Inv}$*; CreERT2* ES cells grew at a similar rate to *Mga*$^{Inv/+}$ ES cells.

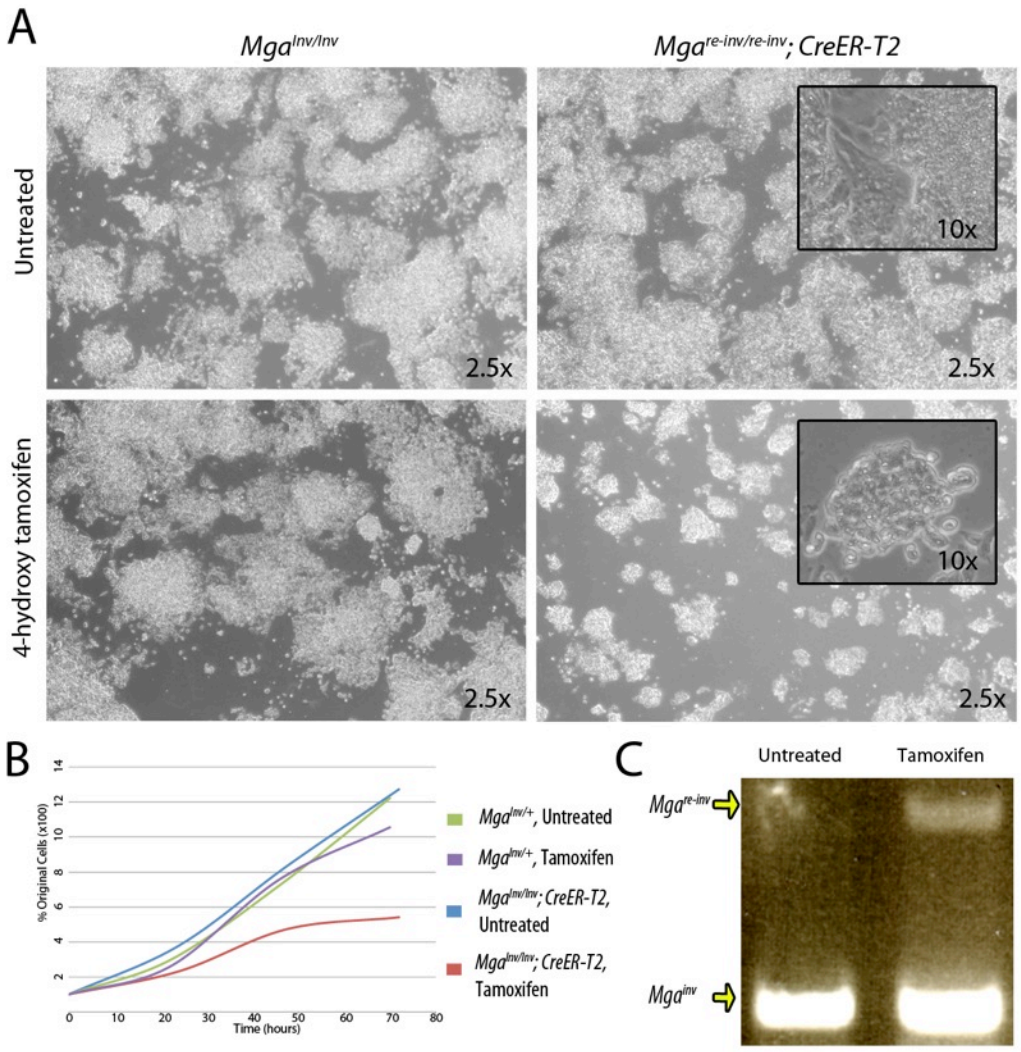

Figure 9. ES cells treated with tamoxifen to induce inversion to the mutated allele. **A.** *Mga*$^{Inv/Inv}$*; CreERT2* ES cells formed smaller and more sparse colonies when treated with 4-hydroxytamoxifen than when untreated, though colony morphology appeared normal in tamoxifen treated cells (A, inset). **B.** *Mga*$^{Inv/Inv}$*; CreERT2* ES cells grew at a slower rate from the time of tamoxifen addition at t=0. **C.** Surviving colonies showed partial inversion from the *Mga*^{Inv} allele to the *Mga*$^{Re\text{-}inv}$ allele.

cultures remained constant, indicating that greater levels of inversion could not be induced before tamoxifen levels became toxic to cells (data not shown). Together, these results indicate that *Mga* is necessary for the survival of ES cells and that the surviving colonies were those that had escaped inversion and thus had at least one functional *Mga* allele.

Apoptosis and cell proliferation in *Mga*$^{GT/GT}$ embryos

Reduced ICM outgrowth of *Mga*$^{GT/GT}$ blastocyst cultures and reduced growth of inversion-induced *Mga*$^{Inv/Inv}$*; CreERT2* ES cells suggests an increase in cell death and/or a decrease in cell proliferation in the ICM or ICM derivatives such as the Epi. To investigate cell proliferation, immunofluorescence with antibodies against phosphorylated histone H3 (phospho-H3) was performed. Counts of the number of positive cells in the Epi did not reveal any difference in the number of mitotic cells in *Mga*$^{GT/GT}$ embryos (3.1 +/- 0.8) compared to *Mga*$^{+/+}$ and *Mga*$^{GT/+}$ embryos (2.8 +/- 0.3) at E4.5 (Fig 10B) (t=0.259, p=0.65) (Figure 10C). The appearance of phospho-H3 nuclear staining can also be used to assess the stage of mitosis that cells are in: prophase nuclei have uniform phospho-H3 staining throughout the nucleus while metaphase and anaphase nuclei have more punctate staining indicative of condensed chromatin. The number of cells that were in prophase in *Mga*$^{GT/GT}$ embryos (1.6 +/- 0.5) was not different from the number of cells in *Mga*$^{+/+}$ and *Mga*$^{GT/+}$ embryos (1.8 +/- 0.3). Similarly, the number of cells in metaphase or anaphase in *Mga*$^{GT/GT}$ embryos (1.5 +/- 0.6) was not different from *Mga*$^{+/+}$ and *Mga*$^{GT/+}$ embryos (1.0 +/- 0.2). Together, these data indicate that there is no defect in progression through the cell cycle in *Mga*$^{GT/GT}$ embryos (Fig 11) (Brenner et al., 2003).

To investigate apoptosis, immunofluorescence of E4.5 day embryos with antibodies against cleaved caspase 9, a marker of fragmented nuclei during apoptosis, was performed (Zhu et al., 2012). A greater proportion of *Mga*$^{GT/GT}$ embryos (7/9) had cleaved caspase 9-positive fragmented nuclei than did *Mga*$^{+/+}$ and *Mga*$^{GT/+}$ littermates (7/47) (p=0.012, Fisher's Exact Probability test) (Fig 10A). There was no difference in the proportion of *Mga*$^{+/+}$ embryos with cleaved caspase 9-positive fragmented nuclei (3/20) compared to *Mga*$^{GT/+}$ embryos (4/27) (p=1.00 Fisher's Exact Probability test) supporting the lack of a heterozygous embryonic phenotype. The higher

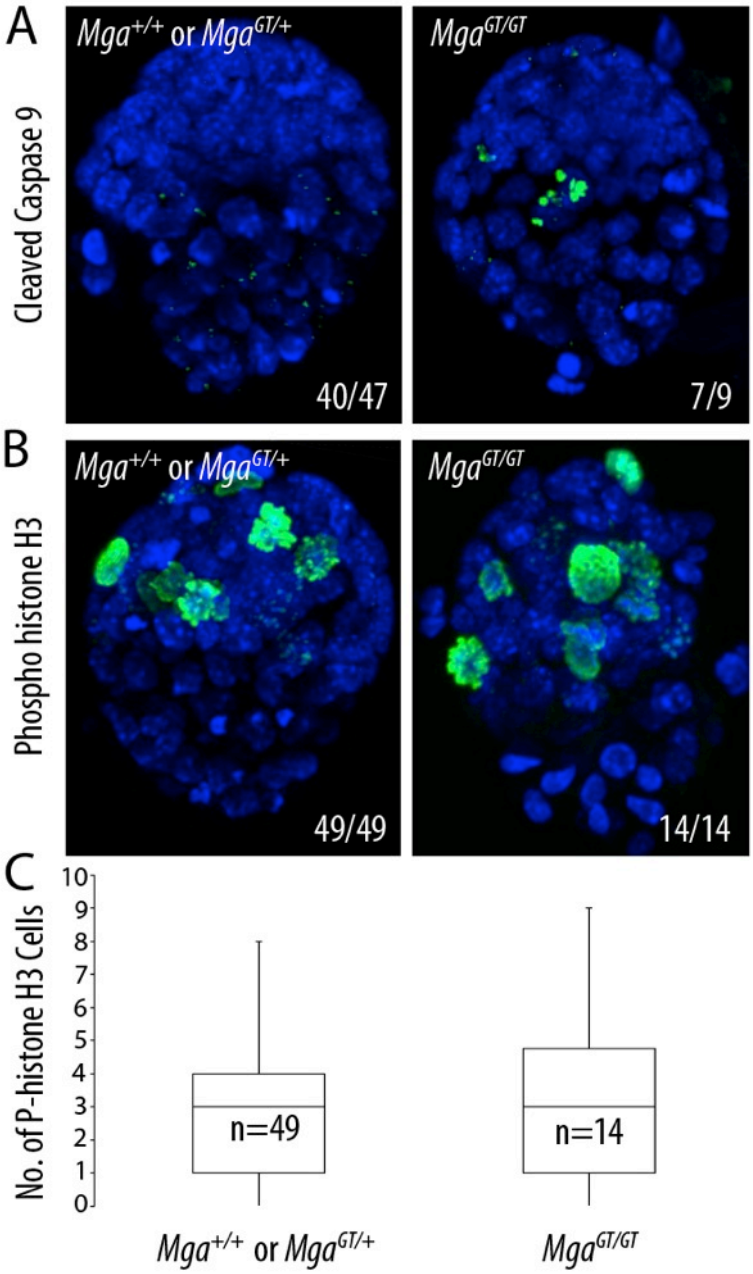

Figure 10. Apoptosis and cell proliferation at E4.5. Numbers indicate the proportion of embryos showing the illustrated expression pattern. A. Immunofluorescence for cleaved caspase 9 shows that more $Mga^{GT/GT}$ embryos had fragmented nuclei than did $Mga^{+/+}$ and $Mga^{GT/+}$ embryos. B. Cell proliferation as measured by phosphorylated histone H3 immunostaining was similar in $Mga^{GT/GT}$ compared to $Mga^{+/+}$ and $Mga^{GT/+}$ embryos. C. Box plots of the number of phospho-histone H3-positive cells showed no difference between $Mga^{GT/GT}$ embryos and $Mga^{+/+}$ and $Mga^{GT/+}$ embryos.

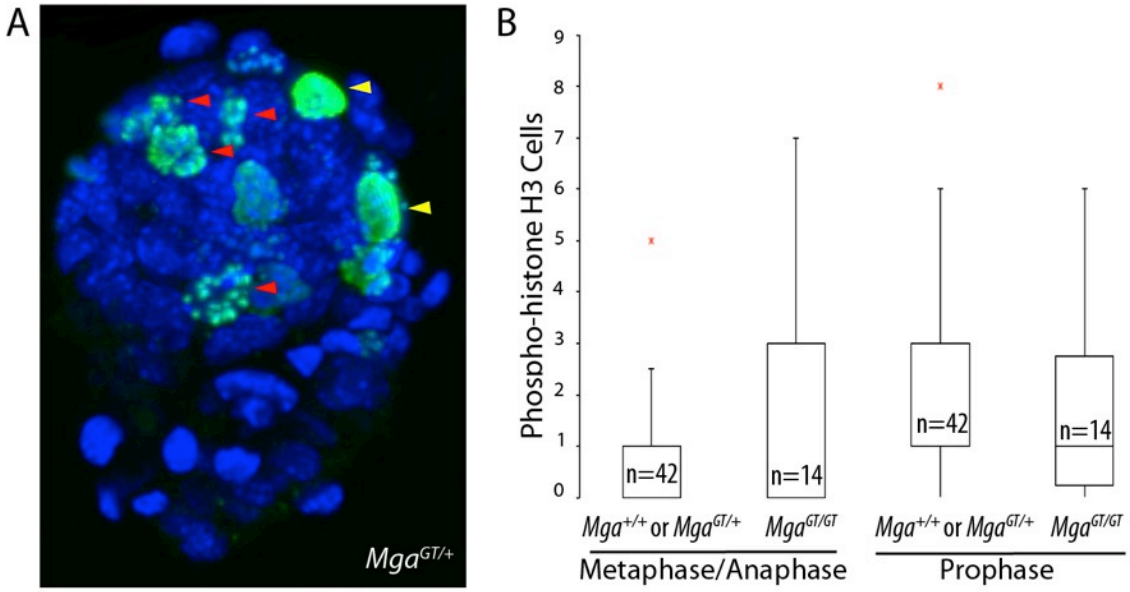

Figure 11. Cell cycle staging in the Epi of embryos at E4.5 A. *Mga*$^{GT/+}$ embryo stained for phospho-histone H3. Cell cycle stage can be determined by the pattern of phospho-histone H3 staining. Prophase nuclei show uniform staining (yellow arrowheads) compared to metaphase and anaphase nuclei, in which condensed chromatin staining is more punctate (red arrowheads). B. Box plots of the number of cells in meta/anaphase or prophase of mitosis. There was no difference in the number of cells in prophase or metaphase/anaphase in *Mga*$^{GT/GT}$ embryos compared to *Mga*$^{+/+}$ and *Mga*$^{GT/+}$ embryos.

incidence of apoptosis in *Mga*$^{GT/GT}$ embryos indicates a defect in the normal function of the cell leading to cell death rather than a defect in cell proliferation.

Differentiation of primitive endoderm in *Mga*$^{GT/GT}$ embryos

Structural integrity of Mga$^{GT/GT}$ *embryos*

To test whether the structural integrity of *Mga*$^{GT/GT}$ embryos was intact, immunofluorescence with antibodies against E-cadherin was performed. E-cadherin forms a thin layer around the compacted Epi and PrE with a thicker layer of staining in the basement membrane of the surrounding TE. *Mga*$^{GT/GT}$ embryos had a similar staining pattern at E3.5 (n=4) and E4.5 (n=2) (Fig 12A, B) indicating that lethality was not the result of the embryo losing its structure.

Gene expression and pluripotency during the differentiation of the embryonic cell layers

At E4.5, just prior to the time that *Mga*$^{GT/GT}$ embryos die, differentiation of the embryonic cell layers has begun. The pluripotent ICM differentiates into two cell layers: the Epi remains pluripotent and becomes a compacted cell layer while the differentiated PE forms an epithelial sheet beneath it. Immunofluorescence with antibodies against the pluripotency marker Nanog, which marks the Epi, and the PE marker Gata4 did not reveal any difference in the formation of cell layers between *Mga*$^{GT/GT}$ (n=3) and *Mga*$^{+/+}$ or *Mga*$^{GT/+}$ embryos (n=4) at E4.5 (Fig 12C, D). Immunofluorescence with antibodies against Oct4, a marker of pluripotency expressed in the Epi, did not generate sufficient signal to be analyzed, so an *Oct4* GFP reporter allele, *Pou5f1*^{tm2Jae} (Lengner et al., 2007), was bred into the *Mga*^{GT} background. Immunofluorescence with anti-GFP antibodies showed a compacted Epi in both the *Mga*$^{+/+}$ and *Mga*$^{GT/+}$ embryos (n=27) and *Mga*$^{GT/GT}$ embryos (n=7) carrying the *Pou5f1*^{tm2Jae} allele (Fig 12E, F). Together, these results indicate that *Mga*$^{GT/GT}$ embryos showed disruption of the spatial and temporal gene expression normally characteristic of the differentiation of embryonic cell layers. Additionally, these results indicate that *Mga*$^{GT/GT}$ embryos do not lose expression of pluripotency markers.

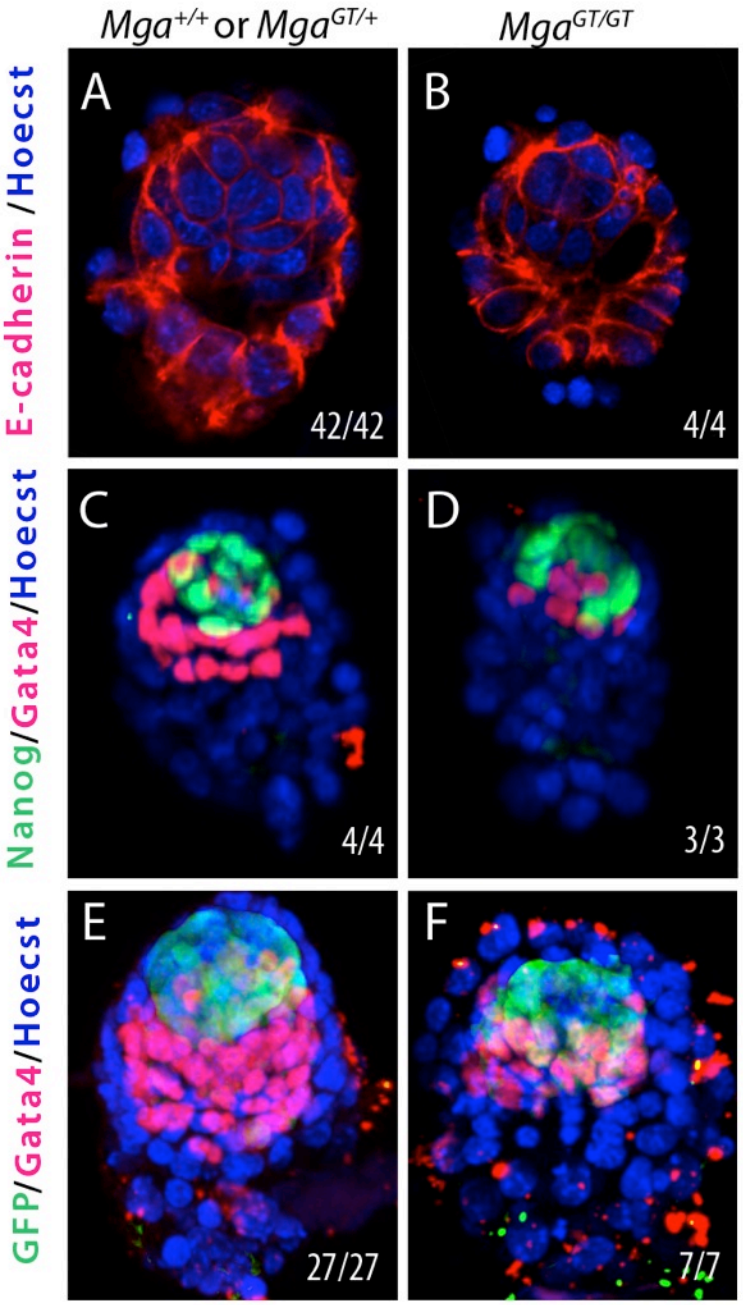

Figure 12. Primitive endoderm differentiation in E4.5 embryos. Numbers refer to the proportion of embryos showing the illustrated expression pattern. A, B. Optical sections of E4.5 embryos show that the E-Cadherin (red) staining pattern is similar in *Mga*$^{GT/GT}$ embryos and *Mga*$^{+/+}$ and *Mga*$^{GT/+}$ embryos. C-F. Projections of z-stacks show that Nanog (green C, D) and Oct4 as measured by GFP reporter (green E, F), markers of the pluripotent Epi, are similar in *Mga*$^{GT/GT}$ embryos compared to *Mga*$^{+/+}$ and *Mga*$^{GT/+}$ embryos, as was the primitive endoderm marker Gata4 (red, C-F).

Maintenance of pluripotent cells in Mga$^{GT/GT}$ embryos

Despite the presence of pluripotency markers at E4.5, the death of the pluripotent cells of the Epi and its *in vitro* derivatives suggest that loss of pluripotent cell self-maintenance could be responsible for the lethality of *Mga*$^{GT/GT}$ embryos. To test maintenance of pluripotency in *Mga*$^{GT/GT}$ embryos, we examined embryos in which diapause was induced (Nichols et al., 2001). Diapause is a natural mechanism of delayed implantation of embryos in mothers who are still nursing a litter, and can be induced experimentally by hormone treatment. During diapause, blastocysts do not implant in the uterus and Epi cells maintain pluripotency but do not undergo the cell proliferation and differentiation evident during normal development.

To determine whether *Mga* is expressed during diapause in normal embryos, RT-PCR of pooled wild-type embryos was done. One day after induction of diapause by tamoxifen and depo-provera injections at E2.5, *Mga* expression is at a level similar to E3.5 embryos before falling and being maintained a low level of expression at 4 days and 7 days of diapause (Fig 13D).

Immunofluorescence using antibodies against the pluripotency marker Nanog, present in the Epi, and the PE marker Gata4 was used to assess the persistence of cell populations throughout diapause. In diapause embryos, similar to the situation in E4.5 day embryos, the Epi forms a compacted group of cells overlying the PE. One day after induction of diapause, *Mga*$^{GT/GT}$ embryos showed spatial gene expression patterns of Nanog and Gata4 that were identical to *Mga*$^{+/+}$ and *Mga*$^{GT/+}$ embryos. The number of Nanog-expressing cells was similar in *Mga*$^{GT/GT}$ embryos (16.5 +/- 1.5) compared to *Mga*$^{+/+}$ and *Mga*$^{GT/+}$ embryos (13.7 +/- 1.2) ($z = 1.17$, $p = 0.24$ Mann-Whitney U test) (Table 3). However, by 4 days after diapause induction, the number of Nanog-expressing cells in *Mga*$^{GT/GT}$ embryos (5.4 +/- 1.0) was smaller than *Mga*$^{+/+}$ and *Mga*$^{GT/+}$ embryos (18.1 +/- 0.9) ($z = 3.240$, $p = 0.001$) (Table 3). The relative position and number of Gata4-expressing cells, however, was similar in in *Mga*$^{GT/GT}$ (21.9+/-2.8) compared to *Mga*$^{+/+}$ and *Mga*$^{GT/+}$ embryos (26.6+/-1.3)($z = 0.98$, $p = 0.33$) (Fig 13A-C, Table 3). By 7 days after diapause induction, there were virtually no Nanog positive cells in *Mga*$^{GT/GT}$ embryoss (0.3+/-0.3 cells), while in *Mga*$^{+/+}$ and *Mga*$^{GT/+}$ embryo Nanog-positive cells persisted (12.5+/-1.4cells) ($z = 2.39$, $p = 0.02$) (Fig 13D, Table 3). In

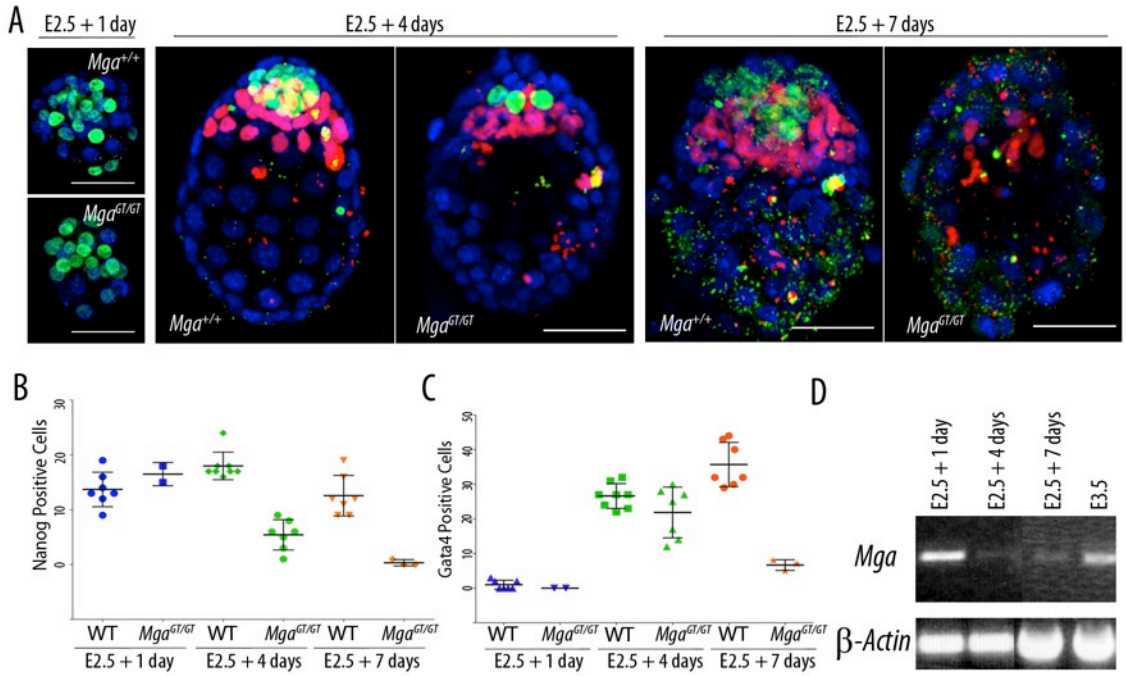

Figure 13. Loss of pluripotent cells during hormonally induced diapause. A. Nanog-positive cells (green) are present initially, but are gradually lost during diapause in *Mga*$^{GT/GT}$ embryos. Gata4-positive cells (red) persist longer but eventually disappear by E2.5+7 days. B, C. The number of Nanog-positive cells is significantly different in *Mga*$^{GT/GT}$ at 4 and 7 days of diapause (B), while Gata4-positive cells are significantly different only at 7 days of diapause (C). "WT" refers to *Mga*$^{+/+}$ and *Mga*$^{GT/+}$ embryos. D. One day after diapause is induced, RT-PCR indicates that in wild type embryos *Mga* is expressed at levels comparable to E3.5 embryos and then declines during diapause.

Table 3. Numbers of cells in differentiated cell layers in hormonally induced diapause embryos. Nanog is a marker of pluripotent Epi and Gata4 is a marker of primitive endoderm. Average number of cells and standard error were calculated on the indicated number of embryos.

Time	Genotype	Nanog-positive cells	Gata4-positive cells	n (embryos)
E2.5 + 1 day	$Mga^{+/+}$ and $Mga^{GT/+}$	13.7 +/- 1.2	1 +/- 0.5	7
	$Mga^{GT/GT}$	16.5 +/- 1.5	0 +/- 0	2
E2.5 + 4 days	$Mga^{+/+}$ and $Mga^{GT/+}$	18.1 +/- 0.9	26.6 +/- 1.3	8
	$Mga^{GT/GT}$	5.4 +/- 1.0	21.9 +/- 2.8	7
E2.5 + 7 days	$Mga^{+/+}$ and $Mga^{GT/+}$	12.6 +/- 1.4	35.7 +/- 2.4	7
	$Mga^{GT/GT}$	0.3 +/- 0.3	6.7 +/- 0.9	3

contrast to earlier time points, the number of Gata4-positive cells was also reduced in $Mga^{GT/GT}$ embryos (6.7+/-0.9) compared to $Mga^{+/+}$ and $Mga^{GT/+}$ embryos (35.7+/-2.4) (z=2.39, p-0.02) (Fig 13A-C, Table 3). The Gata4-expressing cells appeared to have collapsed against the TE in the $Mga^{GT/GT}$ embryos. Moreover, the mutant embryos had cells in the Epi that stained for neither Nanog nor Gata4 (Fig 13D). While formation of embryonic cell layers occurs normally, the declining number of Epi cells in $Mga^{GT/GT}$ embryos during diapause implies that the pluripotent cells of the Epi are not properly maintained without *Mga*. Conversely, the lack of an early effect on Gata4 expressing cells reflects a lack of requirement for *Mga* in PE differentiation.

Regulation of downstream targets of *Mga*

Expression of Myc-target gene Odc1 *in* $Mga^{GT/GT}$ *embryos*

After confirming proper structural integrity, cell layer differentiation, and pluripotency in $Mga^{GT/GT}$ embryos at E4.5, we utilized a candidate gene approach to assess downstream genetic effects of the *Mga* mutation (Table 4). *Odc1* (MGI: 97402, synonym *Odc*), the gene coding for ornithine decarboxylase (ODC), shows a similar expression pattern and embryonic mutant phenotype with *Mga* (Pendeville et al., 2001). ODC catalyzes the decarboxylation of ornithine to form putrescine, the rate-limiting step in the polyamine synthesis pathway for the production of spermine and spermidine (Fig 14A). In addition to the common embryonic phenotype it shares with *Mga*, *Odc1* has 2 E-box sites that have been shown to be able to bind bHLH-Zip domain family members including c-Myc and Mnt (Bello-Fernandez et al., 1993; Nilsson et al., 2004) (Fig 14B).

Immunofluorescence was performed on E4.5 embryos with antibodies against ODC. Projections of confocal stacks showed decreased ODC signal in the Epi of $Mga^{GT/GT}$ embryos (4/6) at E4.5 compared to $Mga^{+/+}$ and $Mga^{GT/+}$ embryos (3/31) (p=0.006; Fisher's Exact Probability test) (Fig 14C). There was also strong signal on the exterior of the TE in all samples, though secondary antibody controls (data not shown) indicated that this was background staining.

Table 4. Candidate genes for *Mga* mutant analysis. Candidate genes were chosen based on similar embryonic phenotype of homozygous mutants. Of these candidates, the presence of E-box sites in a regulatory intron of *Odc1* was unique.

Gene	Mutant Phenotype	Reference
Max	Empty deciduae recovered after implantation, ICM failure in blastocyst culture	(Shen-Li et al., 2000)
Klf5	Embryos not recovered after implantation, ectopic PE development	(Lin et al., 2010)
Notchless	Empty deciduae recovered after implantation, ICM failure in blastocyst culture	(Cormier et al., 2006)
CTCF	Empty deicudea recovered after implantation, ICM failure in blastocyst culture	(Moore et al., 2012)
Oct4	Empty deicudea recovered after implantation, ICM failure in blastocyst culture	(Nichols et al., 1998)
Odc1	Empty deciduae recovered after implantation, ICM failure in blastocyst culture, E-box target sites in regulatory intron	(Pendeville et al., 2001)

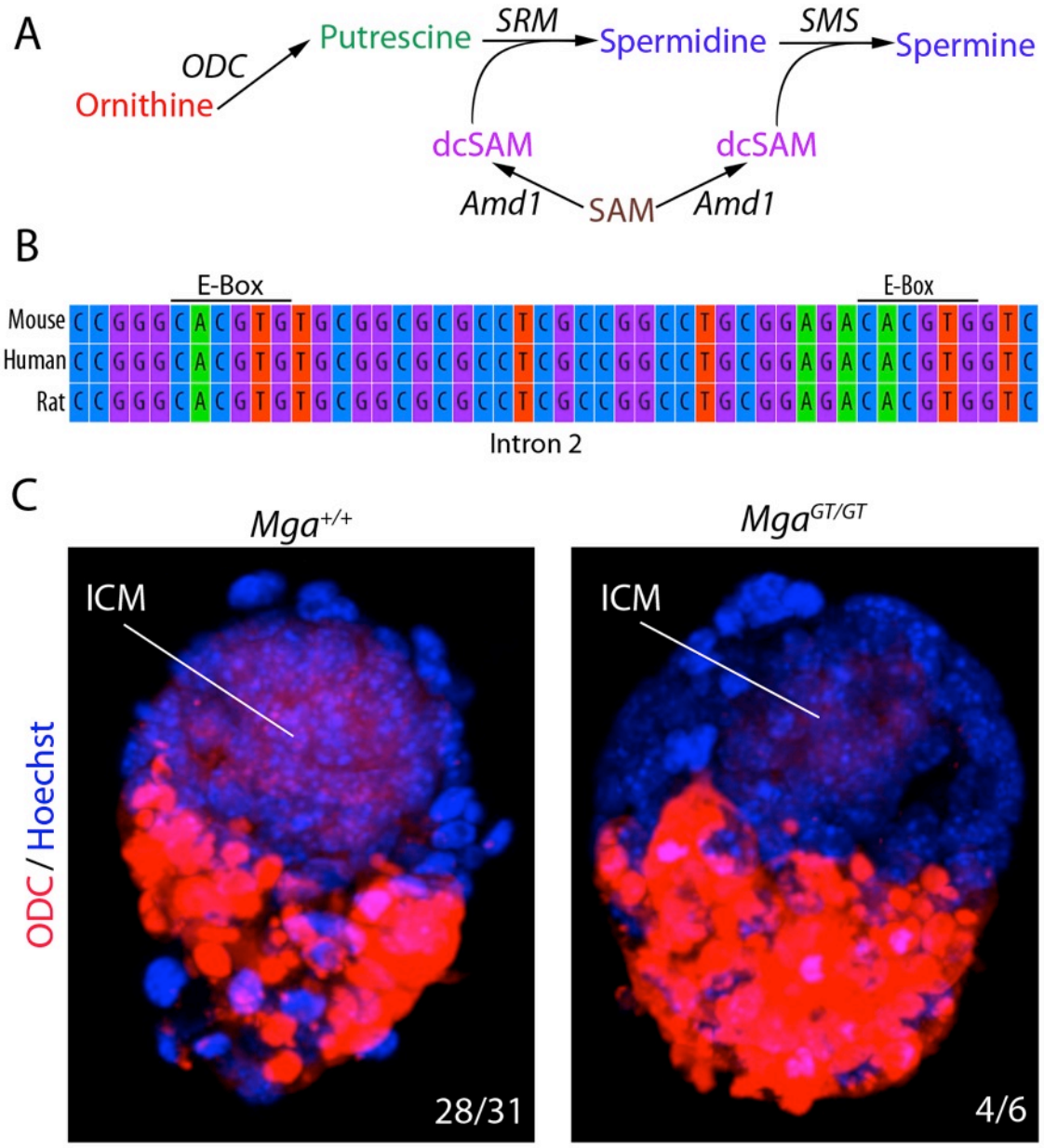

Figure 14. Polyamine synthesis pathway and the expression of Ornithine Decarboxylase (ODC) in E4.5 embryos. A. *ODC* is the rate limiting step in the polyamine synthesis pathway that produces spermine and spermidine. ODC catalyzes the conversion of ornithine to putrescine. Putrescine is then converted into spermidine and spermine with the addition of decarboxylated S-adeonsyl-methionine (dcSAM). B. Two E-box binding sites (CACGTG) are evolutionarily conserved in the second intron. Projections of confocal Z-stacks show lower levels of ODC (red) in the Epi of $Mga^{GT/GT}$ embryos at E4.5. Secondary antibody background is present on the TE of all embryos tested.

ICM growth in the presence of exogenous putrescine

Decreased *Odc1* expression in $Mga^{GT/GT}$ embryos suggests that embryos may lack the ability to produce putrescine and thus may lack the necessary end products of the polyamine synthesis pathway. Putrescine deficiency caused by inhibition of ODC by the small molecule α-difluoromethylornithine (DFMO) can be alleviated by addition of exogenous putrescine to IE6 intestinal crypt cell cultures (Iwama et al., 1990). Similarly, we attempted to rescue embryonic lethality in $Mga^{GT/GT}$ embryos by supplying exogenous putrescine to embryos. Specifically, we supplemented blastocyst cultures with 200μM putrescine and measured the ICM outgrowths following 96 hours of culture, a time after which $Mga^{GT/GT}$ ICM outgrowths had been shown to be deficient in untreated cultures (Fig 8).

The surface area of the ICM outgrowth of $Mga^{GT/GT}$ blastocyst cultures was significantly larger when embryos were treated with putrescine (n=7) than when they were untreated (n=11*)* (t = -4.58, p = 0.0003) (Fig 15A, B). The surface area of the ICM outgrowth in $Mga^{+/+}$ and $Mga^{GT/+}$ cultures, however, was similar with (n=29) or without putrescine (n=24) (t=1.4, p=0.18). None of the treatments affected the outgrowth of trophoblast cells in culture. Notably, the ICM surface area of the putrescine-treated $Mga^{+/+}$ or $Mga^{GT/+}$ cultures (n=29) and $Mga^{GT/GT}$ cultures (n=11) was not significantly different (t = -1.83, p=0.08). Morphologically, the ICM of treated mutants appeared to lack the 3-dimentional structural complexity that was present in $Mga^{+/+}$ or $Mga^{GT/+}$ cultures, though they still appeared larger than untreated $Mga^{GT/GT}$ cultures (Fig 15A). Together, these results indicate that exogenous putrescine is sufficient to at least partially rescue the ICM outgrowth of $Mga^{GT/GT}$ embryos.

ES cell growth in the presence of exogenous putrescine

The rescue of the ICM in blastocyst cultures with exogenous putrescine suggests that the ES cell survival defect of inversion-induced $Mga^{Inv/Inv}$*; CreERT2* ES cells might also be rescued. ES cells were plated in unsupplemented ES media and allowed to attach for 1 day. Cultures were then given ES media that was either unsupplemented, contained tamoxifen to induce inversion, or contained both tamoxifen and 200μM putrescine. Cultures were allowed to grow for an additional 2 days before cells were counted.

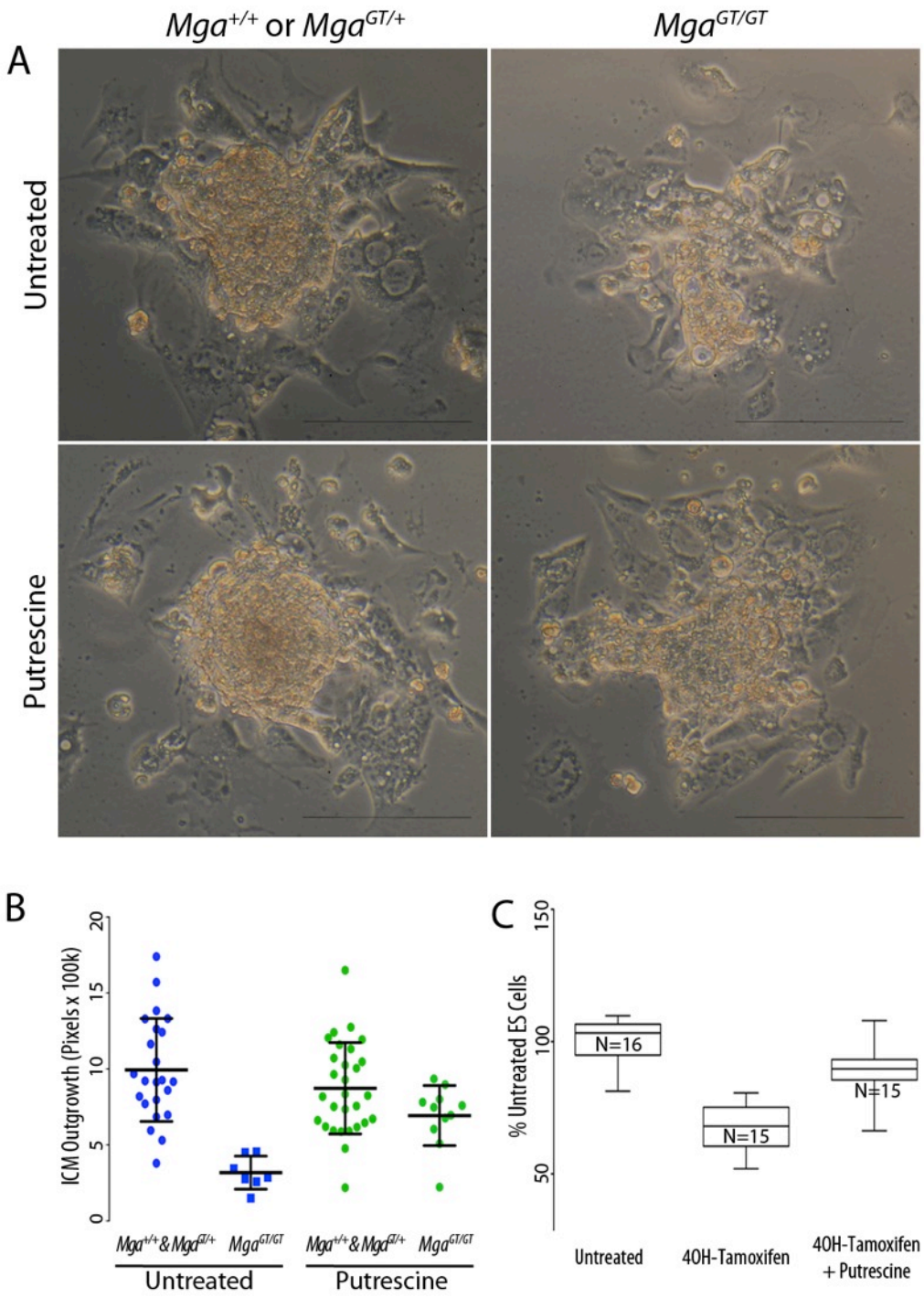

Figure 15. Blastocyst and ES cell culture with or without 200μM putrescine added. A, B. ICM outgrowths of *Mga*$^{GT/GT}$ blastocyst cultures appeared larger when treated with putrescine for 4 days (A). ICM surface area after 4 days of culture of treated *Mga*$^{GT/GT}$ cultures was greater than untreated *Mga*$^{GT/GT}$ cultures and was not different from treated *Mga*$^{+/+}$ or *Mga*$^{GT/+}$ cultures (B). C. Greater numbers of *Mga*$^{Inv/Inv}$*; CreERT2* ES cells that had inversion induced were present after 2 days of culture when treated with putrescine than when untreated.

Cell counts from *Mga*$^{Inv/Inv}$*; CreERT2* cultures treated with tamoxifen were higher when treated with putrescine than when untreated ($t = 6.14$; $p < 0.0001$), but not as high as untreated *Mga*$^{Inv/Inv}$*; CreERT2* ES cells ($t = 3.17$; $p = 0.0036$), suggesting that other factors may be required to compensate for the loss of *Mga* (Fig 15C). Putrescine alone did not affect cell numbers in *Mga*$^{Inv/Inv}$*; CreERT2* cells without tamoxifen, indicating that the rescue effect of exogenous putrescine is due to a deficiency in *Mga*$^{Inv/Inv}$*; CreERT2* ES cells treated with tamoxifen rather than a general effect of the putrescine itself ($t = -0.152$, $p = 0.88$) (Fig 16A).

To ensure that the rescue effect seen in *Mga*$^{Inv/Inv}$*; CreERT2* cultures was specific to putrescine, *Mga*$^{Inv/Inv}$*; CreERT2* cultures were treated with the structurally related cadaverine, another cationic polyamine that has an additional carbon-link in its backbone but is not part of the polyamine synthesis pathway. Cadaverine treatment had no effect on *Mga*$^{Inv/Inv}$*; CreERT2* cultures alone ($t=-0.26$, $p=0.80$) or on cultures that had inversion induced with tamoxifen ($t = 0.05$, $p = 0.96$) (Fig 16A).

To control for the possibility that the rescue effect in *Mga*$^{Inv/Inv}$*; CreERT2* was a result of interaction with CreERT2 or other ES cell components, *Mga*$^{Inv/+}$ ES cells and *Mga*$^{+/+}$*; CreERT2* ES cells were grown and treated with the chemical combinations described above. Neither control cell lines showed any change in cell number with any of the treatments (Fig 16 B, C).

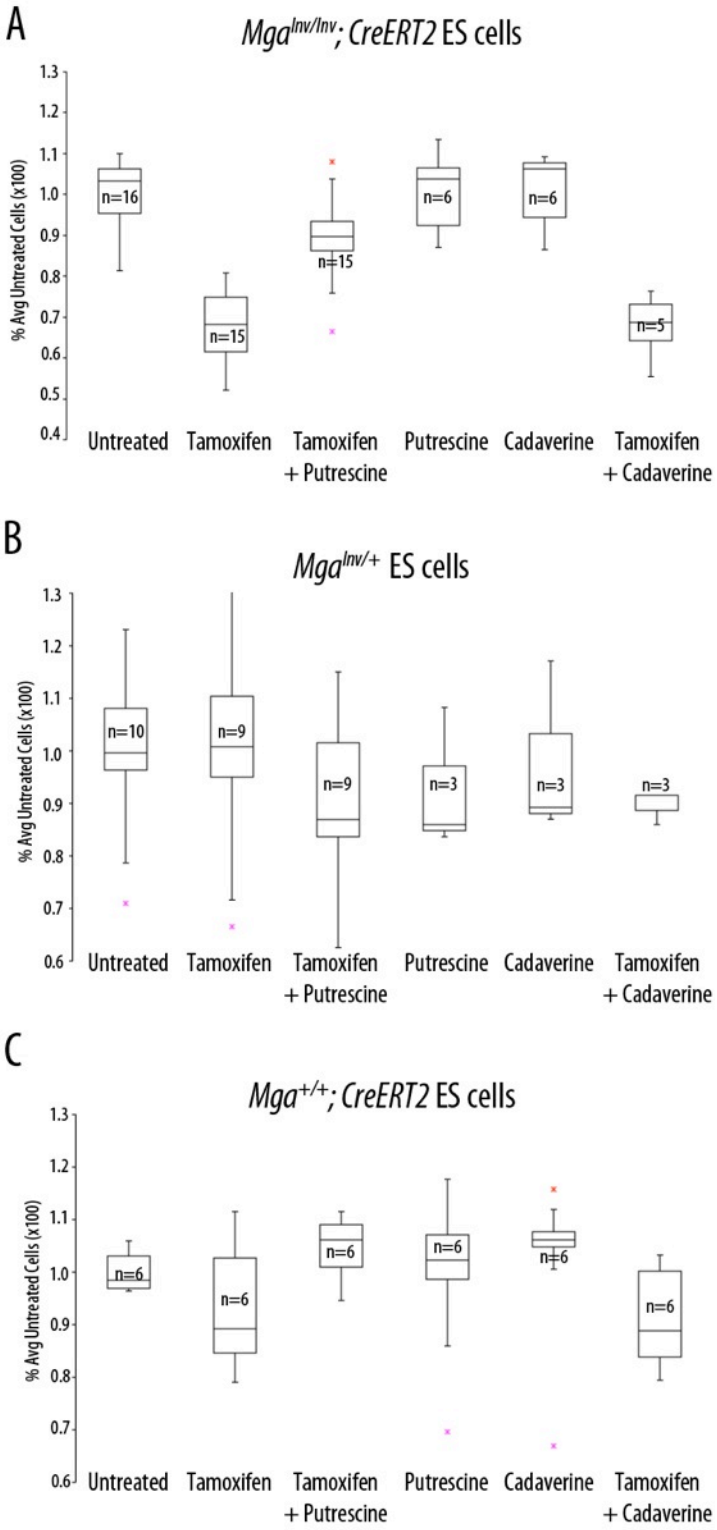

Figure 16. Box plots of cell counts of ES cell cultures treated with tamoxifen, putrescine, and cadaverine. A-C. *Mga*$^{Inv/Inv}$*; CreERT2* (A), *Mga*$^{Inv/+}$(B), and *Mga*$^{+/+}$*; CreERT2* (C) ES cells were treated with the indicated chemicals for 48 hours before cells were counted. Scale indicates the percent of cells present compared to the average number of of the untreated cells. N indicated the number individual cultures counted.

Chapter 3
Discussion

The importance of *Mga* in embryonic development

We used a gene trap allele to assess the role of *Mga* during development (Schnutgen et al., 2005). While this allele is not a knockout allele, we still have insight into its function. The insertion of the gene trap cassette into the 3rd intron does not preclude transcription or translation of this allele; β-galactosidase activity in the embryo demonstrates that it is a functional reporter. Furthermore, the reporter appears to be expressed in the same pattern as endogenous *Mga* as β-galactosidase activity is coincident with detection of the endogenous transcripts by RT-PCR. $Mga^{GT/GT}$ embryos also have a defect in tissues where *Mga* transcripts are detected, notably the Epi derivatives (Yoshikawa et al., 2006). The lack of a phenotype in $Mga^{GT/+}$ embryos provides evidence that the mutant allele is not acting as a dominant negative in spite of the presence of the T-box in the fusion protein. We thus consider the gene trap mutant allele Mga^{GT} to be functionally equivalent to a null allele.

Embryos with a homozygous loss of *Mga* fail to develop past E4.5 with embryonic death occurring during implantation. The expression of *Mga* is restricted to the ICM of embryos at E3.5 and the Epi E4.5, implicating a failure of development of this tissue in the embryonic lethality of *Mga* mutants. This hypothesis is supported by blastocyst cultures, which show *Mga* expression restricted to the ICM outgrowth and a failure of the ICM to expand during culture. Moreover, ES cell culture of $Mga^{Inv/Inv}$; *CreERT2* ES cells that had the conditional allele inverted to a mutant $Mga^{Re\text{-}inv}$ allele by tamoxifen formed smaller and sparser colonies with fewer total cells surviving. Because complete inversion of both alleles was not seen in any cultures, it is likely that the deficit of surviving cells is a result of completely inverted, *Mga* mutant cells dying.

The loss of *Mga* leads to embryonic lethality by increasing the amount of apoptosis in the embryo. Cleaved caspase 9, a marker of apoptosis, is more evident in $Mga^{GT/GT}$ than in $Mga^{+/+}$ and $Mga^{GT/+}$ embryos. The rise in apoptosis is not accompanied

by a change in cell proliferation in the embryo. Increased cell death of the Epi would explain both the stage of embryonic lethality as well as the presence of decidual swellings at the sites of implantation. Because the TE is initially unaffected by the loss of *Mga*, the decidual reaction of the uterus would still proceed, leading to decidual swellings without intact embryos. This phenotype has been noted in other mice that were mutant for ICM- or Epi-specific genes, notably *Oct4* and *Sox2* (Avilion et al., 2003; Nichols et al., 1998).

Because of the similar embryonic phenotype of mutants of *Mga* compared to mutants of genes associated with pluripotency, *Oct4* and *Sox2,* we examined the expression of pluripotency markers at E4.5. The Epi did not appear to lose pluripotency as gauged by expression of *Oct4* and *Nanog*. Additionally, the differentiation of PE was normal in *Mga* mutant embryos at E4.5 as gauged by expression of *Gata4*, as was differentiation of TE as judged by morphology. Together, these data demonstrate that loss of *Mga* does not affect the early differentiation events in the embryo.

To investigate whether pluripotency was maintained in *Mga* mutant embryos, we induced diapause to delay implantation. Strikingly, we found that despite entering diapause with similar numbers of pluripotent cells, the number of Nanog-expressing Epi cells in *Mga* mutant embryos markedly decreases during continued delayed implantation. The number of differentiated, Gata-4 positive PE cells, by contrast, initially remains stable. This suggests that the lack of *Mga* specifically affects the maintenance of the pluripotent cells, not the survival of differentiated cells, which do not initially require *Mga* to survive. Death of differentiated cells later during diapause could be a secondary effect of the lack of Epi, as has been seen in other systems (Strumpf et al., 2005). This effect is exacerbated in diapause when pluripotent cells are challenged in this way to maintain pluripotency for longer periods of time.

Because pluripotent cells were dying without *Mga*, we used a candidate gene approach to identify possible factors responsible this effect. We identified *Odc1,* the gene that codes for the polyamine synthesis enzyme ornithine decarboxylase based on the phenotypic similarity of the mouse mutants as well as the presence of E-box sites in its promoter (Bello-Fernandez et al., 1993; Pendeville et al., 2001). Because Mga has been shown to bind E-box target sites, it was reasonable to propose that loss of *Mga* may have an effect on *Odc*.

We found that ODC was reduced in the Epi of E4.5 day *Mga* mutant embryos. Moreover, we found that culture with exogenous putrescine, the biochemical product of ODC activity, partially rescued cell survival defects in both the Epi outgrowths of blastocyst cultures as well as those in ES cell culture. This suggests that one of the main roles of *Mga* in the preimplantation development of the embryos is to regulate the transcription of *Odc1*, an enzyme critical for the polyamine synthesis pathway. More generally, it suggests that *Mga* plays a crucial role in the survival of pluripotent cell populations not by regulating pluripotency itself, but rather by ensuring that cellular metabolism is functional.

The role of polyamines in embryonic development

Mice deficient for components of the polyamine synthesis pathway have shown that polyamines have an important role in peri-implantation development. *Odc1* mutant mice fail to develop due to a defect in the growth of the ICM during implantation (Pendeville et al., 2001). Knockout of *Amd1,* a crucial enzyme for the production of spermine and spermidine (Fig 12A) also leads to embryonic lethality at the same time. *Amd1*-mutant blastocysts fail to form an ICM outgrowth in blastocyst cultures, implicating failure of ICM development as the cause of embryonic lethality (Nishimura et al., 2002) and suggesting a general role for polyamines in regulating the survival of the ICM and Epi. The importance of polyamines in preimplantation development is reflected in our own findings that embryos lacking the necessary components for the synthesis of polyamines cannot develop properly.

Synthetic disruption of *Odc1* function was also found to affect pluripotent cells *in vitro*. Inactivation of *Odc1* with DFMO in F9 teratocarcinoma cell cultures leads to a decrease in the total number of cells when counted 2 days later. Moreover, cells that did grow were differentiated, suggesting a role for *Odc1* in the maintenance of pluripotent cell populations (Frostesjo et al., 1997). On the other hand, overexpression of *Odc1* promoted self-renewal of ES cells in the absence of LIF. *Odc1* also increased the efficiency of iPS cell generation in the absence of *c-Myc* (Zhao et al., 2012).

Besides ODC itself, other components of the polyamine synthesis pathway have also been linked to survival of pluripotent cell populations. Knockdown of *Amd1* leads to a loss of pluripotency markers and differentiation of ES cultures. Moreover, addition of exogenous spermine to the cultures rescues this defect (Zhang et al., 2012). Together, this highlights the importance of ODC in the function of pluripotent cells, a finding that our results support.

The necessity of polyamines for peri-implantation development could be explained in a number of ways. The first is that the polyamine synthesis pathway is required to generate intermediates for other biological processes, such as DNA methylation. The methylation of cytosine, a critical step during preimplantation development, involves the incorporation of a methyl group from S-adenosyl-methionine (SAM) through the action of *DNA MTase* (Fig 14A). This enzyme is inhibited by high levels of decarboxylated S-adenosylmethionine (dcAdoMet), a reactant in the production of spermine and spermidine. It is possible that in the absence of putrescine, dcAdoMet accumulates and DNA methylation cannot occur. Indeed, synthetic inhibition of ODC with DFMO leads to a decrease in the amount of DNA methylation in teratocarcinoma cells (Frostesjo et al., 1997). Disruption of SAM production leading to preimplantation embryonic lethality is supported by the finding that deletion of S-andeosylhomocysteine hydrolase (*Ahcy*) a key synthetic enzyme for the production of SAM, leads to inhibition of ICM growth (Miller et al., 1994). Further studies to assess the DNA methylation state of *Mga* mutant embryos or ES cells would shed light on this possible mechanism of action.

Another possible explanation for the importance of polyamines in development is that they regulate the expression of genes important for progression through the cell cycle. Unbalancing the polyamine pool by inhibiting ODC with DFMO leads to a decrease in the expression of *c-Myc* in cancer cell lines. The addition of spermidine to the cultures, however, restores normal levels of *c-Myc* expression (Celano et al., 1988). The decrease in *c-Myc* leads to an increase in the amount of *p21Cip1* transcription, a critical necessary for cell cycle progression (Liu et al., 2006). In the mouse model of familial adenomatous polyposis (FAP), polyamine pools are also unbalanced, though in this case through overexpression of *Odc1* in the small intestine and colon. Synthetic

inhibition of ODC in this model alleviates the cancer phenotype, indicating that the proper balance of polyamines is critical for normal proliferation control (Erdman et al., 1999). Further experiments assessing the transcription of downstream genes in rescued blastocyst culture or ES cell cultures could assess whether the Mga-mediated depletion of ODC and disregulation of polyamine pools leads to a loss of control of the cell cycle. The role of *Mga* in the regulation of *c-Myc* transcription and Max network protein function in cancer could also be explored by breeding the *Mga* mutant allele into mouse models of cancer, specifically the APC^{min} mouse that models FAP or other *c-Myc* mutants that model cancer, such as the Eμ-*myc* mouse model of hematocarcinomas (Adams et al., 1985; Erdman et al., 1999).

Polyamines have also been shown to be important for regulating translation in cultured mammalian cells. HeLa cells transfected with *SAT1,* which codes for the catabolic protein SAT1 that is responsible for degrading polyamines by acetylating spermine and spermidine, had a decrease in the production of endogenous proteins and subsequent cell growth arrest. This decrease was not accompanied by any decrease in the synthesis of DNA or RNA indicating a post-transcriptional mechanism of gene regulation (Mandal et al., 2013). It is possible that decreasing the stores of polyamines by decreasing the expression of *Odc1* would lead to a lack of translation and subsequent growth arrest during embryonic development.

A final explanation for the importance of polyamines in peri-implantation development could be that the downstream products of the polyamine synthesis pathway are needed for regulating normal cell cycle progression rather than the polyamines themselves. Genetic profiling of lymphoma samples identified *Amd1* and *eiF5a* as common mutations leading to cancer (Scuoppo et al., 2012). These lymphomas had a deficit of hypusinated-eIF5A, a direct product of polyamine synthesis. Further experiments testing the presence of products of the polyamine synthesis pathway such as hypusine could shed light on how the loss of ODC affects the polyamine pool in mutant embryos or ES cells. Alternately, experiments using the downstream products of the polyamine synthesis pathway to rescue embryos could elucidate which products are specifically required for the peri-implantation development of the mouse embryo.

The interaction of Mga and c-Myc

The finding that *Mga* has a regulatory effect on the expression of *Odc1* is somewhat surprising given a large body of work demonstrating that c-Myc regulates the expression of *Odc1* (Bello-Fernandez et al., 1993; Pendeville et al., 2001). However, a closer examination of the Max network's transcriptional targets provides insight into how Mga might play a role in the regulation of *Odc1* or other E-box targets. It is possible, for example, that Mga and c-Myc compete for available E-box binding sites. Alternately, it is possible that Mga and c-Myc compete for available Max, the obligate heterodimarization partner that allows these genes to bind DNA.

Mga has been shown to directly compete with c-Myc for E-box binding in *in vitro* assays. Co-transfection of *c-Myc* with *Max* in HEK293 cells leads to an increase in transcription of a luciferase reporter driven by an E-box promoter. This effect is abrogated by co-transfection with increasing concentrations of *Mga* plasmid. A similar result is seen in primary rat fibroblasts, in which transfection with *Mga* suppresses *c-Myc* and *Ras*-mediated transformation (Hurlin et al., 1999). The interaction of Max-network members in gene regulation is seen in other systems as well. In neuroblastomas, *Mga* expression correlates positively with *Odc1* expression. There is, however, no correlation, when samples that have normal N-myc levels rather than N-myc amplifications are considered. The fact that variable levels of N-myc can modulate the activity of Mga indicates that Max network proteins are able to regulate the activities of the entire Max network and that changing the cellular levels of any one of these components can have effects on the activities of the others (Geerts et al., 2010).

One explanation for the effects of Mga on the other Max-network proteins is competition for Max binding between proteins of the network. Because Max is necessary for bHLHZip proteins to bind DNA, only the set of bHLHZip proteins that can access Max will be active. The limited cellular stores of Max can only accommodate a finite number of interactions with other Max-network proteins, and by changing the concentration of one of the proteins, it is feasible that others can access newly available Max, or that Max homodimerization becomes favored. Max-network proteins have been

shown to alter the functions of one another when co-expressed in Cos cells (Grinberg et al., 2004), so it is a reasonable hypothesis that this is happening embryonically.

Another explanation for the effects that *Mga* has on putative c-Myc regulated E-box targets is the broad ability of Max-network proteins to bind the canonical E-box. Mnt, for example, has been shown to bind to promoters of multiple genes that are considered c-Myc targets during cell growth but not during quiescence, including notably *Odc1* (Nilsson et al., 2004; Popov et al., 2005). This type of context dependency has been shown with other members of the Max network (Xu et al., 2001; Zervos et al., 1993). It is possible that the *Odc1* promoter is regulated by *Mga* in the context of the peri-implantation embryo, but by other Max-network proteins in other contexts. Alternately, c-Myc may serve to amplify transcription of *Odc1* after induction of transcription by Mga. This notion is supported by the fact that in human colon carcinoma cells and intestinal epithelial cells, *c-Myc* transcription has been shown to be dependent on ODC function. In these studies, ODC must be produced before *c-Myc* transcription begins; it is possible that another factor such as Mga could be responsible for initial *Odc1* transcription with c-Myc amplifying transcription later (Celano et al., 1988; Liu et al., 2006). c-Myc acting as an amplifier of transcription of *Odc1* rather than the as the transcriptional initiator is supported by the role that c-Myc plays in the global amplification of transcription in ES cells (Lin et al., 2012).

A model for the role of *Mga* during embryonic development

Combined with previous work on the Max network of transcription factors, our results suggest a possible mechanism for *Mga* to play a critical role in peri-implantation development of the embryo. *Mga* may interact with other proteins in the Max network, notably c-Myc, to regulate transcription of *Odc1*. In the absence of *Mga*, *Odc1* is downregulated and end products of the polyamine synthesis pathway necessary for the ICM to develop are not produced in sufficient amounts. Further experiments can provide insight into the mechanism of polyamine-depletion-mediated failure of the ICM, though

loss of control of the cell cycle and subsequent apoptosis seems a likely mechanism based on the oncogenic potential of tissues that have aberrant polyamine pools.

Future Directions

One of the most interesting findings of our studies is the necessity of *Mga* in the survival of pluripotent tissues. While it is clear that these cells do not survive in the absence of *Mga*, whether they still retain the differentiation capacity of pluripotent cells before their death is not clear. It is possible that the cell death is a result of a loss of pluripotency. This can be addressed in a number of ways.

First, ES cells lacking *Mga* could be differentiated into embryoid bodies. Some initial work has already been done towards this aim. To ensure that tamoxifen treatment of $Mga^{Inv/Inv}$*; CreERT2* ES cells does not affect the differentiation of these ES cells and that the ES cells do not differentiate in the presence of residual Mga^{Inv} alleles that have not yet undergone inversion, $Mga^{Re\text{-}inv/Re\text{-}inv}$*; CreERT2* ES cells were generated by tamoxifen treatment of $Mga^{Inv/Inv}$*; CreERT2* cells in the presence of putrescine. Single colonies were picked and expanded to generate two subclones that completely lacked Mga^{inv} alleles. These ES cells are able to generate EBs in the absence of putrescine, indicating that *Mga* is not necessary for differentiation, or for survival of differentiated cells. It is unclear, though, whether these ES cells are able to survive long enough with residual putrescine from ES culture to differentiate before no longer needing putrescine as differentiated cells. More detailed studies of the differentiation of these ES cell lines that have had putrescine removed from the media at earlier time points could shed light on this issue. Furthermore, it is unclear whether the EBs formed contain differentiated tissue from all 3 embryonic germ layers. A more detailed analysis of the EBs including embryonic marker analysis could answer this question.

Another way to assess the differentiation capacity of cells lacking *Mga* is to induce differentiation in the ICM of putrescine-rescued $Mga^{GT/GT}$ embryos in culture. Preliminary studies have been performed culturing E3.5 ICMs that were separated from the surrounding TE by immunosurgery to induce differentiation to PE. These studies have shown that without putrescine rescue, mutant ICMs are not able to differentiate into

PE while rescued ICM are, though in reduced numbers compared to $Mga^{+/+}$ or $Mga^{GT/+}$ ICMs. It is unclear whether this descrepency is a result of fewer ICM cells surviving despite the presence of putrescine or of a deficiency in the differentiation capacity of $Mga^{GT/GT}$ ICMs. Marker or transcriptional analysis of rescued ICMs could reveal a defect in the pluripotency transcriptional program that is distinct from the defect in polyamine synthesis.

The importance of *Mga* in the transcription of *Odc1* also raises the possibility that other polyamine synthesis genes are also not transcribed in $Mga^{GT/GT}$ embryos. *Srm*, the gene responsible for synthesizing spermine, for example, has multiple E-box regulatory sequences in its promoter and may be regulated by *Mga* (Forshell et al., 2010). This is supported by preliminary experiments that have shown that exogenous spermine is sufficient to rescue ICM outgrowth in $Mga^{GT/GT}$ blastocyst cultures. There are two possible explanations for this result: the first is that *Mga* is needed to transcribe *Srm*, and that exogenous spermine is able to compensate for the lack of *Srm* in making spermine. The second possibility is that embryos without *Mga* are not producing spermine because of lack of ODC function and the subsequent lack of putrescine. Exogenous spermine may bypass the need for putrescine by supplying the spermine that cannot be made in the absence of putrescine. Immunofluorescence for these components could shed light on the presence or absence of other components of the polyamine synthesis pathway. Alternately, assaying the levels of polyamines could shed light on whether exogenous putrescine is being converted to spermine in $Mga^{GT/GT}$ cultures, or whether $Mga^{GT/GT}$ embryos lack components of the polyamine synthesis pathway other than ODC necessary for the production of the final polyamines.

The deregulation of polyamines and their downstream products in the progression of a number of different cancers is also interesting. As *Mga* is able to affect the polyamine pools by regulating the expression of *Odc1*, it makes an interesting target for studies in cancer models. Specifically, the conditional Mga^{Inv} allele could be bred into the mouse model of human APC. This model has increased expression of *Odc1* and its cancerous phenotype is abrogated by synthetic inhibition of ODC. According to this possible model, *Mga* mutation would slow the progression of tumorogenesis by downregulating of *Odc1*.

Chapter 4
Materials and Methods

Mutant alleles

Mice carrying the Mouse Genome Informatics (MGI) allele *Mga*$^{Gt(E153E01)Wrst}$ were obtained from the German Gene Trap Consortium and alleles derived from it were used in these studies. In the following, the alleles are referred to as *Mga*^{GT} (for gene trap), *Mga*^{Inv} (for FLP-recombinase inverted gene trap) or *Mga*$^{Re\text{-}inv}$ (for Cre-recombinase re-inverted gene trap). ES cell clones were isolated from E14Tg2a ES cells (Sv129P2) after retroviral infection using rsFlpRosaβgeo (FlpRBG; www.genetrap.de). The insertion of FlpRBG in intron 3 of *Mga* was identified by splinkerette PCR (Horn et al., 2007).

Mice and genotyping

Mga mutant mice were obtained from the German Gene Trap Consortium. Analysis of adult mice and embryos was performed on an random bred ICR background (Taconic Farms, Germantown, NY). Offspring were counted at weaning and ear punches or tail tips were digested in PBND lysis buffer (50 mM KCl, 10mM Tris-HCl, (pH8.3), 2.5mM MgCl2-6H2O, 0.1 mg/mL gelatin, 0.45% NP4,0 0.45% Tween20) with 100ug/mL Proteinase K (Roche 03115801001) for PCR genotyping. Mice carrying the *Mga*^{GT} allele were genotyped using a three-primer PCR protocol designed to amplify wildtype and mutant bands using primers AJW360, AJW363, and AJW365. Mice carrying the *Mga*^{Inv} allele were genotyped using primers AJW360, AJW363, and AJW236. *Mga*$^{Re\text{-}inv/+}$ were genotyped using primers AJW360, AJW363, and AJW366. *Mga*$^{Re\text{-}inv/Inv}$ mice were genotyped with AJW360, AJW366, and AJW236 (see table 2 in this chapter). PCR conditions were 4 minutes at 95^{o}C, 32 cycles of 30 seconds at 95 ^{o}C, 30 seconds at 61 ^{o}C, and 40 seconds at 72C, and 5 minutes at 72C. PCR was performed using 2.5uM dNTPs, 1X PCR Buffer (Denville CB3702-7), 1M Betaine [Sigma B2629], 2.5uM primers, and taq that had been prepared in-house previously.

Embryos were generated and collected from timed matings using a vaginal plug as 0.5 days post coitus (defined as E0.5). After analysis, embryos were lysed in 15uL of lysis buffer (10mM Tris pH7.5, 10mM EDTA, 100mM NaCl, 0.5% Sarcosyl, 100ug/mL

Proteinase K) at 55°C for 2 hours and analyzed by genotyping using primers AJW360, AJW363, and AJW365 with Herculase II polymerase (Agilent 600675) according to manufacturer's guidelines with 1M betaine added.

RT-PCR

E0.5 wild type embryos were collected from the oviduct followed by treatment with acid tyrodes solution (Sigma T1788) to remove the zona pellucida. E2.5, 3.5, and 4.5 embryos were collected by uterine flushing using M2 media (Sigma M7167-100mL). For RT-PCR, 42 E0.5 embryos, 26 E2.5, 35 E3.5, and 29 E4.5 embryos were pooled. RNA was isolated using a RNeasy mini kit (Qiagen 74104) and RT-PCR was performed using a OneStep RT-PCR kit (Qiagen 210212) as described, with primers AJW346 and AJW349 for *Mga* and AJW371 and AJW372 for *β-actin*.

β-galactosidase activity assay

Embryos were generated from $Mga^{+/+}$ x $Mga^{GT/+}$ crosses. E3.5 and E4.5 embryos were collected by uterine flushing using M2 media and E5.5, E6.5, and E7.5 embryos by isolating individual deciduae and manually dissecting embryos in cold PBS with 0.1% bovine serum albumin (Sigma A9647-50g). Embryos were fixed for 20 minutes in 4% paraformaldehyde at 4°C and then washed 3 times quickly in PBS with 0.1% Tween20 (Fischer BP337-500).

For whole mount staining, embryos were then incubated in X-Gal staining buffer (1mg/mL 5-Bromo-4-chloro-3-indolyl β-D-galactopyranoside in dimethyl sulfoxide [Sigma B4352], 20mM K_4Fe, 20mM K_3Fe, 2mM $MgCl_2$ in PBS) overnight at 37C. Embryos were then washed 3 times in PBS with 0.1% Tween and fixed in 4% paraformaldehyde before being photographed.

For cryosectioning, embryos were transferred to 20% sucrose overnight and then embedded in O.C.T. Compound (Tissue-Tek 4583). 10-12μm sections were cut and dried and slides were fixed in 4% paraformaldehyde for 10 minutes at 4°C and incubated in X-Gal staining buffer overnight at 37°C. Slides were fixed in 4% paraformaldehyde and then counterstained with Eosin Y (Sigma 318906-500mL) and mounted in Permount (Fisher SP15-500) before photographing.

For greater sensitivity, Salmon-Gal was used to confirm expression patterns (Sundararajan et al., 2012). Embryos were flushed with M2 and fixed briefly at 4C with 4% PFA. Embryos were washed twice with S-Gal rinse solution (0.1% sodium deoxycholate, 0.2% IGEPAL (Sigma I8896), 2mM $MgCl_2$ and 0.1 M phosphate buffer pH 7.3). Embryos were then incubated with 1mg/ml Salmon Gal (6-chloro-3-indolyl-B-D-galactopyranoside, Lab Scientific X668) and 6µg/ml NBT (4-nitro blue tetrazolium chloride, Sigma N6876) dissolved in 70% *N, N*-dimethylformamide in water at 37C for 1 or more days.

Blastocyst outgrowth in vitro

Embryos were generated from $Mga^{GT/+}$ x $Mga^{GT/+}$ crosses and collected at E3.5 by uterine flushing using M2 media. Zona pellucidae were removed by incubation in acid tyrodes solution for approximately 2 minutes at room temperature. Embryos were then plated on tissue culture dishes (BD Falcon 353003) in 20µL drop of ES media (DMEM [Gibco 11965-092], 13% FBS [Hyclone Cat #SH30071.03 Lot #ARG27092], 1% Pen/Strep [Gibco 15070], 1% GlutaMax [Gibco 35050-061], 1% Sodium Pyruvate [Gibco 11360-070], 1% Non-Essential Amino Acids [Gibco 11140-050], 0.1% Beta-Mercaptoethanol [Gibco 21985-023], LIF derived from CHO cells in-house) and covered in mineral oil (Fischer 0122-1). Embryos were cultured at 37°C in 5% CO_2 in air (Bhatnagar et al., 1995). Cultures were photographed daily and the surface area of the ICM and trophoblast was assessed by morphology and quantitated using ImageJ (NIH, http://rsb.info.nih.gov/ij/).

For rescue experiments, embryos were cultured in ES media with 200uM putrescine (Sigma P5780-5g) dissolved in water. Following culture, embryos were scraped off of the dish and genotyped.

Immunohistochemistry

Embryos were generated from $Mga^{GT/+}$ x $Mga^{GT/+}$ crosses and collected by uterine flushing using M2 media. Immunohistochemistry was performed as previously described (Artus et al., 2010). Briefly, embryos were cultured in DMEM/HEPES (Gibco 12430-054) and 10% FBS (Hyclone Cat #SH30071.03 Lot #ARG27092) for 20 minutes at 37°C

and 5% CO_2 and then fixed in 4% paraformaldehyde with 0.1% Tween20 and 0.01% TritonX (Fischer BP151-500) for 10 minutes at room temperature or overnight at 4C. Embryos were then washed in PBT (PBS with 0.1% TritonX) before permeabilization with 0.5% TritonX for 20 minutes at room temperature. After 3x 5 minute washes with PBT, antigens were unmasked with NH_4Cl (Sigma A-4514) in PBT for 10 minutes at room temperature. Following 2x 5 minutes washes, embryos were blocked in 2% donkey serum in PBT for 45 minutes at room temperature. Embryos were then incubated with the first primary antibodies overnight at 4°C in 2% donkey serum. The following day, embryos were washed 3 times with PBT and incubated with the second primary antibody overnight at 4°C in 2% donkey serum. The following day, embryos were washed 3 times with PBT and incubated with secondary antibodies overnight at 4°C in the dark. Embryos were again washed 3 times with PBT and incubated with Hoecst 33342 (Sigma B2261) diluted 1:500 overnight at 4°C in the dark. Embryos were washed 2 more times and then analyzed using a Nikon A1R confocal microscope and NIS Elements v4.0 software with MatTek 35mm petri dishes with coverglass (MatTek P35G-0-10-C). Embryos were then lysed and genotyped with Herculase II polymerase. Statistics were analyzed using Fisher's exact probability test.

Embryonic diapause and immunosurgery

Diapause was induced in pregnant females at E2.5 by subcutaneous injection of 3mg Depo Provera suspended in PBS (Medroxyprogesterone 17-acetate Sigma M1629-1g) and intraperitoneal injection of 20μg tamoxifen in sunflower seed oil (Sigma T5648-1g). Embryos were then flushed from the uterus with M2 1-7 days later.
To perform immunosurgery, embryos were washed twice with Hams F12 media (Gibco 11765-054) and incubated in 20% rabbit anti-mouse serum antibody (Sigma M5774) in Hams F12 for 30 minutes at 37°C in 7% CO_2 in air. Embryos were washed 3 times in Hams F12 before incubation with 20% guinea pig compliment (CalBiochem 234395) in Hams F12 with 1:100 Propidium Iodide (Sigma P4864) and 1:100 Hoechst 33342. Embryos were washed quickly 3 times in Hams F12 and squashed on a glass slide with a glass coverslip before being photographed on a Nikon fluorescent microscope with NIS Elements software.

Immunohistochemistry was performed as described, though the embryos remained intact allowing PCR genotyping after imaging. Statistics were analyzed using Fisher's exact probability test and Mann-Whitney U test.

ES Cells

$Mga^{Inv/Inv}$; CreERT2 and *$Mga^{Inv/+}$* ES cell lines were derived using previously established protocols (Batlle-Morera et al., 2008). Embryos were generated from *$Mga^{Inv/Inv}$; CreERT2 x $Mga^{Inv/+}$; CreERT2* matings and diapause was induced at E2.5. Embryos were flushed with M2 4 days after diapause induction. Immunosurgery was performed as described and isolated ICMs were plated on gelatin-coated tissue culture dishes in mES media supplemented with recombinant human BMP4 (R&D Systems 314-BP-010) and MEK inhibitor PD98059 (Cell Signalling Technology 9900S). After 7-10 days, ICM outgrowths were trypsinized with 0.25% trypsin (Gibco 25200-056) and replated on mitomycin-C (Sigma M4287) treated MEFs. Inversion was induced using 4-hydroxytamoxifen (Sigma H6278). "Inverted" cultures were treated with 200μM putrescine and 200μM cadaverine (Sigma D22606) dissolved in water. For cell count assays, cells were counted and then plated in separate wells, allowed, to attach over night, and then treated the next day. After 48 hours of chemical treatment, cells were trypsinized and counted on a hemocytometer in duplicate or triplicate and the counts averaged. Statistics were analyzed using a Student's t-test.

Table 1 – Primer sequences

Primer Name	Sequence
AJW360	*ATTCCTGTAGGCCCTGGAAG*
AJW363	*CAGGACAACCTGACACCTCTG*
AJW365	*CAGCAGATCCATACCCTGCT*
AJW236	*GGGAGGATTGGGAAGACAAT*
AJW366	*TTTGAGGGGACGACGACAGTAT*
AJW346	*CCTCCAGTGCTGGGTGTTAT*
AJW349	*ACCCTGTTGCCTTCAACATC*
AJW371	*ATATCGCTGCGCTGGTCGTC*
AJW372	*AGGATGGCGTGAGGGAGAGC*
AJW156	*GTCCAATTTACTGACCGTACACC*
AJW157	*GTTATTCGGATCATCAGCTACACC*

Table 2 – Primer combinations for genotyping

Genotypes tested	Primer Combination
$Mga^{+/+}$, $Mga^{GT/+}$, $Mga^{GT/GT}$	AJW360/AJW363/AJW365
$Mga^{Inv/Inv}$, $Mga^{Inv/+}$	AJW360/AJW363/AJW366
$Mga^{Re\text{-}inv/Inv}$	AJW360/AJW366/AJW236

References

Adams, J. M., Harris, A. W., Pinkert, C. A., Corcoran, L. M., Alexander, W. S., Cory, S., Palmiter, R. D. and Brinster, R. L. (1985). The c-myc oncogene driven by immunoglobulin enhancers induces lymphoid malignancy in transgenic mice. *Nature* **318**, 533-538.

Arnold, S. J., Hofmann, U. K., Bikoff, E. K. and Robertson, E. J. (2008). Pivotal roles for eomesodermin during axis formation, epithelium-to-mesenchyme transition and endoderm specification in the mouse. *Development* **135**, 501-511.

Artus, J., Panthier, J. J. and Hadjantonakis, A. K. (2010). A role for PDGF signaling in expansion of the extra-embryonic endoderm lineage of the mouse blastocyst. *Development* **137**, 3361-3372.

Avilion, A. A., Nicolis, S. K., Pevny, L. H., Perez, L., Vivian, N. and Lovell-Badge, R. (2003). Multipotent cell lineages in early mouse development depend on SOX2 function. *Genes & development* **17**, 126-140.

Ayer, D. E., Kretzner, L. and Eisenman, R. N. (1993). Mad: A heterodimeric partner for Max that antagonizes Myc transcriptional activity. *Cell* **72**, 211-222.

Batlle-Morera, L., Smith, A. and Nichols, J. (2008). Parameters influencing derivation of embryonic stem cells from murine embryos. *Genesis* **46**, 758-767.

Baudino, T. A. and Cleveland, J. L. (2001). The Max network gone mad. *Molecular and cellular biology* **21**, 691-702.

Bello-Fernandez, C., Packham, G. and Cleveland, J. (1993). The ornithine decarboxylase gene is a transcriptional target of c-Myc. *Proc. Natl. Acad. Sci. USA* **90**, 7804-7808.

Bernstein, B. E., Mikkelsen, T. S., Xie, X., Kamal, M., Huebert, D. J., Cuff, J., Fry, B., Meissner, A., Wernig, M., Plath, K., et al. (2006). A bivalent chromatin structure marks key developmental genes in embryonic stem cells. *Cell* **125**, 315-326.

Bhatnagar, P., Papaioannou, V. E. and Biggers, J. D. (1995). CSF-1 and mouse preimplantation development in vitro. *Development* **121**, 1333-1339.

Blelloch, R., Venere, M., Yen, J. and Ramalho-Santos, M. (2007). Generation of Induced Pluripotent Stem Cells in the Absence of Drug Selection. *Cell Stem Cell* **1**, 245-247.

Bollag, R. J., Siegfried, Z., Cebra-Thomas, J. A., Garvey, N., Davison, E. M. and Silver, L. M. (1994). An ancient family of embryonically expressed mouse genes sharing a conserved protein motif with the T locus. *Nature genetics* **7**, 383-389.

Brenner, R., Slayden, O., Rodgers, W., Critchley, H., Carroll, R., Jing Nie, X. and Mah, K. (2003). Immunocytochemical assessment of mitotic activity with an antibody to phosphorylated histone H3 in the macaque and human endometrium. *Human Reproduction* **18**, 1185-1193.

Celano, P., Baylin, S. B., Giardiello, F. M., Nelkin, B. D. and Casero, R. A., Jr. (1988). Effect of polyamine depletion on c-myc expression in human colon carcinoma cells. *The Journal of biological chemistry* **263**, 5491-5494.

Chapman, D. L., Garvey, N., Hancock, S., Alexiou, M., Agulnik, S. I., Gibson-Brown, J. J., Cebra-Thomas, J., Bollag, R. J., Silver, L. M. and Papaioannou,

V. E. (1996). Expression of the T-box family genes, Tbx1–Tbx5, during early mouse development. *Developmental Dynamics* **206**, 379-390.

Chazaud, C., Yamanaka, Y., Pawson, T. and Rossant, J. (2006). Early lineage segregation between epiblast and primitive endoderm in mouse blastocysts through the Grb2-MAPK pathway. *Dev Cell* **10**, 615-624.

Cormier, S., Le Bras, S., Souilhol, C., Vandormael-Pournin, S., Durand, B., Babinet, C., Baldacci, P. and Cohen-Tannoudji, M. (2006). The murine ortholog of notchless, a direct regulator of the notch pathway in Drosophila melanogaster, is essential for survival of inner cell mass cells. *Molecular and cellular biology* **26**, 3541-3549.

Davenport, T. G., Jerome-Majewska, L. A. and Papaioannou, V. E. (2003). Mammary gland, limb and yolk sac defects in mice lacking Tbx3, the gene mutated in human ulnar mammary syndrome. *Development* **130**, 2263-2273.

Davis, A., Wims, M., Spotts, G., Hann, S. and Bradley, A. (1993). A null c-myc mutation causes lethality before 10.5 days of gestation in homozygotes and reduced fertility in heterozygous female mice. *Genes & development* **7**, 671-682.

de Luca, C., Kowalski, T. J., Zhang, Y., Elmquist, J. K., Lee, C., Kilimann, M. W., Ludwig, T., Liu, S. M. and Chua, S. C., Jr. (2005). Complete rescue of obesity, diabetes, and infertility in db/db mice by neuron-specific LEPR-B transgenes. *The Journal of clinical investigation* **115**, 3484-3493.

Domashenko, A., Latham, K. and Hatton, K. (1997). Expression of myc-family, myc-interacting, and myc-target Genes During Preimplantation Mouse Development. *Molecular Reproduction and Development* **47**, 57-65.

Downs, K. M., Martin, G. R. and Bishop, J. M. (1989). Contrasting patterns of myc and N-myc expression during gastrulation of the mouse embryo. *Genes & development* **3**, 860-869.

Dubois, N. C., Adolphe, C., Ehninger, A., Wang, R. A., Robertson, E. J. and Trumpp, A. (2008). Placental rescue reveals a sole requirement for c-Myc in embryonic erythroblast survival and hematopoietic stem cell function. *Development* **135**, 2455-2465.

Erdman, S., Ignatenko, N., Powell, M., Blohm-Mangone, K., Holubec, H., Guillen-Rodriguez, J. and Gerner, E. (1999). APC-dependent changes in expression of genes influencing polyamine metabolism, and consequences for gastrointestinal carcinogenesis, in the Min mouse. *Carcinogenesis* **20**, 1709-1713.

Forshell, T. P., Rimpi, S. and Nilsson, J. A. (2010). Chemoprevention of B-Cell Lymphomas by Inhibition of the Myc Target Spermidine Synthase. *Cancer Prevention Research* **3**, 140-147.

Frostesjo, L., Holm, I., Grahn, B., Page, A. W., Bestor, T. H. and Heby, O. (1997). Interference with DNA methyltransferase activity and genome methylation during F9 teratocarcinoma stem cell differentiation induced by polyamine depletion. *The Journal of biological chemistry* **272**, 4359-4366.

Geerts, D., Koster, J., Albert, D., Koomoa, D.-L. T., Feith, D. J., Pegg, A. E., Volckmann, R., Caron, H., Versteeg, R. and Bachmann, A. S. (2010). The polyamine metabolism genes ornithine decarboxylase and antizyme 2 predict aggressive behavior in neuroblastomas with and without MYCN amplification. *International Journal of Cancer* **126**, 2012-2024.

Gibson-Brown, J. J., Agulnik, S. I., Silver, L. M., Niswander, L. and Papaioannou, V. E. (1998). Involvement of T-box genes Tbx2-Tbx5 in vertebrate limb specification and development. *Development* **125**, 2499-2509.

Grandori, C., Cowley, S. m., James, L. p. and Eisenman, R. N. (2000). The Myc/Max/Mad network and the transcriptional control of cell behavior. *Annu Rev Cell Dev Biol* **16**, 653.

Greulich, F., Rudat, C. and Kispert, A. (2011). Mechanisms of T-box gene function in the developing heart. *Cardiovascular Research* **91**, 212-222.

Grinberg, A. V., Hu, C.-D. and Kerppola, T. K. (2004). Visualization of Myc/Max/Mad Family Dimers and the Competition for Dimerization in Living Cells. *Molecular and cellular biology* **24**, 4294-4308.

Habets, P., Moorman, A., Clout, D., van Roon, M., Lingbeek, M., van Lohuizen, M., Campione, M. and Christoffels, V. (2002). Cooperative action of Tbx2 and Nkx2.5 inhibits ANF expression in the atrioventricular canal: implications for cardiac chamber formation. *Genes & development* **16**, 1234-1246.

Hamatani, T., Carter, M. G., Sharov, A. A. and Ko, M. S. H. (2004). Dynamics of Global Gene Expression Changes during Mouse Preimplantation Development. *Developmental cell* **6**, 117-131.

Hammachi, F., Morrison, Gillian M., Sharov, Alexei A., Livigni, A., Narayan, S., Papapetrou, Eirini P., O'Malley, J., Kaji, K., Ko, Minoru S. H., Ptashne, M., et al. (2012). Transcriptional Activation by Oct4 Is Sufficient for the Maintenance and Induction of Pluripotency. *Cell Reports* **1**, 99-109.

Han, J., Yuan, P., Yang, H., Zhang, J., Soh, B. S., Li, P., Lim, S. L., Cao, S., Tay, J., Orlov, Y. L., et al. (2010). Tbx3 improves the germ-line competency of induced pluripotent stem cells. *Nature* **463**, 1096-1100.

Hancock, S. N., Agulnik, S. I., Silver, L. M. and Papaioannou, V. E. (1999). Mapping and expression analysis of the mouse ortholog of Xenopus Eomesodermin. *Mechanisms of Development* **81**, 205-208.

Hayward, W. S., Neel, B. G. and Astrin, S. M. (1981). Activation of a cellular onc gene by promoter insertion in ALV-induced lymphoid leukosis. *Nature* **290**, 475-480.

Horn, C., Hansen, J., Schnutgen, F., Seisenberger, C., Floss, T., Irgang, M., De-Zolt, S., Wurst, W., von Melchner, H. and Noppinger, P. R. (2007). Splinkerette PCR for more efficient characterization of gene trap events. *Nature genetics* **39**, 933-934.

Hu, G., Kim, J., Xu, Q., Leng, Y., Orkin, S. H. and Elledge, S. J. (2009). A genome-wide RNAi screen identifies a new transcriptional module required for self-renewal. *Genes & development* **23**, 837-848.

Hurlin, P., Steingrimsson, E., Copeland, N., Jenkins, N. and Eisenman, R. (1999). Mga, a dual-specificity transcription factor that interacts with Max and contains a T-domain DNA-binding motif. *The EMBO journal* **18**, 7019-7028.

Hurlin, P. J. and Huang, J. (2006). The MAX-interacting transcription factor network. *Seminars in cancer biology* **16**, 265-274.

Hurlin, P. J., Queva, C., Koskinen, P. J., Steingrimsson, E., Ayer, D. E., Copeland, N. G., Jenkins, N. A. and Eisenman, R. N. (1995). Mad3 and Mad4: novel Max-interacting transcriptional repressors that suppress c-myc dependent

transformation and are expressed during neural and epidermal differentiation. *The EMBO journal* **14**, 5646-5659.

Illingworth, R. S., Botting, C. H., Grimes, G. R., Bickmore, W. A. and Eskeland, R. (2012). PRC1 and PRC2 Are Not Required for Targeting of H2A.Z to Developmental Genes in Embryonic Stem Cells. *PLoS ONE* **7**, e34848.

Ivanova, N., Dobrin, R., Lu, R., Kotenko, I., Levorse, J., DeCoste, C., Schafer, X., Lun, Y. and Lemischka, I. R. (2006). Dissecting self-renewal in stem cells with RNA interference. *Nature* **442**, 533-538.

Iwama, K., Wang, J.-Y., Jain, R., Shirley., M. and Leonard., J. (1990). Intestinal ornithine decarboxylase- half-life and regulation by putrescine. *Am. J. Physiol* **258**, G308-G315.

Jedrusik, A., Parfitt, D. E., Guo, G., Skamagki, M., Grabarek, J. B., Johnson, M. H., Robson, P. and Zernicka-Goetz, M. (2008). Role of Cdx2 and cell polarity in cell allocation and specification of trophectoderm and inner cell mass in the mouse embryo. *Genes & development* **22**, 2692-2706.

Johnson, M. H. and McConnell, J. M. L. (2004). Lineage allocation and cell polarity during mouse embryogenesis. *Seminars in Cell & Developmental Biology* **15**, 583-597.

Kim, J., Chu, J., Shen, X., Wang, J. and Orkin, S. H. (2008). An Extended Transcriptional Network for Pluripotency of Embryonic Stem Cells. *Cell* **132**, 1049-1061.

Kispert, A. and Herrmann, B. G. (1993). The Brachyury gene encodes a novel DNA binding protein. *The EMBO journal* **12**, 3211-3220.

Lardelli, M. (2003). The evolutionary relationships of zebrafish genes tbx6, tbx16/spadetail and mga. *Dev Genes Evol* **213**, 519-522.

Lengner, C. J., Camargo, F. D., Hochedlinger, K., Welstead, G. G., Zaidi, S., Gokhale, S., Scholer, H. R., Tomilin, A. and Jaenisch, R. (2007). Oct4 expression is not required for mouse somatic stem cell self-renewal. *Cell Stem Cell* **1**, 403-415.

Lin, Charles Y., Lovén, J., Rahl, Peter B., Paranal, Ronald M., Burge, Christopher B., Bradner, James E., Lee, Tong I. and Young, Richard A. (2012). Transcriptional Amplification in Tumor Cells with Elevated c-Myc. *Cell* **151**, 56-67.

Lin, S. C., Wani, M. A., Whitsett, J. A. and Wells, J. M. (2010). Klf5 regulates lineage formation in the pre-implantation mouse embryo. *Development* **137**, 3953-3963.

Liu, L., Guo, X., Rao, J. N., Zou, T., Marasa, B. S., Chen, J., Greenspon, J., Casero, R. A., Jr. and Wang, J. Y. (2006). Polyamine-modulated c-Myc expression in normal intestinal epithelial cells regulates p21Cip1 transcription through a proximal promoter region. *The Biochemical journal* **398**, 257-267.

Loh, Y.-H., Wu, Q., Chew, J.-L., Vega, V. B., Zhang, W., Chen, X., Bourque, G., George, J., Leong, B., Liu, J., et al. (2006). The Oct4 and Nanog transcription network regulates pluripotency in mouse embryonic stem cells. *Nature genetics* **38**, 431-440.

Lu, R., Yang, A. and Jin, Y. (2011). Dual functions of T-box 3 (Tbx3) in the control of self-renewal and extraembryonic endoderm differentiation in mouse embryonic stem cells. *The Journal of biological chemistry* **286**, 8425-8436.

Malynn, B. A., de Alboran, I. M., O'Hagan, R. C., Bronson, R., Davidson, L., DePinho, R. A. and Alt, F. W. (2000). N-myc can functionally replace c-myc in murine development, cellular growth, and differentiation. *Genes & development* **14**, 1390-1399.

Mandal, S., Mandal, A., Johansson, H. E., Orjalo, A. V. and Park, M. H. (2013). Depletion of cellular polyamines, spermidine and spermine, causes a total arrest in translation and growth in mammalian cells. *Proceedings of the National Academy of Sciences of the United States of America* **110**, 2169-2174.

Meroni, G., Cairo, S., Merla, G., Messali, S., Brent, R., Ballabio, A. and Reymond, A. (2000). Mlx, a new Max-like bHLHZip family member: the center stage of a novel transcription factors regulatory pathway? *Oncogene* **19**, 3266-3277.

Meroni, G., Reymond, A., Alcalay, M., Borsani, G., Tanigami, A., Tonlorenzi, R., Lo Nigro, C., Messali, S., Zollo, M., Ledbetter, D. H., et al. (1997). Rox, a novel bHLHZip protein expressed in quiescent cells that heterodimerizes with Max, binds a non-canonical E box and acts as a transcriptional repressor. *The EMBO journal* **16**, 2892-2906.

Mesbah, K., Harrelson, Z., Theveniau-Ruissy, M., Papaioannou, V. E. and Kelly, R. G. (2008). Tbx3 is required for outflow tract development. *Circulation research* **103**, 743-750.

Miller, M. W., Duhl, D. M., Winkes, B. M., Arredondo-Vega, F., Saxon, P. J., Wolff, G. L., Epstein, C. J., Hershfield, M. S. and Barsh, G. S. (1994). The mouse lethal nonagouti (a(x)) mutation deletes the S-adenosylhomocysteine hydrolase (Ahcy) gene. *The EMBO journal* **13**, 1806-1816.

Mitsui, K., Tokuzawa, Y., Itoh, H., Segawa, K., Murakami, M., Takahashi, K., Maruyama, M., Maeda, M. and Yamanaka, S. (2003). The homeoprotein Nanog is required for maintenance of pluripotency in mouse epiblast and ES cells. *Cell* **113**, 631-642.

Moore, J. M., Rabaia, N. A., Smith, L. E., Fagerlie, S., Gurley, K., Loukinov, D., Disteche, C. M., Collins, S. J., Kemp, C. J., Lobanenkov, V. V., et al. (2012). Loss of Maternal CTCF Is Associated with Peri-Implantation Lethality of <italic>Ctcf</italic> Null Embryos. *PLoS ONE* **7**, e34915.

Murphy, M. J., Wilson, A. and Trumpp, A. (2005). More than just proliferation: Myc function in stem cells. *Trends in cell biology* **15**, 128-137.

Naiche, L. A., Harrelson, Z., Kelly, R. G. and Papaioannou, V. E. (2005). T-box genes in vertebrate development. *Annual review of genetics* **39**, 219-239.

Nichols, J., Chambers, I., Taga, T. and Smith, A. (2001). Physiological rationale for responsiveness of mouse embryonic stem cells to gp130 cytokines. *Development* **128**, 2333-2339.

Nichols, J., Zevnik, B., Anastassiadis, K., Niwa, H., Klewe-Nebenius, D., Chambers, I., Scholer, H. and Smith, A. (1998). Formation of pluripotent stem cells in the mammalian embryo depends on the POU transcription factor Oct4. *Cell* **95**, 379-391.

Nie, Z., Hu, G., Wei, G., Cui, K., Yamane, A., Resch, W., Wang, R., Green, D. R., Tessarollo, L., Casellas, R., et al. (2012). c-Myc is a universal amplifier of expressed genes in lymphocytes and embryonic stem cells. *Cell* **151**, 68-79.

Nilsson, J. A., Maclean, K. H., Keller, U. B., Pendeville, H., Baudino, T. A. and Cleveland, J. L. (2004). Mnt loss triggers Myc transcription targets, proliferation, apoptosis, and transformation. *Molecular and cellular biology* **24**, 1560-1569.

Nishimura, K., Nakatsu, F., Kashiwagi, K., Ohno, H., Saito, T. and Igarashi, K. (2002). Essential role of S-adenosylmethionine decarboxylase in mouse embryonic development. *Genes to Cells* **7**, 41-47.

Ogawa, H., Ishiguro, K., Gaubatz, S., Livingston, D. M. and Nakatani, Y. (2002). A Complex with Chromatin Modifiers That Occupies E2F- and Myc-Responsive Genes in G0 Cells. *Science (New York, N.Y.)* **296**, 1132-1136.

Papapetrou, C., Edwards, Y. H. and Sowden, J. C. (1997). The T transcription factor functions as a dimer and exhibits a common human polymorphism Gly-177-Asp in the conserved DNA-binding domain. *FEBS letters* **409**, 201-206.

Paynton, B. V., Rempel, R. and Bachvarova, R. (1988). Changes in state of adenylation and time course of degradation of maternal mRNAs during oocyte maturation and early embryonic development in the mouse. *Developmental biology* **129**, 304-314.

Pendeville, H., Carpino, N., Marine, J. C., Takahashi, Y., Muller, M., Martial, J. A. and Cleveland, J. L. (2001). The Ornithine Decarboxylase Gene Is Essential for Cell Survival during Early Murine Development. *Molecular and cellular biology* **21**, 6549-6558.

Plusa, B., Piliszek, A., Frankenberg, S., Artus, J. and Hadjantonakis, A.-K. (2008). Distinct sequential cell behaviours direct primitive endoderm formation in the mouse blastocyst. *Development* **135**, 3081-3091.

Popov, N., Wahlstrom, T., Hurlin, P. J. and Henriksson, M. (2005). Mnt transcriptional repressor is functionally regulated during cell cycle progression. *Oncogene* **24**, 8326-8337.

Rikin, A. and Evans, T. (2010). The tbx/bHLH transcription factor mga regulates gata4 and organogenesis. *Developmental Dynamics* **239**, 535-547.

Russ, A. P., Wattler, S., Colledge, W. H., Aparicio, S. A. J. R., Carlton, M. B. L., Pearce, J. J., Barton, S. C., Surani, M. A., Ryan, K., Nehls, M. C., et al. (2000). Eomesodermin is required for mouse trophoblast development and mesoderm formation. *Nature* **404**, 95-99.

Sawai, S., Shimono, A., Hanaoka, K. and Kondoh, H. (1991). Embryonic lethality resulting from disruption of both N-myc alleles in mouse zygotes. *The New biologist* **3**, 861-869.

Sawai, S., Shimono, A., Wakamatsu, Y., Palmes, C., Hanaoka, K. and Kondoh, H. (1993). Defects of embryonic organogenesis resulting from targeted disruption of the N-myc gene in the mouse. *Development* **117**, 1445-1455.

Schnutgen, F., De-Zolt, S., Van Sloun, P., Hollatz, M., Floss, T., Hansen, J., Altschmied, J., Seisenberger, C., Ghyselinck, N. B., Ruiz, P., et al. (2005). Genomewide production of multipurpose alleles for the functional analysis of the mouse genome. *Proceedings of the National Academy of Sciences of the United States of America* **102**, 7221-7226.

Schreiber-Agus, N., Horner, J., Torres, R., Chiu, F. C. and DePinho, R. A. (1993). Zebra fish myc family and max genes: differential expression and oncogenic

activity throughout vertebrate evolution. *Molecular and cellular biology* **13**, 2765-2775.

Scuoppo, C., Miething, C., Lindqvist, L., Reyes, J., Ruse, C., Appelmann, I., Yoon, S., Krasnitz, A., Teruya-Feldstein, J., Pappin, D., et al. (2012). A tumour suppressor network relying on the polyamine-hypusine axis. *Nature* **487**, 244-248.

Shen-Li, H., O'Hagan, R., Harry Hou Jr, H., James Horner II, J., H-W., H.-W. L. and DePinho, R. (2000). Essential role for Max in early embryonic growth and development. *Genes & development* **14**, 17-22.

Showell, C., Binder, O. and Conlon, F. L. (2004). T-box genes in early embryogenesis. *Developmental dynamics : an official publication of the American Association of Anatomists* **229**, 201-218.

Silva, J., Nichols, J., Theunissen, T. W., Guo, G., van Oosten, A. L., Barrandon, O., Wray, J., Yamanaka, S., Chambers, I. and Smith, A. (2009). Nanog is the gateway to the pluripotent ground state. *Cell* **138**, 722-737.

Sinha, S., Abraham, S., Gronostajski, R. M. and Campbell, C. E. (2000). Differential DNA binding and transcription modulation by three T-box proteins, T, TBX1 and TBX2. *Gene* **258**, 15-29.

Stanton, B. R., Perkins, A. S., Tessarollo, L., Sassoon, D. A. and Parada, L. F. (1992). Loss of N-myc function results in embryonic lethality and failure of the epithelial component of the embryo to develop. *Genes & development* **6**, 2235-2247.

Strumpf, D., Mao, C. A., Yamanaka, Y., Ralston, A., Chawengsaksophak, K., Beck, F. and Rossant, J. (2005). Cdx2 is required for correct cell fate specification and differentiation of trophectoderm in the mouse blastocyst. *Development* **132**, 2093-2102.

Sundararajan, S., Wakamiya, M., Behringer, R. R. and Rivera-Perez, J. A. (2012). A fast and sensitive alternative for beta-galactosidase detection in mouse embryos. *Development* **139**, 4484-4490.

Takahashi, K. and Yamanaka, S. (2006). Induction of Pluripotent Stem Cells from Mouse Embryonic and Adult Fibroblast Cultures by Defined Factors. *Cell* **126**, 663-676.

Tanaka, T. S., Kunath, T., Kimber, W. L., Jaradat, S. A., Stagg, C. A., Usuda, M., Yokota, T., Niwa, H., Rossant, J. and Ko, M. S. (2002). Gene expression profiling of embryo-derived stem cells reveals candidate genes associated with pluripotency and lineage specificity. *Genome research* **12**, 1921-1928.

Teo, A. K., Arnold, S. J., Trotter, M. W., Brown, S., Ang, L. T., Chng, Z., Robertson, E. J., Dunn, N. R. and Vallier, L. (2011). Pluripotency factors regulate definitive endoderm specification through eomesodermin. *Genes & development* **25**, 238-250.

van den Berg, D. L. C., Snoek, T., Mullin, N. P., Yates, A., Bezstarosti, K., Demmers, J., Chambers, I. and Poot, R. A. (2010). An Oct4-Centered Protein Interaction Network in Embryonic Stem Cells. *Cell Stem Cell* **6**, 369-381.

Varlakhanova, N. V., Cotterman, R. F., deVries, W. N., Morgan, J., Donahue, L. R., Murray, S., Knowles, B. B. and Knoepfler, P. S. (2010). myc maintains embryonic stem cell pluripotency and self-renewal. *Differentiation; research in biological diversity* **80**, 9-19.

Walker, W., Zhou, Z. Q., Ota, S., Wynshaw-Boris, A. and Hurlin, P. J. (2005). Mnt-Max to Myc-Max complex switching regulates cell cycle entry. *The Journal of cell biology* **169**, 405-413.

Washkowitz, A. J., Gavrilov, S., Begum, S. and Papaioannou, V. E. (2012). Diverse functional networks of Tbx3 in development and disease. *Wiley interdisciplinary reviews. Systems biology and medicine* **4**, 273-283.

Xu, D., Popov, N., Hou, M., Wang, Q., Bjorkholm, M., Gruber, A., Menkel, A. R. and Henriksson, M. (2001). Switch from Myc/Max to Mad1/Max binding and decrease in histone acetylation at the telomerase reverse transcriptase promoter during differentiation of HL60 cells. *Proceedings of the National Academy of Sciences of the United States of America* **98**, 3826-3831.

Yoshikawa, T., Piao, Y., Zhong, J., Matoba, R., Carter, M. G., Wang, Y., Goldberg, I. and Ko, M. S. H. (2006). High-throughput screen for genes predominantly expressed in the ICM of mouse blastocysts by whole mount in situ hybridization. *Gene Expression Patterns* **6**, 213-224.

Zeller, K., Jegga, A., Aronow, B., O'Donnell, K. and Dang, C. (2003). An integrated database of genes responsive to the Myc oncogenic transcription factor: identification of direct genomic targets. *Genome Biology* **4**, R69.

Zervos, A. S., Gyuris, J. and Brent, R. (1993). Mxi1, a protein that specifically interacts with Max to bind Myc-Max recognition sites. *Cell* **72**, 223-232.

Zhang, D., Zhao, T., Ang, H. S., Chong, P., Saiki, R., Igarashi, K., Yang, H. and Vardy, L. A. (2012). AMD1 is essential for ESC self-renewal and is translationally down-regulated on differentiation to neural precursor cells. *Genes & development* **26**, 461-473.

Zhao, T., Goh, K. J., Ng, H. H. and Vardy, L. A. (2012). A role for polyamine regulators in ESC self-renewal. *Cell cycle (Georgetown, Tex.)* **11**, 4517-4523.

Zhu, Q., Jin, L., Casero, R. A., Davidson, N. E. and Huang, Y. (2012). Role of ornithine decarboxylase in regulation of estrogen receptor alpha expression and growth in human breast cancer cells. *Breast Cancer Research and Treatment* **136**, 57-66.

Appendix

Additional publications produced in the course of doctoral research:

1. Medioni, C., et al. (2010). "Expression of *Slit* and *Robo* genes in the developing mouse heart." Dev Dyn **239**(12): 3303-3311.

2. Washkowitz, A. J., et al. (2012). "Diverse functional networks of *Tbx3* in development and disease." Wiley Interdiscip Rev Syst Biol Med **4**(3): 273-283.

Developmental Dynamics

DEVELOPMENTAL DYNAMICS 239:3303–3311, 2010

PATTERNS & PHENOTYPES

Expression of *Slit* and *Robo* Genes in the Developing Mouse Heart

Caroline Medioni,[1†] Nicolas Bertrand,[2†] Karim Mesbah,[3] Bruno Hudry,[3] Laurent Dupays,[4] Orit Wolstein,[5] Andrew J. Washkowitz,[6] Virginia E. Papaioannou,[6] Timothy J. Mohun,[4] Richard P. Harvey,[5,7] and Stéphane Zaffran[2]*

Development of the mammalian heart is mediated by complex interactions between myocardial, endocardial, and neural crest-derived cells. Studies in *Drosophila* have shown that the Slit-Robo signaling pathway controls cardiac cell shape changes and lumen formation of the heart tube. Here, we demonstrate by in situ hybridization that multiple Slit ligands and Robo receptors are expressed in the developing mouse heart. *Slit3* is the predominant ligand transcribed in the early mouse heart and is expressed in the ventral wall of the linear heart tube and subsequently in chamber but not in atrioventricular canal myocardium. Furthermore, we identify that the homeobox gene *Nkx2-5* is required for early ventral restriction of *Slit3* and that the T-box transcription factor Tbx2 mediates repression of *Slit3* in nonchamber myocardium. Our results suggest that patterned Slit-Robo signaling may contribute to the control of oriented cell growth during chamber morphogenesis of the mammalian heart. *Developmental Dynamics 239:3303–3311, 2010.* © 2010 Wiley-Liss, Inc.

Key words: Slit/Robo pathway; cardiac development; mouse; Tbx; atrioventricular canal

Accepted 6 September 2010

INTRODUCTION

Cardiogenesis is one of the earliest and most critical steps during vertebrate organogenesis. Heart development begins when cardiac progenitor cells in the anterior lateral mesoderm cluster in the primary heart field (Harvey, 2002). These cells give rise to the cardiac crescent and linear heart tube containing the future left ventricle and atrioventricular canal (AVC; see Buckingham et al., 2005). Subsequently the heart tube undergoes rightward looping (Harvey, 2002). As looping progresses, cells of the second heart field in splanchnic mesoderm are added to the heart tube to form the outflow tract (OFT), right ventricle, atria and inflow tract regions (Buckingham et al., 2005). Subsequently, atrial and ventricular chambers form through a localized process that involves differential growth or "ballooning" of the outer curvature of the heart tube (Christoffels et al., 2000). Importantly, part of the heart tube, including the OFT, inner curvature, AVC, and inflow tract, escapes this developmental chamber program through the repressive action of the T-box factors, Tbx2 and Tbx3 (Habets et al., 2002; Christoffels et al., 2004b; Harrelson et al., 2004; Bakker et al., 2008). Regionalized gene expression provides evidence for the presence

Additional Supporting Information may be found in the online version of this article.

[1]Institute of Developmental Biology and Cancer, CNRS UMR 6543, Faculté des Sciences, Parc Valrose Nice, France
[2]Inserm UMR_S910, Université de la Méditerranée, Faculté de Médecine de la Timone, Marseille, France
[3]Developmental Biology Institute of Marseille-Luminy, CNRS UMR 6216, Université de la Méditerranée, Marseille, France
[4]Division of Developmental Biology, MRC National Institute for Medical Research, The Ridgeway, Mill Hill, London, United Kingdom
[5]Victor Chang Cardiac Research Institute, Sydney, Australia
[6]Department of Genetics and Development, Columbia University Medical Center, New York, New York
[7]Faculties of Life Sciences and Medicine, University of New South Wales, Kensington, Australia

Grant sponsor: Agence Nationale pour la Recherche; Grant number: ANR-007-MRAR-003; Grant sponsor: NIH; Grant number: 5R37HD033082; Grant sponsor: The European Commission; Grant number: HEALTH-2007-B-223463.

[†]Drs. Medioni and Bertrand contributed equally to this work.

***Correspondence to: Stéphane Zaffran, Inserm UMR_S910, Faculté de Médecine de la Timone, 27 Bd Jean Moulin, 13005 Marseille, France. E-mail: stephane.zaffran@univmed.fr**

DOI 10.1002/dvdy.22449
Published online 12 October 2010 in Wiley Online Library (wileyonlinelibrary.com).

of dorsoventral patterning in the early tube that precedes chamber development (Christoffels et al., 2004a). A retrospective clonal analysis of cardiac cells has shown that myocardium, from the time of its formation, is a polarized and regionalized tissue in which oriented cell growth may be important in shaping the chambers (Meilhac et al., 2004). Although key factors that play a role in forming the heart tube have been identified, including GATA4, NKX2-5, dHAND, TBX5, or RALDH2 (Harvey, 2002), the molecular effectors of cell polarity and cell shape changes remain unknown.

The extracellular-matrix molecule Slit and its Robo (roundabout) family receptors have been implicated in the regulation of cell polarity and morphogenesis during formation of the cardiac tube in *Drosophila* (Qian et al., 2005; MacMullin and Jacobs, 2006; Medioni et al., 2008; Santiago-Martinez et al., 2008). In particular, the Slit-Robo pathway is required for progressive polarization of cardiac cells during migration to the midline (Medioni et al., 2008). In contrast to the single *Slit* and three *Robo* genes in *Drosophila*, three distinct *Slit* genes (*Slit1*, *Slit2*, and *Slit3*) and four distinct *Robo* genes (*Robo1*, *Robo2*, *Rig1*/*Robo3*, and *Robo4*) are found in mammals (Chedotal, 2007). Slit functions as a repulsive ligand for the Robo-family receptors in the central nervous system (CNS), and acts both attractively and repulsively in somatic muscles (Kidd et al., 1998, 1999; Brose et al., 1999; Simpson et al., 2000; Wu et al., 2001). In addition, both gene families display distinct expression patterns outside the CNS (Holmes et al., 1998; Yuan et al., 1999; Strickland et al., 2006). Remarkably, *Slit3* is widely expressed in different organs, including the tongue, kidney, pharynx, umbilical cord vein, heart, lung, and diaphragm (Yuan et al., 1999; Liu et al., 2003; Yuan et al., 2003). Consistent with its expression in non-neural tissues, studies have established that Slit3 is required for angiogenesis and formation of the diaphragm and kidney (Liu et al., 2003; Yuan et al., 2003; Zhang et al., 2009).

The role of the *Drosophila* Slit-Robo pathway in regulating changes in cell shape during cardiac tube formation prompted us to conduct a detailed analysis of murine *Slit* and *Robo* gene expression during mouse heart development. We describe that *Slit3* in particular, shows a specific localization in the ventral region of the forming heart tube and subsequently restriction to chamber myocardium. We show that the homeobox gene *Nkx2-5* is required for the ventral restriction of *Slit3* in the linear heart tube. In addition, we demonstrate that the T-box factors Tbx2 and Tbx20 mediate the restriction of *Slit3* expression to the chamber myocardium. Given the spatial and temporal expression profile of *Slit3* and its role in polarized growth and migration in other tissues, we propose that Slit-Robo signaling may be required for cardiac chamber expansion.

RESULTS AND DISCUSSION

Expression of Mouse *Slit* and *Robo* Genes During Heart Development

Previous studies in *Drosophila* have shown that the Slit-Robo signaling pathway controls cardiac cell polarity and formation of the cardiac lumen (Medioni et al., 2009). Therefore, we decided to analyze the expression pattern of murine *Slit* and *Robo* genes in the developing heart. In contrast to other tissues, detailed analysis of the cardiac expression pattern of *Slit* and *Robo* genes has not been reported (Holmes et al., 1998; Yuan et al., 1999; Holmes and Niswander, 2001; Liu et al., 2003; Yuan et al., 2003). Mouse embryos between 7.5 and 12.5 days of development (E7.5–E12.5) were hybridized with antisense riboprobes for *Slit1*, *Slit2*, *Slit3*, *Robo1*, *Robo2*, *Rig1*/*Robo3*, and *Robo4* (Figs. 1, 2; also see Supp. Fig. S1, which is available online).

Fig. 1. Expression pattern of *Slit* genes during embryonic heart development. Whole-mount in situ hybridization analysis of embryos with *Slit1* (A–D), *Slit2* (E–H), and *Slit3* (I–L) probes. **A:** Ventral view of embryonic day (E) 8.5 embryo showing *Slit1* expression in the ventral midline (arrowhead). *Slit1* is not detected in the forming heart tube. **B:** Lateral view of E9 embryo showing *Slit1* expression in the roof plate (arrowhead), in the floor plate (double arrowhead), and the pharyngeal region (white arrows). **B′:** Frontal section (same embryo depicted in B) showing *Slit1* expression in the mesodermal core of the pharyngeal arch (white arrows) and in the floor plate of the spinal cord. **C:** High magnification picture of heart at late E9.5 showing *Slit1* in atrial wall. **D:** Dissected E12.5 heart showing no expression of *Slit1*. **D′:** In situ hybridization with *Slit1* on section of E12.5 heart. **E:** *Slit2* was not detected in the heart of embryo at E8.5 stage. Note its expression at the ventral midline (arrowhead). **F:** Lateral view of early E9.5 embryo showing *Slit2* expression in the pharyngeal region (asterisk). *Slit2* is also detected in the roof plate (arrowhead), the notochord (double arrowheads) and the somites (white arrowhead). **F′:** Frontal section (same embryo depicted in F) showing *Slit2* expression in the pharyngeal ectoderm surface (arrows). **G:** Dissected E9.5 heart showing no expression of *Slit2*. **H:** A robust expression of *Slit2* is detected in trabeculae of both ventricles at E12.5. **H′:** In situ hybridization on section of E12.5 heart shows expression in the trabeculae (arrowhead). **I,I′:** Ventral views of E7.5 and E8.5 embryos showing *Slit3* expression in the cardiac crescent and the forming heart tube. Expression of *Slit3* is also detected in the ventral midline (black arrowhead) and the somites (white arrowhead) of E8.5 embryo. **J:** Lateral view of early E9.5 embryo showing *Slit3* expression in the heart and the pharyngeal ectoderm surface (asterisk) and in the somites (white arrowhead). **J′:** Frontal section (same embryo depicted in J) showing expression of *Slit3* in pharyngeal ectoderm surface (arrows). **K:** High magnification picture of the heart at late E9.5. Expression of *Slit3* is seen in the outflow tract, the atria and ventricles of the embryonic heart. **L:** At E12.5, expression of *Slit3* is maintained in the right and left atria and in great arteries, the aorta and pulmonary trunk. **L′:** Section of the heart shown in L. ao, aorta; cc, cardiac crescent; ht, heart tube; la, left atrium; lv, left ventricle; oft, outflow tract; pt, pulmonary trunk; ra; right atrium; rv, right ventricle.

Fig. 2. Expression pattern of *Robo* genes during embryonic heart development. Whole-mount in situ hybridization analysis of embryos with *Robo1* (A–D) and *Robo2* (E–H) probes. **A:** Ventral view of early embryonic day (E) 8.5 embryo showing *Robo1* expression in the venous pole (white arrows) of the forming heart tube. **B:** Lateral view of early E9 embryo. *Robo1* expression is detected in the notochord (double arrowhead), the somites (white arrowhead), and the ectodermal pouches of the pharyngeal arches (asterisk) but not in the heart. **C:** High magnification picture of the heart at late E9.5 showing *Robo1* in the cushions (asterisk) of the outflow tract. **D:** Dissected E12.5 heart showing expression of *Robo1* at the base of the great arteries (arrow). **E:** Ventral view of early E8.5 embryo. High *Robo2* expression levels are visible in the neural tube and the venous pole (white arrows) of the forming heart tube. **F:** Lateral view of E9.5 embryo. Weak expression of *Robo2* is detected in the looped heart, the ectoderm of the pharyngeal arches (asterisk) and the notochord (double arrowheads). **G:** High magnification of the heart at E10.5 showing *Robo2* in both atria. **H:** Dissected E12.5 heart showing expression of *Robo2* in the great arteries (arrowheads). ht, heart tube; la, left atrium; lv, left ventricle; oft, outflow tract; ra; right atrium; rv, right ventricle.

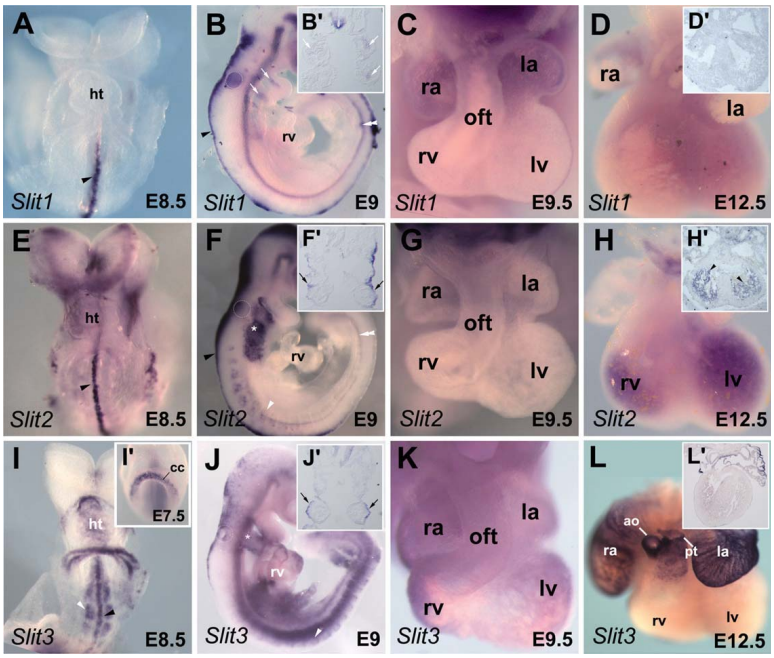
A
ht
Slit1
E8.5
B
B'
rv
Slit1
E9
C
la
ra
oft
rv
lv
Slit1
E9.5
D
D'
ra
la
Slit1
E12.5
E
ht
Slit2
E8.5
F
F'
rv
Slit2
E9
G
ra
la
oft
rv
lv
Slit2
E9.5
H
H'
rv
lv
Slit2
E12.5
I
I'
cc
E7.5
ht
Slit3
E8.5
J
J'
rv
Slit3
E9
K
ra
la
oft
rv
lv
Slit3
E9.5
L
L'
ao
ra
pt
la
rv
lv
Slit3
E12.5

Fig. 1.

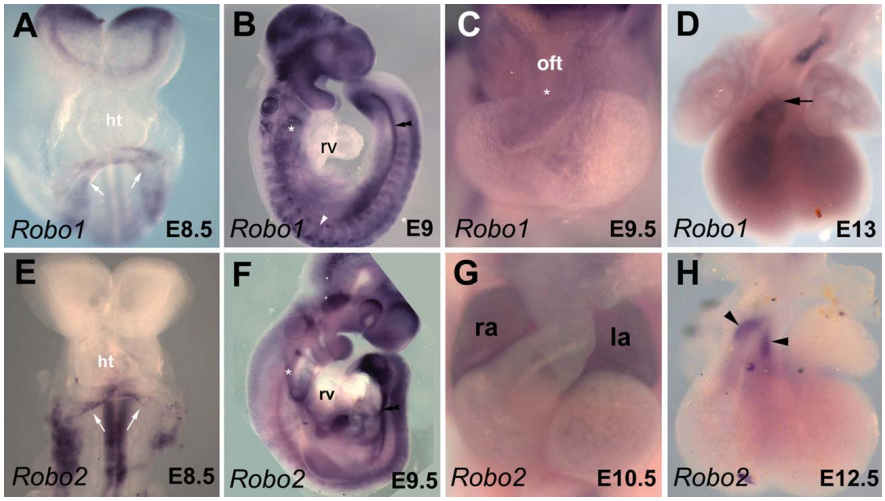
A
ht
Robo1
E8.5
B
rv
Robo1
E9
C
oft
Robo1
E9.5
D
Robo1
E13
E
ht
Robo2
E8.5
F
rv
Robo2
E9.5
G
ra
la
Robo2
E10.5
H
Robo2
E12.5

Fig. 2.

During this period of development, *Slit1* expression was primarily observed in the roof plate and the floor plate (Fig. 1A,B). *Slit1* transcripts were also observed in the mesodermal core of the pharyngeal arches (Fig. 1B,B′). Interestingly, pharyngeal mesoderm has been shown to contribute to the formation of the OFT as well as the pharyngeal arch artery (PAA) development (see Kelly and Buckingham, 2002). At E9.5, *Slit1* expression was detected in the developing heart in the left and right atria (Fig. 1C). However, at E12.5 we did not observe any expression in the heart (Fig. 1D,D′).

Similarly to *Slit1*, *Slit2* expression was observed prominently in neural tissue (Fig. 1E,F). From E8.5 to E9.5, *Slit2* expression was not detected in the myocardium; however, it was highly expressed in the pharyngeal region at these stages (Fig. 1F) as reported by others (Yuan et al., 1999; Calmont et al., 2009). Strong expression of *Slit2* was seen in the pharyngeal surface ectoderm (Fig. 1F″). This tissue has been shown to be a crucial source of signals for fourth PAA formation and remodeling (Kirby, 2007). *Slit2* has also been identified as a downstream target of Tbx1, and is implicated in cardiac neural crest cells (NCC) migration at the time of PAA formation (Calmont et al., 2009). While no clear expression in the embryonic heart was detected at E9.5 (Fig. 1G), a strong expression of *Slit2* was observed in the trabecular region of the ventricular chambers at E12.5 (Fig. 1H,H′). Of interest, the trabecular formation occurs when cardiomyocytes migrate toward the endocardium, which is coincident with upregulation of cell adhesion molecules (Ong et al., 1998). Thus, our observation suggests that other cell signaling molecules such as Slit may be involved in this process.

Slit3 is the earliest *Slit* gene to be expressed in the developing heart. Transcripts were observed in the cardiac crescent at E7.5 and in the linear heart tube at E8.5 (Fig. 1I,I′). At E8.5, *Slit3* expression is observed on the ventral wall of the linear heart tube (see Fig. 3A,B). *Slit3* is also expressed in the ventral midline and developing somites (Fig. 1I,J). Unlike the other *Slit* genes, *Slit3* expression was observed in all compartments of embryonic heart at E9.5, restricted to the outer curvature of the looped heart (Fig. 1J,K). The myocardium of the outer curvature is known to give rise to the ventricular chamber or "working" myocardium (de la Cruz and Markwald, 1999; Christoffels et al., 2000). Analysis of the distribution of clonally related myocytes has demonstrated that different patterns of oriented cell growth underlie regional differences in morphogenesis within the embryonic heart (Meilhac et al., 2004). The expression pattern of *Slit3* and its established role in polarized growth and migration in other tissues suggest implication of Slit-Robo signaling in the oriented cell growth that accompanies ballooning of the ventricular chambers (Christoffels et al., 2004a). By E12.5, expression of *Slit3* was observed only in myocardium of the atria and at the base of the great arteries (Fig. 1L,L′), in agreement with published expression data (Liu et al., 2003). Remarkably, expression of *Slit2* and *Slit3* in ventricular chambers seem to be complementary in the endocardium and myocardium respectively. This observation suggests requirement of a specific Slit ligand during trabeculae formation. Despite that difference, *Slit2* and *Slit3* were detected in the surface pharyngeal ectoderm of embryo at E9.5 (Fig. 1F,F″,J,J′), suggesting redundancy of these molecules during cardiac NCC migration and PAA formation. The Slit-Robo signaling pathway is known to be involved in trunk neural crest migration (Jia et al., 2005). It would be interesting to identify whether Slit-Robo signaling mediates repulsive or attractive signals during cardiac NCC migration.

Robo family members Robo1-4 are the putative receptors for Slit ligands. Whereas *Robo4* is specifically expressed in the vascular endothelium (Supp. Fig. S1; Park et al., 2003), the expression profile of the three other members during heart development has not been analyzed in detail (Yuan et al., 1999; Camurri et al., 2004; Jia et al., 2005). In situ hybridization with *Robo1* and *Robo2* riboprobes showed that these receptors were both expressed in the venous pole of the linear heart tube at E8.5 (Fig. 2A,E). In agreement with a recent study (Calmont et al., 2009), we found *Robo1* expression in migrating NCCs (Fig. 2B). At E9.5, *Robo1* expression was faintly detected in the endocardial cushions of the OFT (Fig. 2C). Later, *Robo1* expression was maintained in the great arteries (Fig. 2D). Unlike other *Robo* genes, a consistent expression of *Robo2* was observed in both atria of the heart at E10.5 (Fig. 2G). At E12.5, *Robo2* expression was observed in the endocardium of the great arteries (Fig. 2H). The specific expression of *Slit* ligand and *Robo* receptor genes in the venous pole at E8.5 and in the atria from E9.5 to E12.5 suggests a role for these molecules in oriented cell growth and migration during atrial morphogenesis (Meilhac et al., 2004). Finally, from our in situ hybridization analysis we did not detect any expression of *Rig1*/*Robo3* and *Robo4* in the developing mouse heart at any timepoint analyzed (Supp. Fig. S1).

Dorsoventral Patterning of *Slit3* Is Controlled by Nkx2-5

As noted above, whole-mount in situ hybridization analysis revealed expression of *Slit3* transcripts in the linear heart tube at E8.5 (Fig. 1I). At this stage, *Slit3* expression is comparable to the expression of the basic helix–loop–helix (bHLH) transcription factor gene, *Hand1*, which is restricted to the ventral wall of the forming heart tube (Fig. 3A–D; Biben and Harvey, 1997; Christoffels et al., 2000; Togi et al., 2004). Although *Slit3* is expressed at high levels in the developing heart, early cardiac defects have not been reported in *Slit3* mutant embryos (Liu et al., 2003; Yuan et al., 2003). However, the expression of *Slit3* detected in the outer curvature of the looped heart and the enlarged right ventricle observed in the hearts of *Slit3* mutant mice (Liu et al., 2003), suggest a role for Slit signaling in ventricular chamber formation. Further studies are required to determine whether subtle changes may exist in the heart of these mutants especially during the formation of the myocardium chambers and the great arteries.

We subsequently examined expression of *Slit3* in mutant mice affecting cardiac morphogenesis. Mutations in the NK-like homeobox gene, *Nkx2-5*/*Csx*, causes early embryonic lethality with cardiac development arrested at

the linear heart tube stage, before looping (Komuro and Izumo, 1993; Lyons et al., 1995; Biben and Harvey, 1997). In *Nkx2-5*$^{-/-}$ embryos, the early expression of *Slit3* was indistinguishable from that in control embryos (Fig. 3E). However, we found that the dorsoventral pattern of *Slit3* expression in the linear heart tube was perturbed and expression was observed throughout the mutant heart tube (Fig. 3E,F). This result suggests that the myocardium of *Nkx2-5*$^{-/-}$ embryos is competent to express *Slit3* but not to interpret signals that restrict expression on the ventral side of the heart. Of note, two putative Nkx2-5 binding motifs (TGAAGTGATG and TAAAGTGGGT) are found in a 3,000 bp Slit3 5′ proximal fragment as predicted using the TFSEARCH program (http://mbs.cbcr.jp/research/db/TFSEARCH.html).

Expression of *Robo* receptor genes in the venous pole (Fig. 2A,E) incited us to examine their expression in *Nkx2-5*$^{-/-}$ embryos. Of interest, we did not detect expression of *Robo2* in the linear heart tube of *Nkx2-5* mutant embryos (Supp. Fig. S2). This observation suggests that Nkx2-5 regulates in a different way *Slit* ligand and *Robo* receptor genes during the formation of the embryonic heart tube.

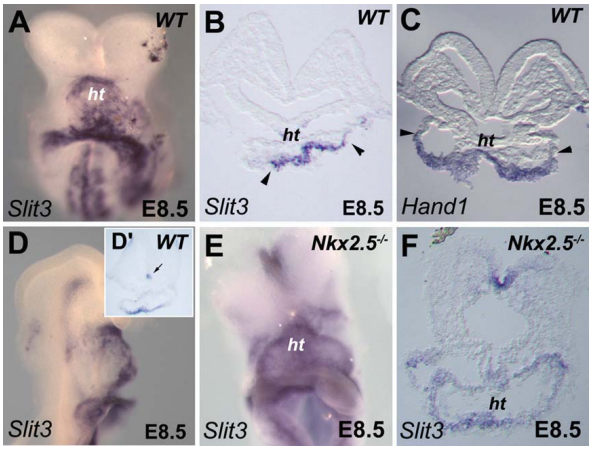

Fig. 3.

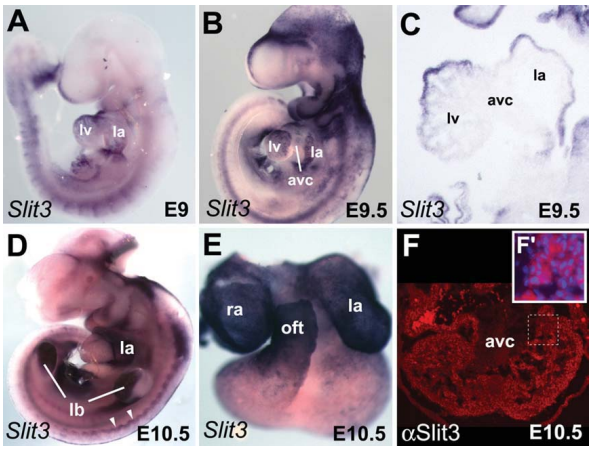

Fig. 4.

Fig. 3. Dorsoventral patterning of *Slit3* expression in the linear heart tube requires Nkx2-5. **A:** Ventral view of embryo at early embryonic day (E) 8.5. *Slit3* is highly expressed in the ventral side of the forming heart tube. **B:** Section (same embryo as depicted in A) showing that *Slit3* expression in the heart tube is strictly ventral as delimited by the arrowheads. **C:** Expression of *Hand1* is shown as a reference to indicate the ventral side (arrowheads) of the heart tube at E8.5. **D,E:** Comparison of *Slit3* expression in wild-type (WT) and *Nkx2-5*$^{-/-}$ embryos at E8.5. **D:** Lateral view of WT embryo showing high expression of *Slit3* in the ventral side of the forming heart tube. **D′:** Section of the embryo shown in D. Note the expression of *Slit3* in the floor plate (arrow). **E:** *Slit3* expression is maintained in *Nkx2-5*$^{-/-}$ embryo. **F:** Section (same embryo as shown in E) reveals that *Slit3* is uniformly expressed in heart of *Nkx2-5*$^{-/-}$ embryo. ht, heart tube; nt, neural tube.

Fig. 4. Dynamic expression pattern of *Slit3* during heart development. In situ hybridization (A–E) and immunofluorescence (F) were used to detect spatial expression of Slit3 in hearts from embryonic day (E) 9 to E10.5. **A,B:** Expression of *Slit3* is detected in the whole heart of E9 embryo, whereas it is down-regulated in the AVC of late E9.5 embryo. **C:** Section (same embryo as depicted in B) showing expression of *Slit3* in the chambers but not in the AVC. Note weak expression of *Slit3* in the trabeculae of the left ventricle. **D:** Lateral view of E10.5 embryo. High expression of *Slit3* is detected in the left atrium. Note *Slit3* expression in the limb buds and the dermomyotome (white arrowheads). **E:** Dissected heart from the embryo shown in D. High expression is observed in the right and left atria and the outflow tract. **F:** Expression of Slit3 protein (red) is detected in the ventricular myocardium and trabeculae but not in the AVC of heart at E10.5. Higher magnification of the trabeculae region delimited by the dotted line is shown in the inset. **F′:** Immunodetection of Slit3 (red) and DAPI (blue) staining. Note Slit3 expression in the cytoplasm. ao, aorta; avc, atrioventricular canal; la, left atrium; lb, limb bud; lv, left ventricle; oft, outflow tract; pt, pulmonary trunk; ra, right atrium; rv, right ventricle.

Regulation of the Chamber-Specific Expression Profile of *Slit3*

In looped hearts (E9–E9.5), *Slit3* expression was confined to the atrial and ventricular myocardium but was clearly absent from the AVC (Fig. 4A–C), a pattern resembling that of *atrial natriuretic factor* (*ANF*; see Supp. Fig. S3A), *Chisel*, and *Connexin40* at this stage (Christoffels et al., 2000). At E10.5 and E12.5 *Slit3* expression was restricted to the atria and the OFT (Figs. 1L, 4C–E). Immunohistochemistry revealed Slit3 protein expression in both atrial and ventricular myocardium at E10.5 (Fig. 4F). The AVC region was negative, confirming our results by in situ hybridization. Detection of Slit3 protein but not mRNA in the ventricles of the heart at E10.5 (Fig. 4E,F) indicates a persistence of the protein in the chamber myocardium. Although *Slit3* expression overlaps with *Robo1* and *Robo2* in the venous pole and later only with *Robo2* in the atria, no *Robo* receptor genes were detected in the ventricular myocardium of the heart (Fig. 2). Despite its favorite link with Robo receptors, Slit contains domains that suggest association with the extracellular-matrix receptors (Chedotal, 2007). Furthermore, recent study in *Drosophila* have proposed that Slit is localized on cardiac cells by association with Dystroglycan (Dg), a proteoglycan (Medioni et al., 2008), and possibly also with αPS3/βPS1 Integrin (MacMullin and Jacobs, 2006).

The absence of *Slit3* gene expression and protein in AVC myocardium suggested potential regulation by the T-box transcriptional repressors *Tbx2* and *Tbx3* that are restricted to nonchamber myocardium (Supp. Fig. S3B,C), where they repress the chamber transcriptional program (Habets et al., 2002; Christoffels et al., 2004b; Harrelson et al., 2004; Bakker et al., 2008; Mesbah et al., 2008). Therefore, we examined *Slit3* expression in mutant embryos deficient for *Tbx2* and *Tbx3*. In situ hybridization on stage-matched embryos revealed activation of *Slit3* in the AVC of E10.5 $Tbx2^{-/-}$ but not $Tbx3^{-/-}$ hearts (Supp. Fig. S4). This observation indicates that Tbx2 alone is sufficient to repress *Slit3* in the nonchamber myocardium of $Tbx3^{-/-}$ hearts, consistent with previous findings on other chamber-specific genes (Bakker et al., 2008; Mesbah et al., 2008). The T-box factor Tbx20 is essential for embryonic chamber formation through its negative regulation of *Tbx2* in the myocardium and endocardium (Cai et al., 2005; Singh et al., 2005; Stennard et al., 2005; Takeuchi et al., 2005). To test the hypothesis that ectopic Tbx2 expression may be able to repress *Slit3* in the forming heart, we analyzed *Slit3* expression in $Tbx20^{-/-}$ embryos. Mutant embryos showed severe cardiac abnormalities including rudimentary ventricular chambers that did not further differentiate (Stennard et al., 2005). We could not detect any *Slit3* expression in $Tbx20^{-/-}$ hearts at E9 (compare Fig. 5B,B′ with 5A,A′). Of interest, *Drosophila Slit* is also perturbed in the embryonic heart tube of *Tbx20*-ortholog ($H15^{nmr}$) mutants (Qian et al., 2005), suggesting a high evolutionary conservation of this regulation pathway. We also examined *Slit3* expression in embryos misexpressing *Tbx2* throughout the embryonic heart under the control of the *XMLC2* promoter (*XMLC2-rtTA/tetO-Tbx2;*) (Dupays et al., 2009). Consistent with our observation in $Tbx20^{-/-}$ embryos, *Slit3* expression was significantly reduced (Fig. 5C,C′). The residual weak expression of *Slit3* observed in these embryos may be explained by the mosaic expression of the transgene at this stage (Dupays et al., 2009). Moreover, we found three conserved T-box binding elements (TBEs; Kispert and Herrmann, 1993; Sinha et al., 2000) in the *Slit3* 5′ proximal promoters (Fig. 5D). The requirement of these TBEs for repression in the AVC and the complementary expression pattern between *Tbx2* (Supp. Fig. S3) and *Slit3* (Fig. 4B) prompted us to study the interaction of Tbx2 with the TBE motifs identified in the *Slit3* promoter using electrophoretic mobility shift assay (EMSA) experiments. Oligonucleotide probes corresponding to the three TBE motifs were used. Tbx2 bound to the wild-type TBE2 motif but not TBE1 and TBE3, because a shifted band was detected only in lanes 11 and 12 (Fig. 5E). However, when the EMSA was performed with a mutated TBE2 motif this binding was abolished (Fig. 5E). Together these results suggest that *Slit3* expression may be directly repressed by Tbx2 during AVC formation.

Conclusion

In this study, we have characterized Slit ligand and Robo receptor gene expression in the developing mouse heart. Our results suggest that Slit-Robo signaling, essential for morphogenesis of the *Drosophila* heart tube, may play roles in oriented cell growth during atrial and ventricular morphogenesis in vertebrates. Furthermore, we identify two upstream regulators of *Slit3* expression, the predominant Slit ligand expressed in the early mouse heart: analysis of *Slit3* expression in different mutant mouse embryos reveals that *Slit3* is restricted to the ventral wall of the linear heart tube by Nkx2-5 regulated mechanisms and excluded from AVC myocardium by the transcriptional repressor Tbx2.

EXPERIMENTAL PROCEDURES

Animals and Tissue Preparation

All experiments involving animals were performed in accordance with French guidelines on the care and use of laboratory animals. After death by CO_2 asphyxiation, embryo mice were removed from timed-pregnant CD1 or mutant mice. The day of vaginal plugging was defined as 0.5. Embryos were genotyped by polymerase chain reaction (PCR) using genomic DNA isolated from yolk sacs. The null alleles $Tbx2^{tm1Pa}$, $Tbx3^{tm1Pa}$, $Tbx20^{lacZ}$, and $Nkx2\text{-}5^{gfp}$ (hereafter referred to as $Tbx2^{-}$, $Tbx3^{-}$, $Tbx20^{-}$, and $Nkx2\text{-}5^{-}$) were maintained on a mixed genetic background (Biben et al., 2000; Davenport et al., 2003; Harrelson et al., 2004; Stennard et al., 2005). Somites were counted for developmental staging and a sample of the yolk sac was taken for PCR genotyping using the following primers. *Tbx3*: the primers 5′-GGC CTC AAG TAG CTT GGA A-3′, 5′-AGG CCA

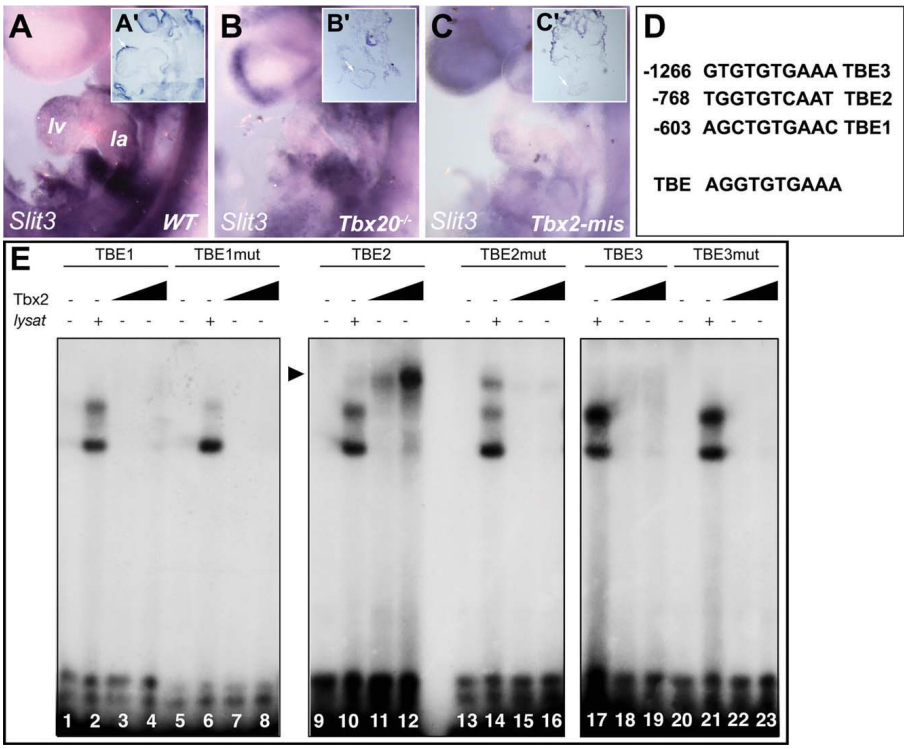

Fig. 5. Disrupted cardiac expression of *Slit3* in *Tbx20* mutant and in *Tbx2*-misexpression embryos. **A–C:** Lateral views of wild-type (WT), *Tbx20*$^{-/-}$ mutant and *Tbx2*-misexpressing embryos. **A′–C′:** Sections of embryos shown in A–C. While *Slit3* is present in the forming heart of WT embryo (A,A′), its expression is not detected in the heart of E9 *Tbx20*$^{-/-}$ embryo (B,B′). **C,C′:** *Slit3* expression is highly reduced in heart misexpressing *Tbx2*. **D:** Sequence of three-conserved T-box binding elements (TBE) found in a *Slit3* 5′ proximal promoter. Numbers indicate position of the sequences from the ATG. TBE sequence shows the T-box binding site as determined previously (Kispert and Herrmann, 1993). **E:** Electrophoretic mobility shift assay shows that Tbx2 binds to the wild-type TBE2 motif (lanes 9–12) but not to the TBE1 (lanes 1–8) and TBE3 (lanes 17–23) motifs. Mutation of the TBE2 motif impairs Tbx2 binding (lanes 13–16). la, left atria; lv, left ventricle.

ACA GAA GAG CAG A-3′, and 5′-CTA AGC CTG ATG GTG TGA G-3′ result in a 350 bp wild-type band and a 500 bp mutant band. *Tbx2*: the primers 5′-CCA GCC AGG GAA CAT AAT GAG G-3′, 5′-CTG TCC CCT GGC ATT TCT GG-3′, and 5′-CCT GCA GGA ATT CCT CGA CC-3′ result in a 180 bp wild-type band and a 88 bp mutant band. *Nkx2-5*: the primers 5′-GAA CCT GGA GCA GCA GCA GCG TAG C-3′ and 5′-CAG AAG GGA AGA GCT TGA GGT TCT C-3′ result in a 308 bp wild-type band and a 1,376 bp mutant band.

The tetO-Tbx2 and xMlc2-rtTA transgenes have been previously described (Dupays et al., 2009). Doxycycline was administered to pregnant females either by intraperitoneal injection (2 mg of Dox in 0.5 ml of 0.9% aqueous NaCl) at the indicated stage or by means of food (2 mg of Dox in 0.5 ml of 0.9% aqueous NaCl) from stages specified.

For early developmental stages whole embryos were fixed in 4% paraformaldehyde (PFA) in phosphate buffered saline (PBS) overnight at 4°C, dehydrated and kept in methanol. Hearts or trunks were dissected and fixed in 4% PFA in PBS overnight at 4°C, transferred to 15% sucrose in PBS, followed by 15% sucrose 7% gelatin, and frozen in liquid nitrogen before cryo-sectioning at 10 μm.

Whole-Mount In Situ Hybridization

Whole-mount in situ hybridization was carried out as published (Zaffran et al., 2004). Probes were labeled according to the manufacturer's instruction using the digoxigenin (DIG) -RNA labeling mix (Roche). The probes used for in situ hybridization were *mSlit2* and *mSlit3* (Yuan et al., 1999), rat *Slit1*, *Robo1*, *Robo2* (Kidd et al., 1998), *Rig1*/*Robo3*, and *mRobo4* 3′-untranslated region

(obtained by PCR). Hybridization signals were then detected by alkaline phosphatase (AP) -conjugated anti-DIG antibodies (1/2,000; Roche), which were followed by color development with NBT/BCIP (nitroblue tetrazolium/5-bromo-4-chloro-3-indolyl phosphate) substrate (Promega). After staining, the samples were washed in PBS and post-fixed. Embryos were imaged using a Zeiss Lumar stereomicroscope coupled to an Axiocam digital camera (AxioVision 4.4, Zeiss). The number of embryos examined was at least 3 for each stage.

Immunohistochemistry

For immunohistochemistry, sections were incubated as described previously (Zaffran et al., 2004). The Slit3 antibody, C-20, was a polyclonal antibody raised against a peptide mapping within an internal region of Slit3 of human origin from Santa Cruz, used at 1/50 dilution. The Robo1 and *Robo2* antibodies were polyclonal antibody raised against ectodomains of rat Robo1 (amino acids 1-892) and rat Robo2 (amino acids 1-855) as described previously (Tamada et al., 2008). Secondary antibodies were donkey anti-goat or anti-rabbit, Alexa 488 used at 1/500 dilution (Molecular Probes). Sections were photographed using a Zeiss Axiovert 200M microscope with an Axiocam camera (AxioVision 4.4, Zeiss).

DNA-Binding Assay

For EMSA, the Tbx2 protein was produced with the TNT (T7) -coupled in vitro transcription/translation system (Promega). Production yields of Tbx2 protein was estimated by [^{35}S]methionine labeling. EMSAs were performed in a 20-μl volume on ice with 10^4 cpm (0.5 ng) of either probes. Probes used were double-stranded: TBE1 (5′-TTTTTGTGTGTGAAAGTGCA), TBE 1mut (5′-TTTTTGTcaaaGAAAGTG CA), TBE2 (5′-TAGTGATGGTGTCAAT ACCGG), TBE2mut (5′-TAGTGATGc aaaCAATACCGG), TBE3 (5′-TGCCTTAGCTGTGAACACTAAT) and TBE3mut (5′-TGCCTTAGCTcaatA CACTAAT) from the *Slit3* promoter. Briefly, 3 or 9 μl of Tbx2 protein was gently added and incubated for 30 min with labeled probes and 0.1 mg of non-specific competitor poly[(dC)] in a binding buffer 5× composition of 20% glycerol, 50 mM Tris-HCl pH7.5, 250 mM NaCl, 2.5 mM ethylenediaminetetraacetic acid, 2.5 mM dithiothreitol, and 0.25 mg BSA then loaded on a 4% polyacrylamide gel in 0.25× TBE buffer. The gel was dried and analyzed with a PhosphoImager.

ACKNOWLEDGMENTS

We thank Dr. David Ornitz for his kind and generous gift of the *Slit2* and *Slit3* vectors, and Dr. Alain Chedotal for providing the *Slit1* and *Robo1*, *Robo2*, and *Robo3* vectors. We thank Dr. Fugio Murakami for generously providing Robo1 and Robo2 antibodies. We express our gratitude to Dr. Florence Besse for allowing Caroline Medioni to complete this work during her post-doc in her lab. We are grateful to Dr. Samir Merabet for allowing Bruno Hudry to carry out part of this work. We thank Dr. Robert Kelly for discussion and comments on the manuscript. S.Z. was funded by grants from the "Agence Nationale pour la Recherche" and V.E.P. was funded by the NIH. K.M. was supported by the European Commission under the FP7 CardioGeNet project.

REFERENCES

Bakker ML, Boukens BJ, Mommersteeg MT, Brons JF, Wakker V, Moorman AF, Christoffels VM. 2008. Transcription factor Tbx3 is required for the specification of the atrioventricular conduction system. Circ Res 102:1340–1349.

Biben C, Harvey RP. 1997. Homeodomain factor Nkx2-5 controls left/right asymmetric expression of bHLH gene eHand during murine heart development. Genes Dev 11:1357–1369.

Biben C, Weber R, Kesteven S, Stanley E, McDonald L, Elliott DA, Barnett L, Koentgen F, Robb L, Feneley M, Harvey RP. 2000. Cardiac septal and valvular dysmorphogenesis in mice heterozygous for mutations in the homeobox gene Nkx2-5. Circ Res 87:888–895.

Brose K, Bland KS, Wang KH, Arnott D, Henzel W, Goodman CS, Tessier-Lavigne M, Kidd T. 1999. Slit proteins bind Robo receptors and have an evolutionarily conserved role in repulsive axon guidance. Cell 96:795–806.

Buckingham M, Meilhac S, Zaffran S. 2005. Building the mammalian heart from two sources of myocardial cells. Nat Rev Genet 6:826–835.

Cai CL, Zhou W, Yang L, Bu L, Qyang Y, Zhang X, Li X, Rosenfeld MG, Chen J, Evans S. 2005. T-box genes coordinate regional rates of proliferation and regional specification during cardiogenesis. Development 132:2475–2487.

Calmont A, Ivins S, Van Bueren KL, Papangeli I, Kyriakopoulou V, Andrews WD, Martin JF, Moon AM, Illingworth EA, Basson MA, Scambler PJ. 2009. Tbx1 controls cardiac neural crest cell migration during arch artery development by regulating Gbx2 expression in the pharyngeal ectoderm. Development 136:3173–3183.

Camurri L, Mambetisaeva E, Sundaresan V. 2004. Rig-1 a new member of Robo family genes exhibits distinct pattern of expression during mouse development. Gene Expr Patterns 4:99–103.

Chedotal A. 2007. Slits and their receptors. Adv Exp Med Biol 621:65–80.

Christoffels VM, Habets PE, Franco D, Campione M, de Jong F, Lamers WH, Bao ZZ, Palmer S, Biben C, Harvey RP, Moorman AF. 2000. Chamber formation and morphogenesis in the developing mammalian heart. Dev Biol 223: 266–278.

Christoffels VM, Burch JB, Moorman AF. 2004a. Architectural plan for the heart: early patterning and delineation of the chambers and the nodes. Trends Cardiovasc Med 14:301–307.

Christoffels VM, Hoogaars WM, Tessari A, Clout DE, Moorman AF, Campione M. 2004b. T-box transcription factor Tbx2 represses differentiation and formation of the cardiac chambers. Dev Dyn 229:763–770.

Davenport TG, Jerome-Majewska LA, Papaioannou VE. 2003. Mammary gland, limb and yolk sac defects in mice lacking Tbx3, the gene mutated in human ulnar mammary syndrome. Development 130:2263–2273.

de la Cruz M, Markwald R, editors. 1999. Living morphogenesis of the heart. Boston: Birkhauser.

Dupays L, Kotecha S, Angst B, Mohun TJ. 2009. Tbx2 misexpression impairs deployment of second heart field derived progenitor cells to the arterial pole of the embryonic heart. Dev Biol 333:121–131.

Habets PE, Moorman AF, Clout DE, van Roon MA, Lingbeek M, van Lohuizen M, Campione M, Christoffels VM. 2002. Cooperative action of Tbx2 and Nkx2.5 inhibits ANF expression in the atrioventricular canal: implications for cardiac chamber formation. Genes Dev 16: 1234–1246.

Harrelson Z, Kelly RG, Goldin SN, Gibson-Brown JJ, Bollag RJ, Silver LM, Papaioannou VE. 2004. Tbx2 is essential for patterning the atrioventricular canal and for morphogenesis of the outflow tract during heart development. Development 131:5041–5052.

Harvey RP. 2002. Organogenesis: patterning the vertebrate heart. Nat Rev Genet 3:544–556.

Holmes G, Niswander L. 2001. Expression of slit-2 and slit-3 during chick development. Dev Dyn 222:301–307.

Holmes GP, Negus K, Burridge L, Raman S, Algar E, Yamada T, Little MH. 1998. Distinct but overlapping expression patterns of two vertebrate slit homologs implies functional roles in CNS development and organogenesis. Mech Dev 79: 57–72.

Jia L, Cheng L, Raper J. 2005. Slit/Robo signaling is necessary to confine early neural crest cells to the ventral migratory pathway in the trunk. Dev Biol 282:411–421.

Kelly RG, Buckingham ME. 2002. The anterior heart-forming field: voyage to the arterial pole of the heart. Trends Genet 18:210–216.

Kidd T, Brose K, Mitchell KJ, Fetter RD, Tessier-Lavigne M, Goodman CS, Tear G. 1998. Roundabout controls axon crossing of the CNS midline and defines a novel subfamily of evolutionarily conserved guidance receptors. Cell 92:205–215.

Kidd T, Bland KS, Goodman CS. 1999. Slit is the midline repellent for the robo receptor in Drosophila. Cell 96:785–794.

Kirby M, editor. 2007. Cardiac development. Oxford: Oxford University Press.

Kispert A, Herrmann BG. 1993. The Brachyury gene encodes a novel DNA binding protein. EMBO J 12:3211–3220.

Komuro I, Izumo S. 1993. Csx: a murine homeobox-containing gene specifically expressed in the developing heart. Proc Natl Acad Sci U S A 90:8145–8149.

Liu J, Zhang L, Wang D, Shen H, Jiang M, Mei P, Hayden PS, Sedor JR, Hu H. 2003. Congenital diaphragmatic hernia, kidney agenesis and cardiac defects associated with Slit3-deficiency in mice. Mech Dev 120:1059–1070.

Lyons I, Parsons LM, Hartley L, Li R, Andrews JE, Robb L, Harvey RP. 1995. Myogenic and morphogenetic defects in the heart tubes of murine embryos lacking the homeo box gene Nkx2-5. Genes Dev 9:1654–1666.

MacMullin A, Jacobs JR. 2006. Slit coordinates cardiac morphogenesis in Drosophila. Dev Biol 293:154–164.

Medioni C, Astier M, Zmojdzian M, Jagla K, Semeriva M. 2008. Genetic control of cell morphogenesis during Drosophila melanogaster cardiac tube formation. J Cell Biol 182:249–261.

Medioni C, Senatore S, Salmand PA, Lalevee N, Perrin L, Semeriva M. 2009. The fabulous destiny of the Drosophila heart. Curr Opin Genet Dev 19: 518–525.

Meilhac SM, Esner M, Kerszberg M, Moss JE, Buckingham ME. 2004. Oriented clonal cell growth in the developing mouse myocardium underlies cardiac morphogenesis. J Cell Biol 164: 97–109.

Mesbah K, Harrelson Z, Theveniau-Ruissy M, Papaioannou VE, Kelly RG. 2008. Tbx3 is required for outflow tract development. Circ Res 103:743–750.

Ong LL, Kim N, Mima T, Cohen-Gould L, Mikawa T. 1998. Trabecular myocytes of the embryonic heart require N-cadherin for migratory unit identity. Dev Biol 193:1–9.

Park KW, Morrison CM, Sorensen LK, Jones CA, Rao Y, Chien CB, Wu JY, Urness LD, Li DY. 2003. Robo4 is a vascular-specific receptor that inhibits endothelial migration. Dev Biol 261:251–267.

Qian L, Liu J, Bodmer R. 2005. Slit and Robo control cardiac cell polarity and morphogenesis. Curr Biol 15: 2271–2278.

Santiago-Martinez E, Soplop NH, Patel R, Kramer SG. 2008. Repulsion by Slit and Roundabout prevents Shotgun/E-cadherin-mediated cell adhesion during Drosophila heart tube lumen formation. J Cell Biol 182:241–248.

Simpson JH, Kidd T, Bland KS, Goodman CS. 2000. Short-range and long-range guidance by slit and its Robo receptors. Robo and Robo2 play distinct roles in midline guidance. Neuron 28:753–766.

Singh MK, Christoffels VM, Dias JM, Trowe MO, Petry M, Schuster-Gossler K, Burger A, Ericson J, Kispert A. 2005. Tbx20 is essential for cardiac chamber differentiation and repression of Tbx2. Development 132:2697–2707.

Sinha S, Abraham S, Gronostajski RM, Campbell CE. 2000. Differential DNA binding and transcription modulation by three T-box proteins, T, TBX1 and TBX2. Gene 258:15–29.

Stennard FA, Costa MW, Lai D, Biben C, Furtado MB, Solloway MJ, McCulley DJ, Leimena C, Preis JI, Dunwoodie SL, Elliott DE, Prall OW, Black BL, Fatkin D, Harvey RP. 2005. Murine T-box transcription factor Tbx20 acts as a repressor during heart development, and is essential for adult heart integrity, function and adaptation. Development 132:2451–2462.

Strickland P, Shin GC, Plump A, Tessier-Lavigne M, Hinck L. 2006. Slit2 and netrin 1 act synergistically as adhesive cues to generate tubular bi-layers during ductal morphogenesis. Development 133:823–832.

Takeuchi JK, Mileikovskaia M, Koshiba-Takeuchi K, Heidt AB, Mori AD, Arruda EP, Gertsenstein M, Georges R, Davidson L, Mo R, Hui CC, Henkelman RM, Nemer M, Black BL, Nagy A, Bruneau BG. 2005. Tbx20 dose-dependently regulates transcription factor networks required for mouse heart and motoneuron development. Development 132: 2463–2474.

Tamada A, Kumada T, Zhu Y, Matsumoto T, Hatanaka Y, Muguruma K, Chen Z, Tanabe Y, Torigoe M, Yamauchi K, Oyama H, Nishida K, Murakami F. 2008. Crucial roles of Robo proteins in midline crossing of cerebellofugal axons and lack of their up-regulation after midline crossing. Neural Dev 3:29.

Togi K, Kawamoto T, Yamauchi R, Yoshida Y, Kita T, Tanaka M. 2004. Role of Hand1/eHAND in the dorso-ventral patterning and interventricular septum formation in the embryonic heart. Mol Cell Biol 24:4627–4635.

Wu JY, Feng L, Park HT, Havlioglu N, Wen L, Tang H, Bacon KB, Jiang Z, Zhang X, Rao Y. 2001. The neuronal repellent Slit inhibits leukocyte chemotaxis induced by chemotactic factors. Nature 410:948–952.

Yuan W, Zhou L, Chen JH, Wu JY, Rao Y, Ornitz DM. 1999. The mouse SLIT family: secreted ligands for ROBO expressed in patterns that suggest a role in morphogenesis and axon guidance. Dev Biol 212:290–306.

Yuan W, Rao Y, Babiuk RP, Greer JJ, Wu JY, Ornitz DM. 2003. A genetic model for a central (septum transversum) congenital diaphragmatic hernia in mice lacking Slit3. Proc Natl Acad Sci U S A 100:5217–5222.

Zaffran S, Kelly RG, Meilhac SM, Buckingham ME, Brown NA. 2004. Right Ventricular Myocardium Derives From the Anterior Heart Field. Circ Res 95: 261–268.

Zhang B, Dietrich UM, Geng JG, Bicknell R, Esko JD, Wang L. 2009. Repulsive axon guidance molecule Slit3 is a novel angiogenic factor. Blood 114: 4300–4309.

Focus Article

Diverse functional networks of *Tbx3* in development and disease

Andrew J. Washkowitz, Svetlana Gavrilov, Salma Begum and Virginia E. Papaioannou*

The T-box transcription factor Tbx3 plays multiple roles in normal development and disease. In order to function in different tissues and on different target genes, Tbx3 binds transcription factors or other cofactors specific to temporal or spatial locations. Examining the development of the mammary gland, limbs, and heart as well as the biology of stem cells and cancer provides insights into the diverse and common functions that Tbx3 can perform. By either repressing or activating transcription of target genes in a context-dependent manner, Tbx3 is able to modulate differentiation of immature progenitor cells, control the rate of cell proliferation, and mediate cellular signaling pathways. Because the direct regulators of these cellular processes are highly context-dependent, it is essential that Tbx3 has the flexibility to regulate transcription of a large group of targets, but only become a active on a small cohort of them at any given time or place. Moreover, *Tbx3* must be responsive to the variety of different upstream factors that are present in different tissues. Only by understanding the network of genes, proteins, and molecules with which Tbx3 interacts can we hope to understand the role that Tbx3 plays in normal development and how its aberrant expression can lead to disease. Because of its myriad functions in disparate developmental and disease contexts, *Tbx3* is an ideal candidate for a systems-based approach to genetic function and interaction.

How to cite this article:
WIREs Syst Biol Med 2012, 4:273–283. doi: 10.1002/wsbm.1162

INTRODUCTION

The T-box family of genes is an ancient and evolutionarily conserved group of transcription factor genes defined by their DNA-binding domain, known as the T-box. First discovered in mouse, the T-box family derives its name from the mesoderm-specification gene *Brachyury* (*T*).[1] Each T-box factor binds a specific core sequence, the T-half-site, found in the promoters of target genes, often in tandem or in different orientations. These T-half sites are accompanied by other transcription factor binding sites, giving them specificity.[2] It is the interactions with these other transcription factors that allow T-box genes to play a variety of roles during disparate development processes.[3]

*Correspondence to: vep1@columbia.edu
Department of Genetics and Development, Columbia University Medical Center, New York, NY, USA

The 17 members of the T-box gene family in mouse have been grouped into five subfamilies based on sequence similarity. *Tbx3* is a member of the Tbx2 subfamily, a group that also includes *Tbx2*, *Tbx4*, and *Tbx5*. This subfamily arose during a tandem duplication event followed by chromosomal duplication and dispersion. *Tbx3* and *Tbx2* are closely related members sharing 90% amino acid identity in the T-box and having many overlapping areas of expression.[4]

During normal mouse development, *Tbx3* expression begins in the inner cell mass of the blastocyst, and then appears in the extraembryonic mesoderm during gastrulation. During organogenesis, *Tbx3* is expressed in the nervous system, skeleton, eye, heart, kidney, lungs, pancreas, and mammary gland.[5] There are two known isoforms of Tbx3 that result from differential splicing in the second intron, Tbx3 and Tbx3+2a, which includes 20 extra amino acids in the DNA binding domain of the protein.[6] While both have been detected, there is no known unique role for

one or the other specific isoform in development. A null allele of *Tbx3* has been generated and homozygous mutant mice have defects in a number of structures such as the limbs, mammary glands, and heart. These mutants die by embryonic day (E) 16.5 with greater than 50% dead by E11.5, most likely because of yolk sac defects. A number of different organ-specific effector genes and transcription factors are aberrantly expressed in these mutants.[7]

In humans, *TBX3* mutations have been linked to ulnar-mammary syndrome (UMS, MIM 181450), a disease with variable penetrance characterized by shortened forelimbs, defective apocrine gland and genital development, and heart abnormalities.[8,9] This phenotype is similar to that seen in *Tbx3* mutant mice, although in humans the phenotype is seen in heterozygotes whereas in mice, only homozygotes have severe defects. The spectrum of affected organs in UMS is characteristic of diseases associated with T-box factors and is indicative of the complex transcriptional networks in which these genes participate during development.[10] *Tbx3* mutations have also recently been found to impact the pluripotency of embryonic stem cells and the invasiveness of cancer.[11–15]

For *Tbx3* to play a part in the development of so many different organs, it must interact with a network of genes and proteins specific to each spatial and temporal location of action. While Tbx3 most likely binds to its target promoters as a monomer, other factors are known to enhance Tbx3-mediated transcriptional activation or repression, hinting at a large network of factors that give specificity to Tbx3 activity.[16,17] In addition, Tbx3 has been shown to have both activation and repression domains which may be modulated by other cofactors to ensure the proper function of the protein in each context.[18] Only by understanding the function of *Tbx3* by a systems approach in a variety of developmental contexts can we hope to unravel the network of genes of which *Tbx3* is a part.

Tbx3 IN DEVELOPMENT

Tbx3 in Mammary Gland Development

The initiation and growth of the mammary gland is dependent on fibroblast growth factor (FGF) and WNT signaling and involves reciprocal interactions between the epidermis and the underlying mesenchyme in bilateral 'milk lines'. Mesenchyme induces the formation of mammary placodes in five specialized areas along each flank of the embryo. The epidermal placode forms a mammary bud which in turn influences the surrounding mesenchyme to form the primary mammary mesenchyme. *Tbx3* is initially expressed in the mesenchyme of the milk line prior to placode formation and then appears in the mammary placodes as one of the earliest markers of mammary epithelium. Expression in the mesenchyme gradually decreases while epithelial expression is maintained.[5,7,19,20] During late gestation, *Tbx3* is expressed in mammary mesenchyme surrounding the nipple (Figure 1(a)) and in postnatal females it has been detected in virgin, pregnant, lactating and involuting mammary glands.[21]

UMS in humans is characterized by variable abnormalities of the mammary gland ranging from normal to hypoplastic breasts, with missing or supernumerary nipples. A loss of function mutation of mouse *Tbx3* results in the failure of mammary placode induction in homozygous females and aplasia or a decrease in the extent of branching of the ductal tree in heterozygous females. This effect on the developing mammary gland is independent of the repression of the Tbx3 target gene $p19^{ARF}$.[19] Although there is no evidence regarding the direct regulation of *Tbx3* in mammary gland development or on its direct downstream targets, both WNT and FGF signaling feed into the *Tbx3* regulatory network. Fgfr2b and Fgfr1/2c are upstream of *Tbx3* expression, and *Wnt10b*, *Lef1*, and FGF signaling are all lost in the absence of *Tbx3*,[7,20] indicating feed-forward and feedback loops of regulation for the maintenance and/or induction of *Tbx3* expression (Figure 2). Similarly, *Bmp4* overexpression inhibits *Tbx3* expression in the mammary mesenchyme while, reciprocally, overexpression of *Tbx3* represses *Bmp4*.[22] Tbx3, in combination with FGF signaling, may be upstream of *Nrg3*, a growth factor implicated in the initiation of mammary placodes, but the evidence is circumstantial.[23,24]

The closely related T-box gene, *Tbx2*, is expressed in the mesenchyme but not the epithelium during mammary development and although mutation of *Tbx2* by itself does not result in a mammary gland phenotype, a genetic interaction with *Tbx3* is evident in double heterozygous females by an exacerbation of mammary aplasia.[19]

Tbx3 in Limb Development

In vertebrates, limbs develop as a set of lateral bulges from the lateral plate mesoderm on either side of body axis. The initial events in limb development involve proliferation of the lateral plate mesoderm and induction of the apical ectodermal ridge (AER).[25] Three signaling centers, the AER, the zone of polarizing activity (ZPA) and the nonridge ectoderm, are necessary for growth and patterning of limb buds, processes which involve complex signaling through the FGF and Sonic hedgehog (SHH) pathways.[26] All four

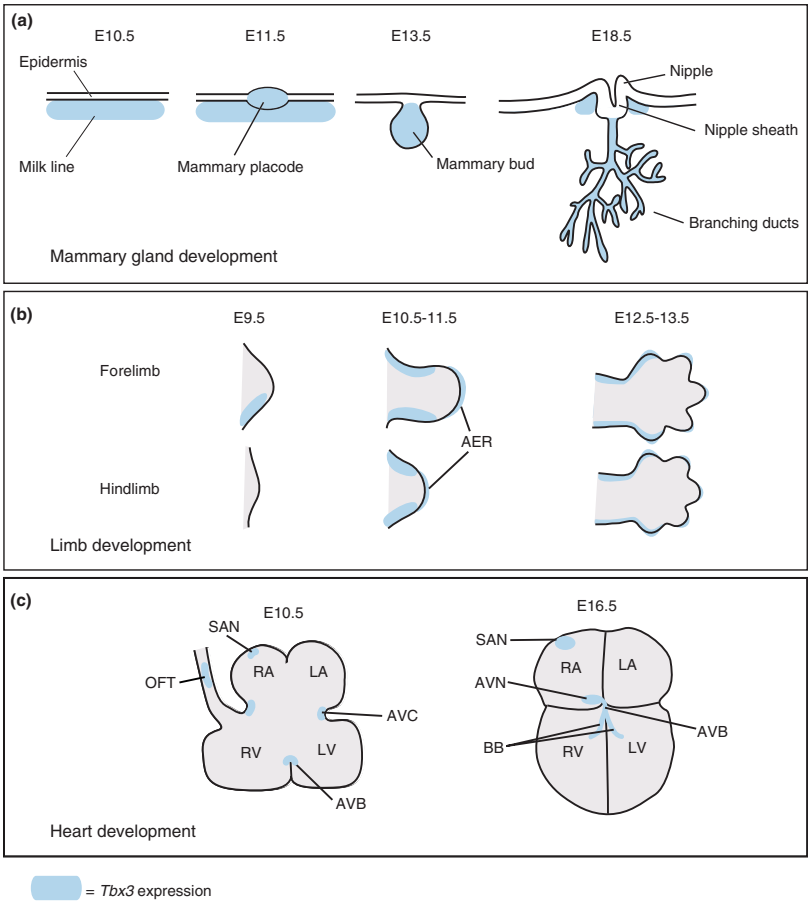

FIGURE 1 | Expression of *Tbx3* (blue) in developing organ systems at different stages. (a) In mammary gland, *Tbx3* is first expressed at E10.5 in the mesenchymal milk line and then appears as one of the earliest markers of the epithelial thickenings known as the mammary placodes. It continues to be expressed in the epithelium as the placode expands into the mammary bud and eventually forms the branching ductal system. Near term (E18.5), mesenchyme surrounding the nipple expresses *Tbx3*. (b) *Tbx3* is first expressed in the posterior margin of the early limb buds and then in the posterior and anterior margins of both fore and hind limbs by E10.5. It is also expressed in the AER, continuously at first and then limited to the tips of the digits by E12.5. (c) *Tbx3* is expressed in the AVC, SAN, OFT and atrioventricular bundle (AVB) starting around E10.5. It fully delineates the cardiac conduction system at E14.5 with expression in the SAN, AVN, AVB, and the bundle branches (BB).

members of the *Tbx2* subfamily are expressed during limb development. In mice, *Tbx3* expression is first detected at the posterior margin of the early limb buds, and shortly thereafter in the anterior and posterior proximal mesenchyme and AER. As the limb bud elongates, *Tbx3* anterior and posterior expression domains are expanded in the mesenchyme. By E13.5, expression in the AER is limited to the tips of the digits[5,27](Figure 1(b)). A similar pattern is observed in the chick.[28–31]

In UMS, posterior structures of the fore limb, for example, the ulna and the fifth digit are missing.[8] Mice homozygous for the *Tbx3* null allele similarly exhibit missing or abnormal posterior fore limb

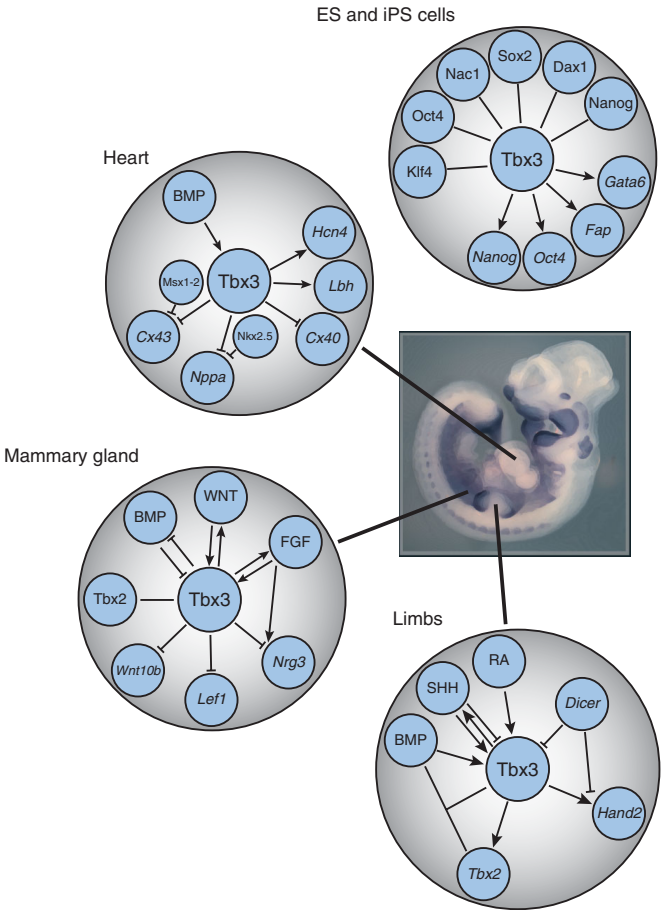

FIGURE 2 | Diagram of known regulatory pathways and downstream targets of *Tbx3* in the development of heart, mammary gland and limbs, as well as in embryonic and iPS stem cells. The variety of factors involved illustrates the context-dependent nature of Tbx3 interactions.

elements, but unlike UMS also show severe hind limb abnormalities.[7]

Little is known about the direct regulation of *Tbx3* in limb development. Studies in the chick indicate that *Tbx3* expression in the posterior of the limb buds is controlled via different mechanisms than in the anterior. The posterior domain of *Tbx3* expression depends on the ZPA signaling cascade and is regulated positively by Shh, but the anterior expression domain is negatively regulated by Shh and is dependent on continuous signaling by anteriorly produced BMPs, suggesting a potential role for *Tbx3* in the antero-posterior patterning of the limb.[31] A recent study places retinoic acid (RA) signaling upstream of *Tbx3* in the limbs (RD Ballim, C Mendelsohn, VE Papaioannou, S Prince, personal communication). In mice, *Shh* and *Hand2* appear to be downstream targets of Tbx3.[7] Studies in chick have implicated *Tbx3* in positioning the limb along the main body axis through a genetic interplay between *Hand2* and *Gli3*, but the interrelationship of these genes is not clear.[32] Inactivation of *Dicer* in mice

results in a posterior shift and a delayed formation of hind limb bud which is accompanied by altered transcription of *Tbx3*, *Hand2* and *Gli3*. This study showed that microRNA is also capable of inhibiting *Tbx3* and *Hand2* expression *in vitro*. Hence, *Tbx3* and *Hand2* might be downstream of Dicer-mediated regulation in limb bud positioning[33] (Figure 2).

Tbx2 has a similar spatiotemporal expression pattern in limb buds in both chick and mice[27,29–31] and is downregulated in *Tbx3* mutants.[7] Experiments in the chick have shown that *Tbx3* and *Tbx2* together specify the identity of posterior digits, acting through regulation of interdigital BMP signaling,[34] possibly indicating a genetic interaction.

Tbx3 in Heart Development

The transformation from linear heart tube to the four-chambered heart is accomplished by the differential cell growth and distinct gene programs adopted by different regions in the heart. Starting at E9.5, the working myocardium cells undergo rapid and sustained proliferation to form the muscular chambers of the heart. The intervening regions of non-chamber myocardium, meanwhile, are held relatively mitotically inactive to form the constrictions between the chambers that will eventually become components of the cardiac conduction system (CCS).

Tbx3 expression is first detected in the heart at E8.5 and as the heart undergoes looping *Tbx3* expression delineates the developing nodal conduction system with expression in the sinoatrial node (SAN) and atrioventricular node (AVN), as well as the endocardial cushions in the atrioventricular canal (AVC) and the mesenchyme of the outflow tract (OFT) (Figure 1(c)). This expression pattern is almost identical to that of *Tbx2* although no genetic interaction has been demonstrated in this tissue. *Tbx3* is thought to have two distinct roles in the developing CCS: first, the modulation of cell division resulting in constrictions between chambers, and secondly, the repression of a chamber-specific gene program and concomitant promotion of a conduction system-specific gene program. Despite the assumption that *Tbx3* mutant embryos die at midgestation due to yolk sac deficiencies, their hearts have altered morphology including double outlet right ventricle, incomplete ventricular septation, and delayed aortic arch formation.[35] These malformations are a result of increased cell division in the AVC and OFT leading to a lack of constriction.[36] Mutant hearts also have ectopic expression of chamber myocardium genes, such as *Cx40*, *Cx43,* and *Nppa*, in the non-chamber AVC, a phenotype resembling that of *Tbx2* mutants. Conversely, CCS-specific genes *Hcn4* and *Lbh* are upregulated in regions where *Tbx3* ectopic expression is induced, and functional conduction tissue develops[37] (Figure 2).

On a protein level, it appears that Tbx3 regulates its targets by cooperatively binding their promoters along with other transcription factors. For example, Tbx3 has been shown to bind cooperatively with Msx1 and Msx2 in the repression of *Cx43*.[16] Similarly, Tbx2 has been shown to bind to Nkx2.5 and repress *Nppa*, a known Tbx3 target. However, in the absence of Tbx2, Tbx5 binds to Nkx2.5 and activates *Nppa*[38] (Figure 2). This suggests a regulatory mechanism whereby binding competition with a network of transcription factors determines which gene program will be expressed in a given tissue.

Tbx3 mutant heart abnormalities result from increased cell division in the regions of *Tbx3* expression implicating *Tbx3* in the regulation of cell dynamics in the process of heart looping and growth. Conversely, despite its role in the regulation of the gene expression profile of the CCS, *Tbx3* mutant hearts have normal conduction velocity and several of the conductive structures are present. This discrepancy is likely due to the functional overlap of *Tbx3* with *Tbx2*, which has been shown to bind to and regulate many of the same targets. Nonetheless, some patients with UMS show conduction defects in line with abnormal development of conduction structures.[9] These defects are similar to those in mice mutant for *Tbx2*, highlighting the potential functional overlap with *Tbx3* in the development of the CCS.[39]

Tbx3 IN STEM CELL BIOLOGY

In addition to its key roles in development, *Tbx3* also plays a role in both the establishment and maintenance of pluripotency in embryonic stem (ES) cells and induced pluripotent stem (iPS) cells. ES cells are derived from the inner cell mass (ICM) of preimplantation blastocysts and rely on the LIF/STAT3 pathway to maintain pluripotency. In the embryo, *Tbx3* is first expressed in the ICM[7] and this expression is recapitulated in ES cells. *Tbx3* expression is highest when ES cells are undifferentiated and decreases as cells differentiate into embryoid bodies, suggesting its importance in the maintenance of pluripotency.[13]

In ES cells, *Oct4* and *Nanog*, two recognized markers of pluripotency, act as repressors of differentiation toward a trophectoderm and endodermal fate, respectively. Similarly, *Tbx3* is able to block differentiation into mesoderm, ectoderm, trophectoderm, and neural crest cell fates.[11,13] ES cells treated with shRNA against *Tbx3* downregulate both *Oct4* and *Nanog,* and show differentiated morphology and reduced

alkaline phosphatase activity. To function as a mediator of pluripotency, Tbx3 is able to act with Klf4 to regulate the expression of *Nanog* specifically, lying at the center of a LIF-independent pluripotency pathway in ES cells.[40] In addition to blocking differentiation, *Tbx3* also appears to play a role in the differentiation of ES cells into extraembryonic endoderm (ExEn) as overexpression of *Tbx3* in ES cells induces differentiation into cells with ExEn morphology as well as expression of ExEn markers such as *Gata6*.[13] This dual functionality suggests that *Tbx3* takes part in a complex regulatory network where it is able to function both as a repressor of specific cell fates and an activator of others. In this way, ES cells are poised to differentiate into a given cell type quickly when the proper signals are received: the relief of one repression module allows the activation of another. The complexity of *Tbx3* in the pluripotency network is evident as the promoter of *Tbx3* itself is bound by a number of transcription factors at the core of the genetic regulation circuit of pluripotency[12] (Figure 2). Mechanistically, Tbx3 is able to regulate transcription at the level of DNA, but also on an epigenetic level: Tbx3 binding to the *Gata6* promoter is necessary to activate transcription but Tbx3 is also able to mediate the histone methylation of H3K27me3 at the *Gata6* promoter.[13]

In addition to the maintenance of pluripotency, *Tbx3* may also play a role in the establishment of pluripotency in iPS cells. Fibroblasts with induced expression of *Tbx3* in combination with the reprogramming factors *Sox2*, *Oct4,* and *Klf4* express pluripotency markers more rapidly than fibroblasts without. Moreover, iPS cells with induced *Tbx3* expression contributed to enhanced germ line contribution and transmission.[41]

Tbx3 IN CANCER

Tbx3 is amplified and/or overexpressed in many tumors[42–55] (Table 1). Accumulating evidence suggests that *Tbx3* contributes to tumorigenesis through interaction with components of several major oncogenic pathways (Figure 3), some with which *Tbx3* is known to interact in other contexts. Activation of the canonical Wnt-β-catenin pathway has been linked to many types of cancer. β-Catenin plays dual roles depending on intracellular localization: in the nucleus it acts as the main effector of WNT signaling and at the plasma membrane as a component of adherens junctions where it links E-cadherin with the actin cytoskeleton.[56] *Tbx3* is a downstream target of the Wnt-β-catenin pathway in liver tumorigenesis, and recent evidence suggests that there is a feedback loop by which Tbx3 can upregulate β-catenin.[46] Thus, *Tbx3* could be a critical mediator of cellular responses to proliferative and anti-apoptotic signals delivered by β-catenin. Interestingly, Tbx3 represses E-cadherin,[47] which has been implicated in metastasis of invasive epithelial tumors.[57] Together these findings suggest that *Tbx3* can enhance tumor invasiveness through both E-cadherin repression and β-catenin upregulation. Additionally, phorbol ester 12-*O*-tetradecanoylphorbol-13-acetate (TPA) treatment leads to downregulation of E-cadherin, and as TPA activates *TBX3* in a PKC-dependent manner,[58] it is possible that upregulation of *TBX3* is mediating this process.

As in normal mammary gland development, FGF signaling is upstream of *TBX3* expression in breast cancer.[61] Moreover, estrogen can upregulate TBX3 levels in breast cancer via paracrine FGF9–FGFR3 signaling and the upregulation of TBX3 expands the pool of functional estrogen receptor (ER) -negative cancer stem-like cells. This implies that resistance to anti-estrogen therapy which is common in breast cancer might be accompanied by an increase in FGF–TBX3 signaling and a consequent increase in the proportion of cancer stem-like cells. Thus, targeting of the FGF–TBX3 pathway could be a useful strategy for refractory breast cancers. Moreover, TBX3 can affect the equilibrium of cell type differentiation within breast epithelial cancers, which is context-dependent for a given cancer cell population.[62] Together these studies suggest that *TBX3* could play important roles in cell plasticity within breast cancer.

Upregulation of *Tbx3* suppresses the expression of *ARF* ($p19^{ARF}$ in mouse and $p14^{ARF}$ in humans) and possibly $p16^{INK4a}$ and promotes the bypass of senescence through inactivation of p53 via ARF-MDM2-p53 tumor suppressor pathway.[15,23,42,63,64] Tbx3 can also directly repress the $p21^{Cip1/WAF1}$ promoter[6] and bypass senescence independently of p53. The knockdown of Tbx3 in both melanoma and breast cancer cell lines leads to reduction in anchorage-independent growth, migration and tumor formation, and a decrease in pro-senescence factors that results in increased proliferation.[14] It was previously suggested that Tbx3 and its splice variant Tbx3+2a, are functionally distinct in inhibition of senescence.[42] However, a subsequent study convincingly demonstrated that both isoforms function as anti-senescence factors, bind the same T-half-site and target the same genes.[6] Also, Tbx3 can promote Ras and c-Myc associated transformation.[15,65] These findings together imply that Tbx3 cooperates with oncogenic Ras and c-Myc by suppressing ARF activity. A recent study identified *GATA3* and *GLI3* as

TABLE 1 | Incidence of *Tbx3* Expression in Human Cancers and Corresponding Normal Tissue in the Mouse

Cancer	No. (%) of Specimens with *TBX3* Expression	Method of Detection	Corresponding Normal Expression of *Tbx3*	References
Breast	48/50 (96)	WB and real time PCR	Mammary epithelium and mesenchyme of developing gland	42,44,51
Melanoma[1]	7/12 (58)	WB	Melanocytes[2]	47
Pancreatic	7	Microarray	Developing pancreas	53,55,59
Cervical	48	Microarray	Unknown	45
Ovarian	21/29 (70)	MALDI-Tof-MS	Not detected (unpublished)	44
Prostate	ND	GWAS	Adult prostate	42,43,49
Colorectal	1	RT-PCR	Adult colon	42,52
Liver	(70–87)	Microarray and WB	Hepatoblasts	46,60
Gastric	1	Microarray	Developing stomach	50,59
Glioblastoma	ND	Microarray	Developing CNS	54
Pheochromocytoma	ND	Microarray	Adult adrenal gland	42,48

GWAS, genome-wide association study; ND, not determined; MALDI-Tof-MS, matrix-assisted laser desorption/ionization time of flight mass spectrometry; RT-PCR, reverse transcriptase–polymerase chain reaction; WB, western blot.
Cancers listed are those in which *TBX3* has been shown to be amplified and/or overexpressed.
[1]Melanoma cell lines *in vitro*.
[2]Also present in human melanocyte cell lines.

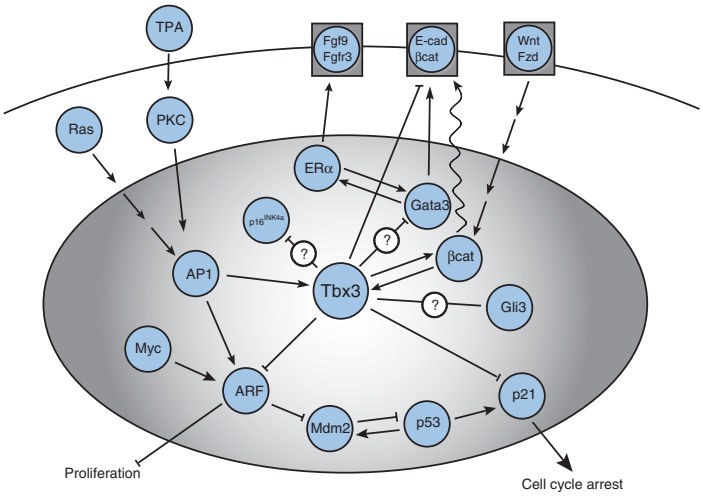

FIGURE 3 | The Tbx3 interactome in cancer. Known and hypothetical molecular interactions between Tbx3 and components of several signaling pathways important in oncogenesis are drawn from a variety of contexts.

putative TBX3 downstream targets in breast cancer.[66] Although chromatin immunoprecipitation analysis confirmed direct binding of TBX3 to both of these targets, the functional significance of these findings is not known. Interestingly, GATA3 was shown to inhibit breast cancer metastasis by directly upregulating E-cadherin levels.[67] It is tempting to speculate that TBX3 could be repressing *GATA3* or alternatively affecting E-cadherin levels by binding to both GATA3 and E-cadherin. *Gli3* belongs to the hedgehog (Hh) signaling network and is required for normal mammary bud formation.[68] As deregulation of Hh

pathway is implicated in a wide variety of aggressive and metastatic cancer, the predicted Tbx3–Gli3 interaction warrants further investigation.

CONCLUSION

The *Tbx3* transcriptional network is highly context dependent. This flexibility allows the protein to assume different functions that are specialized for the time and place of expression. Nonetheless, there are common themes that run through the network that hint at more general functions for the gene. In the heart and ES cells, *Tbx3* blocks the differentiation of multipotent tissues. This inhibition of differentiation may play a role in cancers when *Tbx3* is overexpressed or amplified: induction of an undifferentiated 'stem-like' cancer cell by Tbx3 may initiate the process of tumor formation and cell migration. This repressive function is evident in *in vitro* assays where a transcriptional repression module has been noted.[69] Conversely, Tbx3 can induce differentiation in different contexts. In ES cells, for example, Tbx3 promotes differentiation into ExEn. In the mammary gland as well, Tbx3 induces differentiation of the mammary placodes. Indeed, by binding to tissue-specific transcription factors, Tbx3 may be able to either repress or activate the differentiation of multipotent progenitors in a context-dependent manner.

Tbx3 also appears to play a role in cell proliferation in a number of different contexts: in the heart, *Tbx3* depletion leads to an excess of cell proliferation in the structures where it is normally expressed. Cell proliferation might also be altered in the limb in the absence of *Tbx3* as mice deficient for the gene have shortened fore and hind limbs, a phenotype that is largely recapitulated in human UMS. This role is highlighted in cancers where *TBX3* is overexpressed or amplified as it results in the bypass of senescence through inactivation of the p53 pathway, while the knockdown of TBX3 leads to an increase in proliferation.

Finally, *Tbx3* appears to play a role as a mediator of cellular signaling by modulating a number of signaling pathways. Tbx3 can control WNT signaling in the mammary gland and limb buds, as well as in various cancer models. FGF and SHH signaling are also modulated by Tbx3 in various contexts. As with cell proliferation, Tbx3 may be able to regulate these pathways generally, but rely on specific signals to impart specificity to this function.

In order for it to assume such distinct functions, Tbx3 interacts with other factors to give a regional and temporal specificity to its action. Given the evidence of Tbx3 functioning in protein complexes with transcription factors of myriad different families and as a competitor for binding to transcriptional targets, it is reasonable to conclude that Tbx3 is able to mediate a specific set of activities, but that available cofactors determine how it will act in specific contexts. The necessity of these cofactors in determining what function Tbx3 will have makes it an important target for studying with a systems-based approach.

REFERENCES

1. Herrmann BG, Labeit S, Poustka A, King TR, Lehrach H. Cloning of the *T* gene required in mesoderm formation in the mouse. *Nature* 1990, 343:617–622.
2. Tada M, Smith JC. T-targets: clues to understanding the functions of T-box proteins. *Dev Growth Differ* 2001, 43:1–11.
3. Papaioannou VE, Silver LM. The T-box gene family. *Bioessays* 1998, 20:9–19.
4. Agulnik SI, Garvey N, Hancock S, Ruvinsky I, Chapman DL, Agulnik I, Bollag R, Papaioannou V, SIlver LM. Evolution of mouse *T-box* genes by tandem duplication and cluster dispersion. *Genetics* 1996, 144:249–254.
5. Chapman DL, Garvey N, Hancock S, Alexiou M, Agulnik SI, Gibson-Brown JJ, Cebra-Thomas J, Bollag RJ, Silver LM, Papaioannou VE. Expression of the T-box family genes, *Tbx1-Tbx5*, during early mouse development. *Dev Dyn* 1996, 206:379–390.
6. Hoogaars WM, Barnett P, Rodriguez M, Clout DE, Moorman AF, Goding CR, Christoffels VM. TBX3 and its splice variant TBX3 + exon 2a are functionally similar. *Pigment Cell Melanoma Res* 2008, 21:379–387.
7. Davenport TG, Jerome-Majewska LA, Papaioannou VE. Mammary gland, limb and yolk sac defects in mice lacking *Tbx3*, the gene mutated in human ulnar mammary syndrome. *Development* 2003, 130:2263–2273.
8. Bamshad M, Lin RC, Law DJ, Watkins WC, Krakowiak PA, Moore ME, Franceshini P, Lala R, Holmes LB, Gebuhr TC, et al. Mutations in human *TBX3* alter limb, apocrine and genital development in ulnar-mammary syndrome. *Nat Genet* 1997, 16:311–315.
9. Linden H, Williams R, King J, Blair E, Kini U. Ulnar Mammary syndrome and *TBX3*: expanding the phenotype. *Am J Med Genet A* 2009, 149A:2809–2812.
10. Packham EA, Brook JD. T-box genes in human disorders. *Hum Mol Genet* 2003, 1:R37–R44.

11. Ivanova N, Dobrin R, Lu R, Kotenko I, Levorse J, DeCoste C, Schafer X, Lun Y, Lemischka IR. Dissecting self-renewal in stem cells with RNA interference. *Nature* 2006, 442:533–538.
12. Kim J, Chu J, Shen X, Wang J, Orkin SH. An extended transcriptional network for pluripotency of embryonic stem cells. *Cell* 2008, 132:1049–1061.
13. Lu R, Yang A, Jin Y. Dual functions of T-box 3 (Tbx3) in the control of self-renewal and extraembryonic endoderm differentiation in mouse embryonic stem cells. *J Biol Chem* 2011, 286:8425–8436.
14. Peres J, Davis E, Mowla S, Bennett DC, Li JA, Wansleben S, Prince S. The highly homologous T-box transcription factors, TBX2 and TBX3, have distinct roles in the oncogenic process. *Genes Cancer* 2010, 1:272–282.
15. Rowley M, Grothey E, Couch FJ. The role of Tbx2 and Tbx3 in mammary development and tumorigenesis. *J Mammary Gland Biol Neoplasia* 2004, 9:109–118.
16. Boogerd KJ, Wong LY, Christoffels VM, Klarenbeek M, Ruijter JM, Moorman AF, Barnett P. Msx1 and Msx2 are functional interacting partners of T-box factors in the regulation of Connexin43. *Cardiovasc Res* 2008, 78:485–493.
17. Coll M, Seidman JG, Muller CW. Structure of the DNA-bound T-box domain of human TBX3, a transcription factor responsible for ulnar-mammary syndrome. *Structure* 2002, 10:343–356.
18. Carlson H, Ota S, Campbell CE, Hurlin PJ. A dominant repression domain in Tbx3 mediates transcriptional repression and cell immortalization: relevance to mutations in Tbx3 that cause ulnar-mammary syndrome. *Hum Mol Genet* 2001, 10:2403–2413.
19. Jerome-Majewska LA, Jenkins GP, Ernstoff E, Zindy F, Sherr CJ, Papaioannou VE. *Tbx3*, the ulnar-mammary syndrome gene, and *Tbx2* interact in mammary gland development through a p19Arf/p53-independent pathway. *Dev Dyn* 2005, 234:922–933.
20. Eblaghie MC, Song SJ, Kim JY, Akita K, Tickle C, Jung HS. Interactions between FGF and Wnt signals and *Tbx3* gene expression in mammary gland initiation in mouse embryos. *J Anat* 2004, 205:1–13.
21. Platonova N, Scotti M, Babich P, Bertoli G, Mento E, Meneghini V, Egeo A, Zucchi I, Merlo GR. TBX3, the gene mutated in ulnar-mammary syndrome, promotes growth of mammary epithelial cells via repression of p19ARF, independently of p53. *Cell Tissue Res* 2007, 328:301–316.
22. Cho KW, Kim JY, Song SJ, Farrell E, Eblaghie MC, Kim HJ, Tickle C, Jung HS. Molecular interactions between Tbx3 and Bmp4 and a model for dorsoventral positioning of mammary gland development. *Proc Natl Acad Sci U S A* 2006, 103:16788–16793.
23. Howard B, Ashworth A. Signalling pathways implicated in early mammary gland morphogenesis and breast cancer. *PLoS Genet* 2006, 2:e112.
24. Howard B, Panchal H, McCarthy A, Ashworth A Identification of the *scaramanga* gene implicates Neuregulin3 in mammary gland specification. *Genes Dev* 2005, 19:2078–2090.
25. King M, Arnold JS, Shanske A, Morrow BE. T-genes and limb bud development. *Am J Med Genet A* 2006, 140:1407–1413.
26. Martin GR. The roles of FGFs in the early development of vertebrate limbs. *Genes Dev* 1998, 12:1571–1586.
27. Gibson-Brown JJ, Agulnik SI, Chapman DL, Alexiou M, Garvey N, Silver LM, Papaioannou VE. Evidence of a role for *T-box* genes in the evolution of limb morphogenesis and the specification of forelimb/hindlimb identity. *Mech Dev* 1996, 56:93–101.
28. Gibson-Brown JJ, Agulnik SI, Silver LM, Niswander L, Papaioannou VE. Involvement of T-box genes *Tbx2-Tbx5* in vertebrate limb specification and development. *Development* 1998, 125:2499–2509.
29. Gibson-Brown JJ, Agulnik SI, Silver LM, Papaioannou VE. Expression of T-box genes *Tbx2-Tbx5* during chick organogenesis. *Mech Dev* 1998, 74:165–169.
30. Logan M, Simon HG, Tabin C. Differential regulation of T-box and homeobox transcription factors suggests roles in controlling chick limb-type identity. *Development* 1998, 125:2825–2835.
31. Tümpel S, Sanz-Ezquerro JJ, Isaac A, Eblaghie MC, Dobson J, Tickle C. Regulation of *Tbx3* expression by anteroposterior signalling in vertebrate limb development. *Dev Biol* 2002, 250:251–262.
32. Rallis C, Buono JD, Logan MPO. *Tbx3* can alter limb position along the rostrocaudal axis of the developing embryo. *Development* 2005, 132:1961–1970.
33. Zhang Z, O'Rourke JR, McManus MT, Lewandoski M, Harfe BD, Sun X. The microRNA-processing enzyme *Dicer* is dispensable for somite segmentation but essential for limb bud positioning. *Dev Biol* 2011, 351:254–265.
34. Suzuki T, Takeuchi J, Koshiba-Takeuchi K, Ogura T. *Tbx* genes specify posterior digit identity through Shh and BMP signaling. *Dev Cell* 2004, 6:43–53.
35. Mesbah K, Harrelson Z, Theveniau-Ruissy M, Papaioannou VE, Kelly RG. Tbx3 is required for outflow tract development. *Circ Res* 2008, 103:743–750.
36. Ribeiro I, Kawakami Y, Buscher D, Raya A, Rodriguez-Leon J, Morita M, Rodriguez Esteban C, Izpisua Beloment JC. Tbx2 and Tbx3 regulate the dynamics of cell proliferation during heart remodeling. *PLoS One* 2007, 2:e398.
37. Hoogaars WM, Engel A, Brons JF, Verkerk AO, de Lange FJ, Wong LY, Bakker ML, Clout DE, Wakker V, Barnett P, et al. Tbx3 controls the sinoatrial node gene program and imposes pacemaker function on the atria. *Genes Dev* 2007, 21:1098–1112.

38. Habets PEMH. Cooperative action of Tbx2 and Nkx2.5 inhibits ANF expression in the atrioventricular canal: implications for cardiac chamber formation. *Genes Dev* 2002, 16:1234–1246.
39. Aanhaanen WTJ, Boukens BJD, Sizarov A, Wakker V, de Gier-de Vries C, Anderson RH, Kispert A, Moorman AF, Christoffels VM. Defective Tbx2-dependent patterning of the atrioventricular canal myocardium causes accessory pathway formation in mice. *J Clin Invest* 2011, 121:534–544.
40. Niwa H, Ogawa K, Shimosato D, Adachi K. A parallel circuit of LIF signalling pathways maintains pluripotency of mouse ES cells. *Nature* 2009, 460:118–122.
41. Han J, Yuan P, Yang H, Zhang J, Soh BS, Li p, Lim SL, Cao S, Tay J, Orlov YL, et al. Tbx3 improves the germline competency of induced pluripotent stem cells. *Nature* 463:1096–1100.
42. Fan W, Huang X, Chen C, Gray J, Huang T. *TBX3* and its isoform *TBX3+2a* are functionally distinctive in inhibition of senescence and are overexpressed in a subset of breast cancer cell lines. *Cancer Res* 2004, 64:5132–5139.
43. Gudmundsson J, Besenbacher S, Sulem P, Gudbjartsson DF, Olafsson I, Arinbjarnarson S, Agnarsson BA, Benediktsdottir KR, Isaksson HJ, Kostic JP, et al. Genetic correction of PSA values using sequence variants associated with PSA levels. *Sci Transl Med* 2010, 2:62ra92.
44. Lomnytska M, Dubrovska A, Hellman U, Volodko N, Souchelnytskyi S. Increased expression of cSHMT, Tbx3 and utrophin in plasma of ovarian and breast cancer patients. *Int J Cancer* 2006, 118:412–421.
45. Lyng H, Brovig RS, Svendsrud DH, Holm R, Kaalhus O, Knutstad K, Oksefjell H, Sundfor K, Kristensen GB, Stokke T. Gene expressions and copy numbers associated with metastatic phenotypes of uterine cervical cancer. *BMC Genom* 2006, 7:268.
46. Renard CA, Labalette C, Armengol C, Cougot D, Wei Y, Cairo S, Pineau P, Neuveut C, de Reynies A, Dejean A, et al. Tbx3 is a downstream target of the Wnt/β-catenin pathway and a critical mediator of β-catenin survival functions in liver cancer. *Cancer Res* 2007, 67:901–910.
47. Rodriguez M, Aladowicz E, Lanfrancone L, Goding CR. Tbx3 represses E-cadherin expression and enhances melanoma invasiveness. *Cancer Res* 2008, 68:7872–7881.
48. Suh I, Shibru D, Eisenhofer G, Pacak K, Duh QY, Clark OH, Kebebew E. Candidate genes associated with malignant pheochromocytomas by genome-wide expression profiling. *Ann Surg* 2009, 250:983–990.
49. Witte JS. Personalized prostate cancer screening: improving PSA tests with genomic information. *Sci Transl Med* 2010, 2:62ps55.
50. Yamashita S, Tsujino Y, Moriguchi K, Tatematsu M, Ushijima T. Chemical genomic screening for methylation-silenced genes in gastric cancer cell lines using 5-aza-2′-deoxycytidine treatment and oligonucleotide microarray. *Cancer Sci* 2006, 97:64–71.
51. Yarosh W, Barrientos T, Esmailpour T, Lin L, Carpenter PM, Osann K, Anton-Culver H, Huang T. TBX3 is overexpressed in breast cancer and represses p14 ARF by interacting with histone deacetylases. *Cancer Res* 2008, 68:693–699.
52. Zhang JF, He ML, Qi D, Xie WD, Chen YC, Lin MC, Leung PC, Zhang YO, Kung HF. Aqueous extracts of Fructus Ligustri Lucidi enhance the sensitivity of human colorectal carcinoma DLD-1 cells to doxorubicin-induced apoptosis via Tbx3 suppression. *Integr Cancer Ther* 2011, 10:85–91.
53. Cavard C, Audebourg A, Letourneur F, Audard V, Beuvon F, Cagnard N, Radenen B, Varlet P, Vacher-Lavenu MC, Perret C, et al. Gene expression profiling provides insights into the pathways involved in solid pseudopapillary neoplasm of the pancreas. *J Pathol* 2009, 218:201–209.
54. Etcheverry A, Aubry M, de Tayrac M, Vauleon E, Boniface R, Guenot F, Saikali S, Hamlat A, Riffaud L, Menei P, et al. DNA methylation in glioblastoma: impact on gene expression and clinical outcome. *BMC Genom* 2010, 11:701.
55. Hansel DE, Rahman A, House M, Ashfaq R, Berg K, Yeo CJ, Maitra A. Met proto-oncogene and insulin-like growth factor binding protein 3 overexpression correlates with metastatic ability in well-differentiated pancreatic endocrine neoplasms. *Clin Cancer Res* 2004, 10(18 Pt 1):6152–6158.
56. Schmalhofer O, Brabletz S, Brabletz T. E-cadherin, β-catenin, and ZEB1 in malignant progression of cancer. *Cancer Metastasis Rev* 2009, 28:151–166.
57. Kowalski PJ, Rubin MA, Kleer CG. E-cadherin expression in primary carcinomas of the breast and its distant metastases. *Breast Cancer Res* 2003, 5:R217–R222.
58. Mowla S, Pinnock R, Leaner VD, Goding CR, Prince S. PMA-induced up-regulation of TBX3 is mediated by AP-1 and contributes to breast cancer cell migration. *Biochem J* 2010, 433:145–153.
59. Begum S, Papaioannou VE. Dynamic expression of *Tbx2* and *Tbx3* in developing mouse pancreas. *Gene Expr Patterns* 2011.
60. Suzuki A, Sekiya S, Buscher D, Izpisua Belmonte JC, Taniguchi H. Tbx3 controls the fate of hepatic progenitor cells in liver development by suppressing *p19ARF* expression. *Development* 2008, 135:1589–1595.
61. Fillmore CM, Gupta PB, Rudnick JA, Caballero S, Keller PJ, Lander ES, Kuperwasser C. Estrogen expands breast cancer stem-like cells through paracrine FGF/Tbx3 signaling. *Proc Natl Acad Sci U S A* 2010, 107:21737–21742.
62. Gupta PB, Fillmore CM, Jiang G, Shapira SD, Tao K, Kuperwasser C, Lander ES. Stochastic state transitions

give rise to phenotypic equilibrium in populations of cancer cells. *Cell* 2011, 146:633–644.

63. Lingbeek ME, Jacobs JJ, van Lohuizen M. The T-box repressors *TBX2* and *TBX3* specifically regulate the tumor suppressor gene *p14ARF* via a variant T-site in the initiator. *J Biol Chem* 2002, 277:26120–26127.
64. Brummelkamp TR, Kortlever RM, Lingbeek M, Trettel F, MacDonald ME, van Lohuizen M, Bernards R. TBX-3, the gene mutated in Ulnar-Mammary Syndrome, is a negative regulator of p19ARF and inhibits senescence. *J Biol Chem* 2002, 277:6567–6572.
65. Carlson H, Ota S, Song Y, Chen Y, Hurlin PJ. Tbx3 impinges on the p53 pathway to suppress apoptosis, facilitate cell transformation and block myogenic differentiation. *Oncogene* 2002, 21:3827–3835.
66. Mosca E, Bertoli G, Piscitelli E, Vilardo L, Reinbold RA, Zucchi I, Milanesi L. Identification of functionally related genes using data mining and data integration: a breast cancer case study. *BMC Bioinform* 2009, 10(Suppl 12):S8.
67. Yan W, Cao QJ, Arenas RB, Bentley B, Shao R. GATA3 inhibits breast cancer metastasis through the reversal of epithelial-mesenchymal transition. *J Biol Chem* 2010, 285:14042–14051.
68. Hatsell SJ, Cowin P. Gli3-mediated repression of Hedgehog targets is required for normal mammary development. *Development* 2006, 133:3661–3670.
69. He M, Wen L, Campbell CE, Wu JY, Rao Y. Transcription repression by *Xenopus* ET and its human ortholog TBX3, a gene involved in ulnar-mammary syndrome. *Proc Natl Acad Sci U S A* 1999, 96:10212–10217.

FURTHER READING

Naiche LA, Harrelson Z, Kelly R, Papaioannou VE. T-box genes in vertebrate development. *Annu Rev Genet* 2005, 39:219–239. http://omim.org/entry/181450

